# ELECTROCHEMICAL IMPEDANCE SPECTROSCOPY STUDY

# OF THE

# ULTRAVIOLET EXPOSURE OF BALLISTIC RESISTANT

# POLYMER MATRIX COMPOSITES

**A Thesis**
**Submitted to the Graduate Faculty**
**of the**
**North Dakota State University**
**of Agriculture and Applied Science**

**By**

**Drew Adam Pavlacky**

**In Partial Fulfillment**
**for the Degree of**
**MASTER OF SCIENCE**

**Major Degree:**
**Materials and Nanotechnology**

**January 2012**

**Fargo, North Dakota**

North Dakota State University
Graduate School

**Title**

Electrochemical Impedance Spectroscopy Study of the Ultraviolet Exposure

of Ballistic Resistant Polymer Matrix Composites

**By**

Drew Adam Pavlacky

The Supervisory Committee certifies that this ***disquisition*** complies with North Dakota State University's regulations and meets the accepted standards for the degree of

**MASTER OF SCIENCE**

SUPERVISORY COMMITTEE:

(Dr. Victoria Gelling)
Co-Chair

(Dr. Chad Ulven)
Co-Chair

(Dr. Dean Webster)

(Dr. Xinnan Wang)

Approved by Department Chair:

01/13/2012
Date

(Dr. Erik Hobbie)
Signature

## ABSTRACT

This study examined the effect of ultraviolet radiation on ballistic resistant polymer matrix composites. Two composite systems studied included a phenolic matrix with either S2 Glass® or Kevlar® fiber laminates. These composites were weathered in ultraviolet conditions and the effects were quantified with multiple destructive and non-destructive testing. Electrochemical impedance spectroscopy (EIS) was used as a non-destructive evaluation method which is a commonly used experiment in the corrosion community. Circuit modeling the EIS spectra produced both resistive and capacitive characteristics inherent of the composite materials. Surface characterization was performed to determine if degradation was occurring at the composite surface. Techniques included: color, gloss, surface profilometry, and water contact angle. Tensile and flexural destructive experimentation revealed the influence of the ultraviolet exposure on the mechanical properties. It was determined that the resistive portion of the EIS response correlated well with the ultimate tensile strength of the S2 Glass® fiber composites.

## ACKNOWLEDGEMENTS

I would like to thank all the people who have supported me through my entire journey as a graduate student. First, I would like to thank my supervisory committee members Dr. Victoria Gelling (co-advisor), Dr. Chad Ulven (co-advisor), Dr. Dean Webster, and Dr. Xinnan Wang. The constant guidance offered in the classroom and laboratory by my committee was greatly appreciated. Thank you to Sioux Manufacturing Corporation of Fort Totten, North Dakota whom supplied the ballistic resistant composites for their contribution to my research. The Gelling lab members were also extremely helpful in answering difficult questions, especially Christopher Vetter in the area of thesis formatting. Heidi Docktor was always willing to help with all instrumentation questions which was greatly appreciated. Numerous initial investigations were performed by the undergraduate student Tryg Bredeson which was a very important phase of research. I also always appreciated the help I received from Dr. Ulven's group members, Mike Ehresmann and Jeffrey Flynn, who helped conduct the mechanical and ballistic experimentation. In the same instance, I would like to thank all students, faculty, and staff of the Coatings and Polymeric Materials, Mechanical Engineering, and Materials and Nanotechnology departments for their help and encouragement. I would like to thank the Army Research Laboratory for funding this research throughout the duration of my graduate career. ND EPSCoR also provided funding which was helpful in completion of my degree.

## DEDICATION

This thesis is dedicated to my wife, Erin, for always being there for me and guiding me through difficult times as we shared the experience of graduate research together. It's amazing how our independent decisions made when we were friends led to the greatest thing that ever could have happened! I love you more than you will ever know.

This thesis is also dedicated to my parents, Butch and Gail,
and immediate family who taught me how to be the person I am today.

I also have the best advisors and friends a person could ever have and their guidance and friendship kept me sane over the past few months.

It is because of all of you that I've made it to where I am today. Thank You!

## PREFACE

The thesis entitled “Electrochemical Impedance Spectroscopy Study of the Ultraviolet Exposure of Ballistic Resistant Polymer Matrix Composites” was written as the author saw the need for a quick, inexpensive, and quantitative method for polymer matrix composites in structural applications. Most importantly, the quantitative nature of the impedance method would be more conducive for correlation to the mechanical properties, so that impedance could be used to know when structures would “fail”. The thesis experimental chapters were then fashioned in logical order to display the impedance change, why the impedance was changing, and how the change in impedance influenced the mechanical properties.

The first experimental chapter, Chapter 3, was to determine if a change in the impedance would be observed for the ballistic resistant composite materials after exposure to ultraviolet radiation. Changes were observed in the impedance response, so more commonly found non-destructive methods of surface characterization were then instituted to show the surface characteristics changing during ultraviolet exposure. The literature review found in the introduction chapter determined which surface characterization techniques would be most useful and cost efficient to reinforce the fact that degradation was occurring. Initially, it was hypothesized that if a change in the impedance occurred from increased porosity, then the mechanical properties should correlate to that impedance change. The last experimental chapter, Chapter 5, investigates the mechanical properties of the weathered composites along with the correlation to the electrochemical impedance results. The final chapter, Chapter 6, of the thesis then entails the general conclusions from the entire study as well as future experimentation to be completed for further validation of

using this impedance method for non destructive evaluation of polymer composite structures.

## TABLE OF CONTENTS

## LIST OF TABLES

## LIST OF FIGURES

# CHAPTER 1. APPLICATIONS, ULTRAVIOLET DEGRADATION, AND NON-DESTRUCTIVE EVALUATION OF POLYMER MATRIX COMPOSITES

## 1.1 Introduction

A polymer matrix composite (PMC) is a combination of two distinct phases with the polymeric phase being continuous (i.e., matrix or binder) and the other phase discontinuous (i.e., fiber, inclusions, etc.).[1] The combination of these materials, when correctly selected, provide a desirable material with physical, mechanical, thermal, and electrical properties which are typically more beneficial than each phase alone. The improvements in properties give rise to the extensive use of these materials in the aerospace, defense, automotive, industrial, and civil infrastructure sectors. Many PMCs have a low density, which is attributed to the low density of the polymeric matrix, and when combined with the high strength and high modulus of fibrous inclusions the resulting composite has a high specific strength and specific modulus.[2] PMCs with advanced fibers (i.e., carbon, aramid, various glasses, and other polymeric fibers) have properties that far exceed traditional and advanced metallic alloys on a per density basis.[2]

However, one major drawback of PMCs is their susceptibility to degradation in outdoor exposure. Some PMCs will undergo thermal oxidation in ambient conditions which occurs when polymeric chains are severed from the thermal energy input and oxygen, readily available in the atmosphere, forms a bond with the radical present on the exposed chain end.[3] The overall result is a loss of long range continuity in the polymer which will lead to a noticeable change in many properties of the material when enough oxidation reactions occur throughout the bulk polymer. Hydrolysis is another aspect of degradation that occurs in PMCs which causes degradation of the chain when water is

present. Of utmost concern for the polymeric matrix, and occasionally the fiber, is photodegradation which is caused by solar radiation in the ultraviolet (UV) wavelengths. One particular fiber with relatively low resistance to UV degradation is an aramid based polymer such as Kevlar®.[4] Much like thermal oxidation, an exposed chain end combines with ambient oxygen to form a peroxy containing structure. The breaking of the chain causes a loss of chain stability and a corresponding decrease in the ability to support mechanical and thermal stressors. Chain scission can also deteriorate the transfer of mechanical stresses from the matrix to fiber influencing the mechanical properties. Polymers and fibers, such as phenolics, epoxies, and aramids, contain aromatic groups within the polymeric chain. Aromatic groups are ring structures with multiple carbon-carbon double bonds which form a chemical structure of resonance where the electrons must be shared to remain stable. The use of aromatic polymers and fibers is beneficial because these materials are typically stronger and undergo less expansion upon thermal and mechanical loading as the rings in the chain cause significant interference to chain movement. Photodegradation of PMCs can lead to void or pore formation within these materials which is undesirable in many aspects.

Pore formation in the polymeric matrix provides sites for crack initiation or propagation when subjected to various stressors. Non-destructive evaluation (NDE) is used to investigate cracks, voids, delaminations, and other defects within the matrix material by non-evasive methods. Typically, NDE is used for an initial investigation of a PMC after manufacturing to determine void content as well as providing a method to improve the processing of these composites. Another sector of NDE usage is in structural health monitoring of the matrix after mechanical damage has occurred. The most common

methods used for NDE of PMCs are thermography, acoustic emission, ultrasonic techniques, and x-ray radiography.[2] As mentioned, these methods are considered, for the most part, to be non-destructive, however, some materials may be degraded upon exposure to the NDE technique. The results obtained from common NDE experiments are typically qualitative allowing for interpretation of the results. This causes the technique to be highly dependent upon the person performing the NDE technique. Ideally, an NDE technique is desired where the results are quantifiable, leading to a mathematical and statistical means for evaluating a PMC. The measurement should also be repeatable and have the ability to be conducted quickly. One experimental method with these desirable characteristics is electrochemical impedance spectroscopy (EIS), which is commonly used in the coatings industry to monitor coating degradation and corrosion.[5]

The establishment of the two electrode EIS technique, as opposed to the traditional three electrode technique, and the emergence of PMCs in multiple structural applications lead to the possibility of EIS as a structural health monitoring technique. In the late 1980s, carbon fiber reinforced polymers (CFRPs) became the subject of EIS experimentation utilizing the three electrode technique where the conductive fiber could act as the working electrode. Figure 1.1 displays the distinction between the two electrode and three electrode EIS techniques.

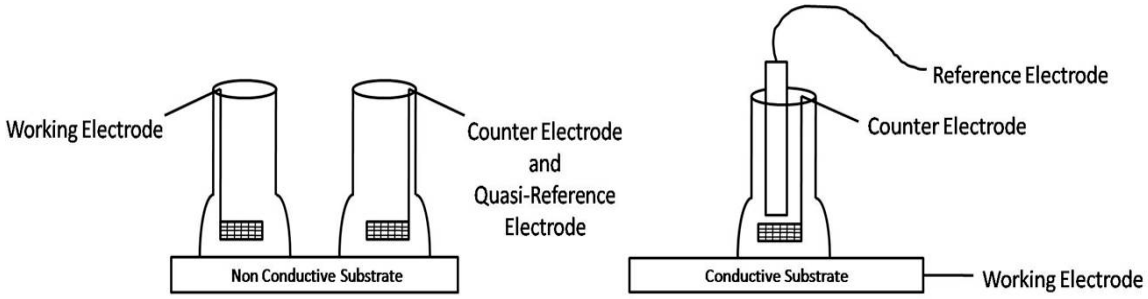


**Figure 1.1 – Two electrode technique (left) and three electrode technique (right)**

The research in this area led to many observations depending on the stimuli causing delaminations between the fiber and matrix. The use of carbon fiber as an electrode had many distinct advantages due to the previous work accomplished in the research of carbon electrodes for electrochemical measurements.[6] However, the aforementioned measurement technique is not suitable for use with bulk non-conducting PMCs. Therefore, it was not until 2008 when the two electrode technique was introduced to monitor the bulk material EIS response non-conducting PMCs. Unlike the local measurements performed on conductive fibers within an insulating matrix, the EIS experiments were performed in a global sense, which may provide correlation with other bulk properties (i.e., strength, stiffness, thermal expansion, etc.). Therefore, it was observed that two-electrode EIS is a suitable NDE technique for PMCs and that this technique has not been extensively researched or utilized to date.

**1.2 Polymer Matrix Composites: Applications and Advantages**

As mentioned previously, PMCs have higher specific modulus and specific strength compared to metallic alloys. Until recently, the main components of structural bearing components within many engineering sectors have been comprised of predominantly metallic alloys with the composite materials making contributions in primarily non-load bearing applications. The first use of PMCs in aircraft applications occurred during the metal shortage during World War II.[1] Non- structural aircraft parts such as ducts, engine covers, and radomes were manufactured with PMCs to save metal. Eventually, the success of these parts (i.e., easily processed and structurally stable) transferred to the initial design of structural components comprised of PMC material. One of the first aircraft to be designed with a large portion of PMC as the structural component was the AV-8B aircraft

designed in the 1970s and 1980s for use as a ground attack aircraft.[7] Original designs suggested that 23.3%, by weight, of the fuselage and wing substructures were comprised of a graphite fiber embedded within an epoxy matrix. This aircraft's development led Boeing and Airbus to design the Boeing 777 and Airbus 340 with 13% and 15% of their structural components comprised of polymeric composites by weight.[8] A major milestone in the use of PMCs occurred when Boeing's Dreamliner 787 was reported to be designed with 50 weight percent of composites, distributed throughout the entire aircraft.[9] The specific strength and modulus of PMCs are typically much higher than the metallic alloys traditionally used in aerospace applications; for instance, carbon fiber/epoxy matrix composites have a specific strength and modulus roughly two to four times higher than mild steel and one and a half to two and a half times higher than commonly used aluminum alloys.[2] The differences become even more prominent when comparing to a low density fibers like Kevlar®, Spectra®, and Dyneema®, which are polymeric in nature.

In the civil engineering sector, the use of PMCs has also been explored for the replacement and retrofitting of concrete structures.[10-11] Both the use of retrofitting concrete structures with PMCs and the development of fiber reinforced polymer (FRP) beams for replacement of steel reinforcement have been utilized in this sector. Both these replacements stem from the corrosion issues of the interior steel reinforcement. Once the corrosion process occurs in the steel reinforcements, voluminous rust causes cracking at the steel reinforcement/concrete interface. When combined with cyclic loading from traffic and pedestrians, cracks initiated at the interface can be propagated to the surface of the concrete. To combat the complete destruction and replacement of beams, PMC wrapping of the column structures is a solution used to delay further corrosion and also provides a

structural support. [12] Specific equipment, Robo-Wrapper®, is used with polymer pre-impregnated unidirectional fibers to wrap the beam structure and cure the matrix material after application.[13] The most typical PMC used in this application is epoxy matrix/carbon fiber due to the relative high elongation and high strength. Strong PMC beams containing carbon reinforced polymers have also been utilized in the replacement of steel reinforcements to offset the metallic corrosion. Many PMC combinations have been explored in this area which usually include numerous combinations of common matrix and reinforcement materials. Another area of investigation is disposing of the concrete element and replacing these bridge and support structures with PMCs. The first all-composite bridge designed for pedestrians was erected in Israel almost four decades ago in 1975. Now, composite bridges which support vehicles have been built in many states with the first being constructed in Kansas.[14] On the other hand, these structures are expensive, compared to the concrete bridges. Another area of concern is the long-term durability of these structures as the technology and materials are relatively new.

Defense applications are another major market in which PMCs have found a niche.[1] Kevlar® and Twaron® fibers woven into plies and then surrounded by stiff matrix materials (i.e., epoxies and phenolics) have found many uses in ballistic shielding applications including the up-armoring of military vehicles and bunker containment materials.[15] These materials are also being utilized in the door separating passengers from pilots in some commercial aircrafts for protection purposes. Another fiber reinforcement used in this area includes S2 Glass® and R Glass® which are a less expensive alternative to an aramid (i.e., Kevlar® or Twaron®) fiber. The applications can be identical, but typically the aramid fiber has a lower density making it more suitable when weight

restrictions are a concern. High performance polyethylene (HPPE) including Spectra® and Dyneema® are garnering attention in the hard personnel armor which also contain a polymeric binder.[16] Common applications include helmets and armor plates for insertion into clothing. Other organic fibers in ballistic armor are poly-phenylenebenzobisoxazole (PBO) and poly-diimadazo-pyridinylene-dihydroxy-phenylene (M5).[16] However, PBO is known to hydrolytically degrade from exposure to ambient atmospheric conditions. Also, the processing of M5 is considered difficult, compared to the other fibers, making these fibers not as common.

As mentioned, PMCs have excellent properties on a per density basis such as specific strength and specific modulus. These attributes also lead to these composite systems performing well in ballistic applications. Ballistic penetration is directly related to how well a material absorbs energy along with how fast that material distributes that energy. Polymeric fibers embedded within a matrix perform very well in this area as the sonic velocity (i.e., relates to the velocity of energy transfer) and specific energy absorption are both on a per density basis.[16] Figure 1.2 displays the areas encompassing several types of PMC fibers with respect to their energy absorption and sonic velocities.[16]

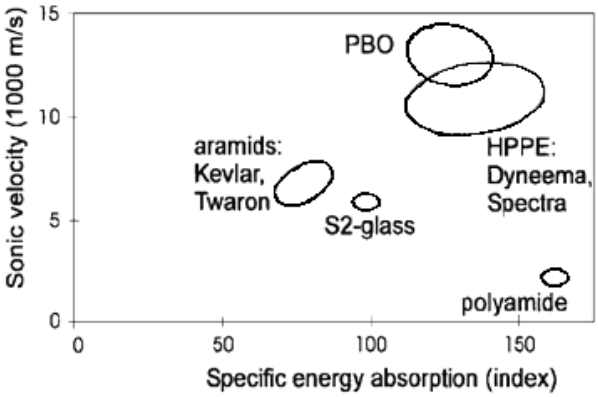


**Figure 1.2 - Fiber performance on basis of ballistic properties**

**[With kind permission from Springer Science+Business Media: Journal of Materials Science, Ballistic protection mechanisms in personal armour, 36, 2001, pages 3137-3142, M. Jacobs, Figure 3]**

Typically, ballistic resistant PMCs also have high smoke and flame retardant capabilities which are two more important attributes for defense applications. To accomplish flame retardant matrix, a substitution reaction of the matrix polymer incorporates a halogen (i.e., fluorine, chlorine, bromine, iodine) to reduce the oxygen at the area of combustion.[17] A typical substituted polymer is a phenolic as the highly aromatic backbone is difficult to ignite with flame and halogenation is relatively easy with the numerous hydroxyls present. Another commonly halogenated matrix material is epoxy which also has aromatic groups present within the polymeric chain.

One main reason for PMC success in many applications is the ease of manufacturing complex geometries. When the first aircraft parts were made during the metal shortage of World War II, manufacturers noted that much time could be saved with hand lay-up of the difficult duct structures in aircraft as opposed to bending and riveting metal.[1] Additionally, new technologies in processing have made parts far more robust with continuously more automation within PMC manufacturing.[18] Autoclaving of PMCs uses a combination of pressure and a vacuum along with heat to consolidate and cure thick and complex geometries with minimal void content.[19] Resin transfer methodologies (vacuum assisted resin transfer molding, expansion resin transfer molding, Seeman's composite resin infusion molding process, etc.) have also been used with promise in manufacturing complex PMC components.[1] Lastly, compression molding using high pressures and heat has been used to produce thick composite parts with reasonably low void content on a per thickness basis.[1]

Another aspect regarding the success of PMCs is the fiber architecture design which can be engineered to have minimal fiber content by aligning fiber in the directions of

incurred stressing. Fiber architecture can be accomplished within some composite processing techniques including: extrusion, pultrusion, fiber placement, and filament winding. Additionally, fiber weaving into fiber plies and the subsequent orientation and stacking of these plies along with the woven pattern can determine strength directionality.[1] The emergence of three dimensional weaving is another proponent to the likelihood of PMC's stable market in many advanced applications.[20] With all these capabilities for fiber orientation much weight can be saved in the part and also the entire structure. In the aerospace and transportation sectors, part weight is always a major design consideration with the increasing price of fuel.

PMCs have many advantages over traditional monolithic metals, but a downfall of these materials is their weathering in outdoor exposure from the presence of heat, water, and ultraviolet radiation. The influence of ultraviolet radiation can have several undesirable effects which can directly influence the desired performance of the aforementioned applications.

### 1.3 Ultraviolet Radiation Weathering of Polymer Matrix Composites

Various forms of degradation occur when reinforced polymers are placed into their functioning environment. The three main forms of weathering degradation which cause a chemical change include: thermal degradation, hydrolysis, and photodegradation.[3] Thermal degradation and hydrolysis are unlike photodegradation as the entire bulk material can undergo degradation reactions after exposure while photodegradation is usually a surface phenomenon. As mentioned previously, radical formation is achieved once a degradation initiation reaction occurs which usually combines with oxygen to form various carbonyl containing groups. These carbonyl groups can further undergo free radical

reactions to produce highly oxidative species.[21] Also, the hydroxyl radicals are of concern as a further initiator of degradation reactions. In some polymers, both thermal initiation and photo-oxidation can occur in synergy to further excel the degradation. The overall process is highly sophisticated and dependent on polymer chemistry, but a simplified reaction scheme of the degradation process in organic polymers is presented in Figure 1.3.[21]

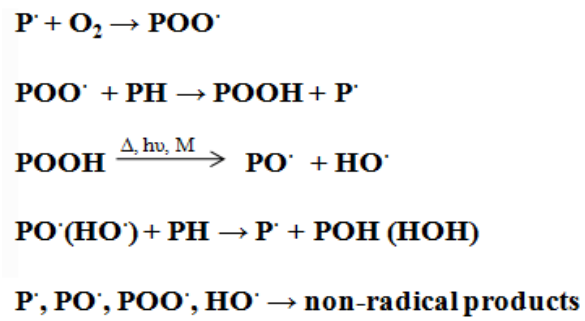


**Figure 1.3 - Generalized reaction scheme of organic polymers via photodegradation**

**[With kind permission from Springer Science+Business Media: Progress in Polymer Science, Photostabilization of coatings. Mechanisms and performance, 25, 2000, pages 1261-1335, Pospíšil, J. and S. Nešpurek, Scheme 25-29]**

In Figure 1.3, "P" represents the polymeric structure and the "P·" is the radical form of the polymer after a stimuli of enough energy has produced a free radical. The chain scission decreases the overall stability of the polymer which effects transfer of stimuli to the fiber and, thus, the entire PMC structure is compromised. Fibers and inclusions, if possessing an appropriate chemical structure, can also undergo photodegradation resulting in a loss of integrity. Photodegradation can even lead to complete deterioration of the polymeric rich top layer present in many PMCs by a process known as chalking.[22] Chalking results in a white powder formation from the oxidation processes which consists of degraded polymer and various other components depending on the material system. A similar phenomenon termed blooming is the migration of degraded species causing a dull appearance.[23]

PMCs that are degraded from ultraviolet exposure display significant changes to surface characteristics; however, if the UV source is of the correct wavelength and the exposure time is great enough, sufficient damage can be done to interior layers of the PMC. Two of the most easily noticeable changes, visible by the human eye, are gloss and color change.[23] Unfortunately, very little literature investigates these two phenomena quantitatively for PMCs. Most literature in this area cites a noticeable change in color and gloss without stating the results as a quantitative value.[24-29] However, some studies were performed to investigate polymer degradation use the yellowness index which monitors the yellowing of the polymer over exposure time by numerical color measurements.[30-32] This is often done by purely monitoring the b* value of the CIE Lab coordinate system, or by using the tristimulus values of color with the following Equation 1.1.

$$YI = \frac{100(1.28X - 1.06Z)}{Y} \qquad (1.1)$$

In Equation 1.1, *X*, *Y*, and *Z* are tristimulus values dependent on the object, illumination source, and standard observer.[33] This index only utilizes one aspect of color change from UV degradation while two other color coordinates can also be monitored. Of particular concern is the L* value of the CIE (i.e., Commission Internationale de L'éclairage) Lab color scale which can be used to determine the amount of chalking that has occurred with the PMC.[34] In a numerical sense, a total color change can be calculated by measuring the L*, a*, and b* coordinates differences in the Euclidean color space which is displayed in Equation 1.2.[35]

$$\Delta E = (\Delta L^2 + \Delta a^2 + \Delta b^2)^{1/2} \qquad (1.2)$$

Ahmad Thimizir et al. investigated a natural kenaf fiber in poly(butylene succinate) after radiation exposure to a natural atmosphere in Malaysia.[36] Both the polymer and fiber had proper chemical structures for photodegradation to occur through multiple reaction forms depending on the wavelengths of radiation present.[37] It was observed that all color values were modified over an exposure time of six months, with the largest contribution of color change coming from the L* value of color due to polymer chalking. Correria et al. examined the gloss and color change of polyester matrix/glass fiber composites under UV exposure for long (i.e., greater than 2000 hours) exposure times.[38] It was found that considerable changes were observed in the b* and L* values for the samples subjected to only UV exposure. These large differences, especially in the b* value, gave a large total color change from initial experimentation to the end of exposure. Also, the change in gloss was attributed to many effects, but surface roughening effects were thought to be the main proponent by the authors. Equation 1.3 was derived by Toporets and is used to quantify the surface roughness when comparing the reflectance values of the pristine surface to that of the weathered surface.[39]

$$\frac{R_s}{R_0} = exp\left[-\left(\frac{4\pi\sigma\cos\theta}{\lambda}\right)^2\right] \qquad (1.3)$$

In Equation 1.3, $R_s$ is the reflectance of the rough surface, $R_o$ is the initial reflectance of the polymer, $\sigma$ is the root mean square deviation from the mean height, $\theta$ is the angle of the gloss measurement, and $\lambda$ is the wavelength of the illuminant. The surface roughness usually increases with exposure which corresponds to a larger $\sigma$ value and, thus, a larger decrease in the exponentially decaying function. The rough surface reflectance is decreased which directly correlates to lower gloss values.

Another surface characteristic studied is the surface roughness after exposure to UV radiation. The effect can vary from surface wrinkling and void creation to complete degradation of the polymeric top layer to expose fiber ends. Scanning electron microscopy (SEM) is a commonly used technique to observe fiber pull-out, matrix micro-cracking, and matrix erosion at the surface of the composite structure.[40-46] In lengthy weathering experiments, the debonding between fiber plies was observed via SEM.[29] SEM micrographs can also distinguish the form of failure that occurred within the PMCs when fracture surfaces are examined. The fracture surface examination provides information on the failure mode and whether it was due to matrix or fiber centered properties or a combination of the two in the form of delamination.[24, 47] Figure 1.4 displays common degradation characteristics observed in carbon fiber/epoxy matrix.[28]

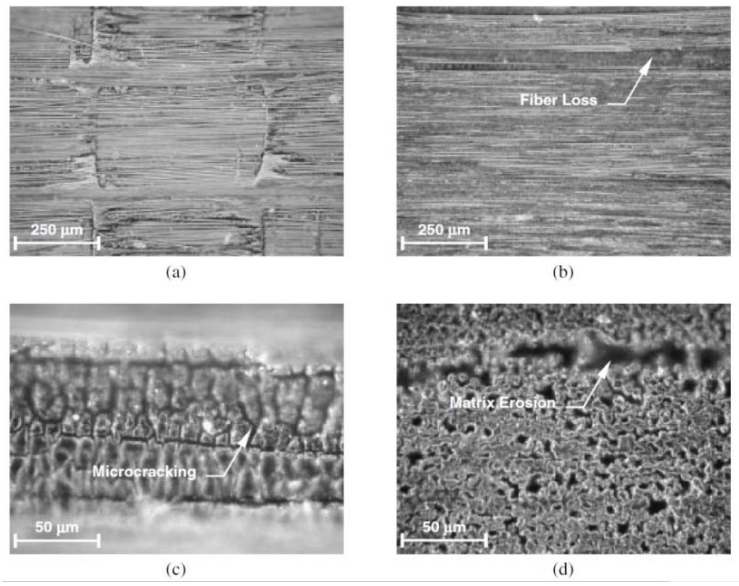


**Figure 1.4 – Scanning electron micrographs of a) pristine PMC b) PMC exhibiting fiber loss at low magnification c) matrix cracking of PMC at high magnification and d) matrix erosion of PMC all after 1000 hours of accelerated exposure**

**[With kind permission from Sage Publications: Journal of Composite Materials, Degradation of carbon fiber-reinforced epoxy composites by ultraviolet radiation and condensation, 36, 2002, page 2713, Kumar, B.,Singh, R., Nakamura, T., Figure 10]**

Another common method of surface investigation is optical microscopy which can be used to monitor pore content, depth of pore and void formation, fiber pull-out, and various other characteristics.[28, 48-49] Other surface phenomena that have also been studied are the area of surface energies and resistivity for photodegraded composites. Findings in this area have concluded that the wavelength of ultraviolet radiation present influences the surface energy, surface resistivity and contact angle. Therefore, the degradation products formed from the matrix material are also dependent on the radiation energy.[50]

A major area of concern with degraded PMCs is the presence of voids which indicate a mass loss of the part or structure. Mass loss can be attributed to degraded polymer being removed from the surface, or if enough matrix is removed, loss of fiber.[28, 43, 45] Additionally, the presence of pores also leads to an increased solution or water absorption.[38, 51-54] Micelli and Nanni studies with glass and carbon fiber composites exhibited an increase of water absorption with increased time and temperature.[52] However, the uptake of water correlated with the trends observed in the mechanical testing of the composites. Depending on the solution, which varies with the composite's application, hydrolysis and polymeric oxidation may occur if oxidizing agents are present in the solution. Chin et al. also investigated solution uptake of composite samples subjected to artificial UV exposure.[53] Three forms of solution were used to weather PMCs comprised of polyester and vinyl ester resins for extended time frames. A concrete alkaline solution, produced from concrete mixing, was of concern as the study focused on these PMCs function in as concrete reinforcement. The final conclusion was that the composites were oxidized which caused changes composite structure.

UV photo-oxidation and the resulting degradation reactions can cause significant mechanical damage if the radiation is of a low enough wavelength (i.e., higher energy) and/or for extended periods of time. Flexural properties are more dependent on the matrix phase of composites than tensile properties as the load is applied out-of-plane of the fiber orientation. This causes increased dependence on the matrix to fiber load transfer. Matrix dominated properties are observed to change after relatively short weathering periods.[36, 38, 40, 48-49, 55-57] In some instances, the flexural modulus can increase due to increased crosslinking, either from under-cured composites or photodegradation induced crosslinking from free radicals, and then decrease after further exposure.[29, 51, 58]

A study conducted by George and Dursch investigated numerous high strength composites in a low earth orbit for a duration of 69 months.[58] The results displayed increased composite flexural modulus and strength over this duration. Figure 1.5 reveals two composites that increased the flexural strength or both the flexural strength and modulus.[58]

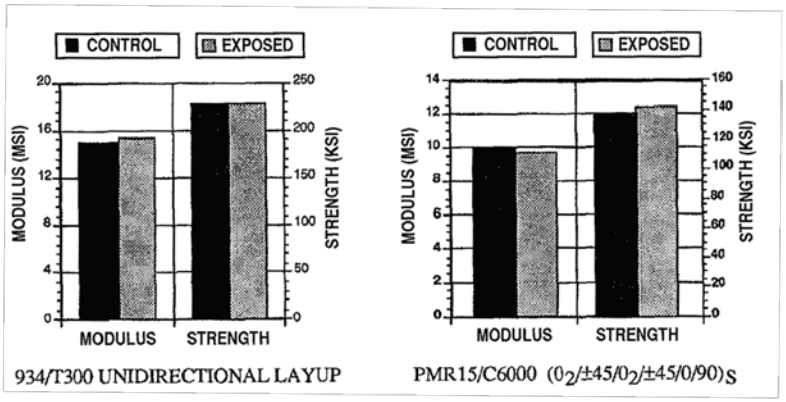


**Figure 1.5 - Two composites systems subjected to low earth orbit and the corresoponding flexural properties**

**[Reprinted by permission from the society for the Advancement of Material and Process Engineering (SAMPE): Journal of Advanced Materials, Low earth orbit effects on organic composites flown on the long duration exposure facility, 25, 1994, 10-19, George, P. and Dursch, H., Figure 7]**

The PMC systems 934/T300 and PMR15/C6000 designate an epoxy matrix/graphite fiber and polyimide matrix/graphite fiber, respectively. The 934/T300 PMC was made in a unidirectional fiber orientation while the PMR15/C6000 was a composite constructed of numerous stacked fiber plies. It was also concluded from this research that carbon fiber/epoxy matrix composites had both a higher modulus and strength than the polyimide matrix/ graphite fiber composites. However, low earth orbit exposure does not provide similar conditions to that found on Earth's surface, but is a form of accelerated exposure as photodegradation and increased oxidation reactions are occurring.

Transverse tensile loading of unidirectional composites are also highly dependent on the matrix properties. A transverse tensile measurement corresponds to a tensile loading in a direction 90° from the fiber orientation. This form of experimentation on PMCs provides better insight into how the matrix was affected due to UV exposure which normally decreases the strength and modulus.[28, 44] Kumar et al. studied both longitudinal (i.e., in the fiber direction) and transverse tensile properties of epoxy matrix/carbon fiber composites.[28] It was observed that the longitudinal moduli and strengths did not change from the original values as the fiber phase was not affected by UV radiation. Carbon fiber is not susceptible to UV degradation which is the reason for the modulus remaining constant with increasing exposure. Likewise, the transverse modulus did not change dramatically during exposure, but the transverse strength did change substantially. The transverse modulus is an out-of-phase loading scenario which is more dependent on the matrix; however, the small strains associated in this regime do not promote large differences from short exposure. Figure 1.6 exhibits the change observed for various weathering cycles and the corresponding transverse strengths.[28]

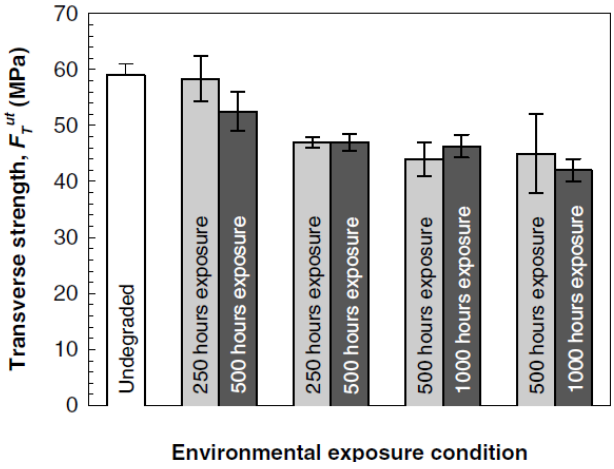


**Figure 1.6 - Transverse strengths of (from left to right) undegraded PMC, UV exposure only PMC, Moisture exposure only PMC, sequential exposure, and cyclic exposure of UV and moisture**

**[With kind permission from Sage Publications: Journal of Composite Materials, Degradation of carbon fiber-reinforced epoxy composites by ultraviolet radiation and condensation, 36, 2002, page 2713, Kumar, B., Singh, R., Nakamura, T., Figure 15]**

It can be concluded that these composites appear to be more sensitive to moisture than UV exposure. However, 500 hours of UV exposure changed the transverse strength significantly from the initial strength. These examples indicate that the longitudinal strength and modulus are not greatly affected by UV induced degradation, but the degree of UV susceptibility is dependent on the fiber architecture and fiber type.

The tensile properties are commonly reported measurements for PMCs that have been exposed to UV radiation. Depending on the fiber, drastically different results can be obtained. For instance, carbon or graphite and glass fiber exhibit tensile properties that demonstrate little change after weathering due to the fibrous material not undergoing degradation reactions.[26, 28, 38, 42, 45, 59-60] Similarly, the compressive strength of composites is dominated by the fiber which demonstrates little change if the fiber itself is not susceptible to UV degradation.[61] However, most natural fiber PMCs are known to

display decreasing tensile mechanical properties when exposed to ultraviolet radiation for durations long enough to remove the polymeric top layer.[56, 62-64] For instance, Shubhra et al. studied the utilization of randomly oriented silk fibers in a polypropylene matrix for durability after several forms of weathering.[63] It was observed that the composite systems displayed a higher loss of tensile strength with increased ageing. Figure 1.7 displays the loss of tensile strength with increased exposure time for polypropylene/rubber matrix ratios with 20% silk fiber by weight.[63]

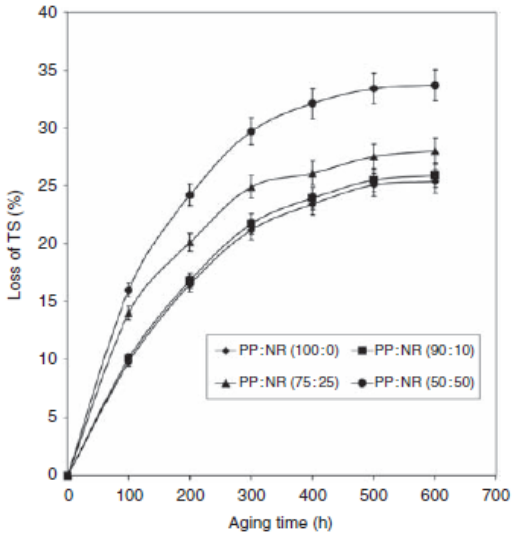


**Figure 1.7 - Loss of tensile strength over ageing time for varying ratios of polypropylene (PP) to natural rubber (NR)**

**[With kind permission from Sage Publications: Journal of Reinforced Plastics and Composites, Effect of matrix modification by natural rubber on the performance of silk-reinforced polypropylene composites, 29, 2010, page 3338, Shubhra, Q., Saha, M., Alam, A., Beg, M., Khan, M., Figure 2]**

Polymeric fibers such as ultra high molecular weight polyethylene (UHMWPE) have also displayed a decrease in mechanical tensile properties when UV radiation is administered to the composite.[65] If the duration of exposure is long enough and the radiation administered to the samples is the certain wavelength, considerable damage can accumulate thus affecting the tensile strength substantially. Segovia et al. determined that

7000 hours of exposure to artificial weathering gave undeniably large decreases in tensile strength for several types of two dimensional fiber layup composites. The artificial weathering was also conducted at UV intensities of 1700 watts per square meter.[66]

Lastly, infrared spectroscopy has been used to provide an indication of the extent of photodegradation as new chemical constituents form and the initial chemical structure is altered. Depending on the matrix, many forms of chemical reactions can occur producing a variety of degraded compounds. One of the degraded functional groups produced is the carbonyl group which was referenced earlier and can be observed in pristine organic polymers.[36, 38, 67] Correia et al. found an increase in the carbonyl peak at 1730 $cm^{-1}$ with an increase in UV exposure for an isopthalic polyester matrix/glass fiber PMC.[38] Figure 1.8 displays the trend of an increasing carbonyl peak with exposure time.[38]

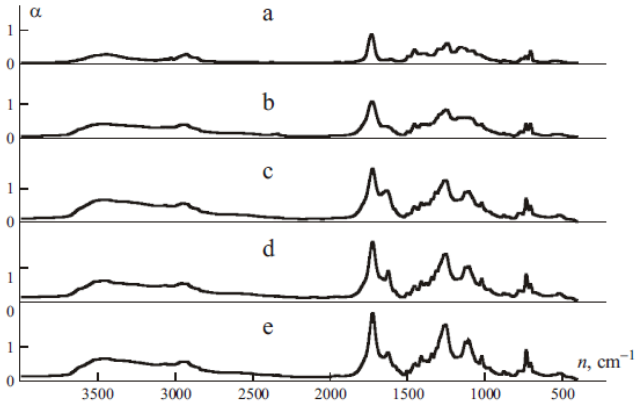


**Figure 1.8 - Infrared spectra of UV weathered PMC for a) reference b) 1642 hours c) 3304 hours d) 4839 hours and e) 6480 hours showing increased carbonyl content**

**[With kind permission from Springer Science+Business Media: Mechanics of Composite Materials, Durability of pultruded glass-fiber-reinforced polyester profiles for structural applications, 42, 2006, pages 325-338, Correia, J., Cabral-Fonseca, S., Branco, F., Ferreira, J., Eusebio, M., Rodrigues, M., Figure 10]**

It was concluded that the extent of weathering is dependent on many factors such as the form of exposure and PMC type. In a mechanical sense, an area of great concern is pore development which can alter material properties. To monitor the extent of weathering

in these structures without permanent destruction (i.e., mechanical testing), non-destructive evaluation techniques have been introduced.

## 1.4 Non-Destructive Evaluation of Polymer Matrix Composites: Traditionally Accepted Methods

The goal of non-destructive evaluation (NDE) of PMCs is to determine areas containing voids, pores, and delaminations within a structure. NDE techniques can be performed with PMCs that are in their unused state or for scheduled structural health monitoring of a composite part over time. The traditionally used and widely accepted methods of NDE are: thermography, acoustic emission, ultrasonic techniques, and x-ray radiography.[2] As the name suggests, each evaluation technique is typically non-destructive, but each method can be detrimental depending on the PMC. For instance, acoustic emission monitors the noise emitted by the PMC when stresses are applied. Noise is emitted when fiber breakage, matrix cracking, or fiber-matrix delamination occurs which is destructive. Thermography requires a temperature increased from ambient conditions and maintained for a period of time to determine void areas. This can be degrading if the matrix is highly susceptible to thermal oxidation. Each method has positive and negative aspects, but all methods tend to have relatively quick measurements, repeatable results, and qualitative imagery where the interpretations of the results are user specific.

Thermography is a NDE methodology which exploits the differences in thermal conductivities of air and polymers to observe air entrapment within PMC via void formation or delamination creation via an infrared camera.[2] The energy source can be either external or internal. An external source is radiant heating of the composite and an internal source is accomplished from the heat generation from fatigue cycling of the

composite. Originally, this inspection method had poor resolution compared to other NDE methods, but now with the immergence of liquid crystal technology the resolution has improved.[68] Instead of the traditional heating methods, where the composite's surface temperature is increased, the use of pulse thermography and cooling techniques has also been instituted.[69] Numerous forms of active (i.e., heat source containing) thermography are available, ranging from continuously modulated radiation to bursts as short as 2 milliseconds.[70] However, most methods do have a negative aspect. Pulse thermography typically discovers only surface defects of thicker cross sectional parts where development of major mechanical flaws are not detected.[71] If continuous thermally exposed samples are examined with thermography, thermal oxidation reactions will increase in number and accelerate the degradation process which is undesirable. Another area for concern is the detection limit of this method. As assumed, larger defects are relatively easy to detect, but large defects below the surface can be difficult to observe in thick or multi-ply PMCs. Composites with similar fiber and matrix thermal conductivities are also difficult to examine via thermography. Thus, investigation of polymeric fiber PMCs is difficult which is a negative aspect considering the emergence of polymeric fibers. Also, thin defects, such as fiber disbonding, are difficult to detect when occurring parallel to the heat source.[72]

Acoustic emission is a NDE that monitors the release of energy, in the form of sound waves, from PMCs. Energy release can be incurred through fiber breakage, matrix cracking, and complete delamination of fiber from matrix.[2] This method is traditionally used when fatigue or mechanical investigation is being conducted on composites as the acoustic microsensors can measure the energy releasing events in real-time as compared to

other NDE methods. The sound is emitted by the composite, captured by the emitter, and the signal amplified, filtered, conditioned, and converted to usable data. The frequency and amplitudes of the energy release are then studied and interpreted to determine which effect is occurring during the recorded energy release. By grouping these events into frequency bins for examination, it can be determined which effect may be the main contributing factor to the composite failure.[73] Also, mechanical degradation mechanisms may have one or more frequencies at which the sound response is generated leading to results that have to be heavily analyzed before the mechanism can be found.[74] This method leads to many quantitative results where statistical analysis is important, but the one negative aspect is the noise emitted is associated with a mechanism that compromises the stability of the composite. The measurement can only be accomplished with a specimen that is being degraded, causing this methodology to be less ideal than other accepted methods.

Ultrasonic NDE techniques use sound waves (i.e., frequencies between 1 and 25 MHz) as an external source to determine internal voids.[2] The wave can bounce off the sample skin layer (i.e., the depth of penetration dependent on material and wave frequency) or can go through the sample with the voids and defects scattering the wave such that the signal is not caught by the receiver to display a void. The measurement is performed on a point by point basis which is called an A-scan, and combining multiple A-scans produce a line of points known as a B-scan. If all B-scans are sorted in order and placed on one plane, the combination is known as a C-scan. These measurements are typically performed in a fluid medium to dissipate the loss effects that would be present in air. The fluid medium can cause degradation when subjected to this environment for extended periods of time. On the other hand, development of new sensors is paving a niche in the area of in-air

measurements.[75-76] An example of a typical C-scan is displayed in Figure 1.9 for the damage caused by impacts of varying energies in three composite systems.[77]

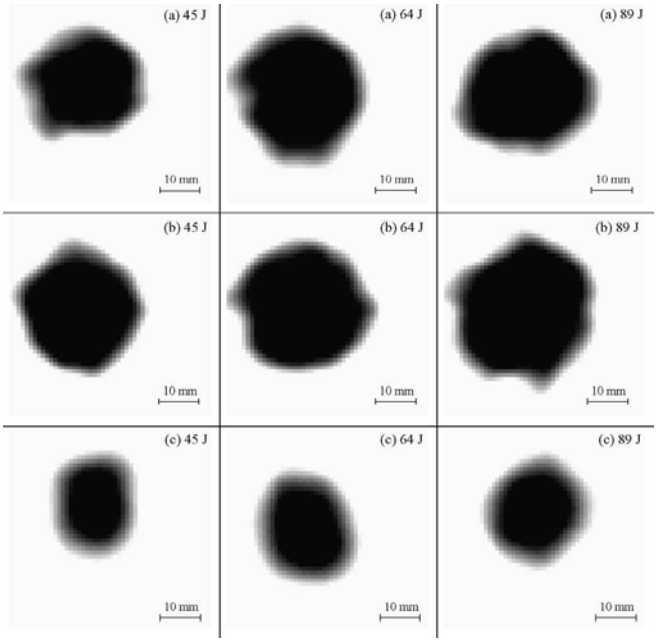


**Figure 1.9 - C-scans for 45 J, 64 J, and 89 J (from left to right) impacts on composite systems containing (a) carbon fiber (b) carbon and E Glass fiber and (c) carbon and Kevlar fiber**

**[With kind permission from Springer Science+Business Media: Journal of Materials Processing Technology, Air-coupled ultrasonic C-scan technique in impact response testing of carbon fibre and hybrid: glass, carbon and Kevlar/epoxy composites, 157-158, 2004, pages 513-522, Imielińska, K., Castaings, M., Wojtyra, R., Haras, J., Clezio, E., Hosten, B. Figure 7]**

The pulse echo method is usually the most popular method for in-service measurements as it requires only one side of the composite to be accessible.[78] Pulse-echo measurements are typically performed on thick samples (i.e., greater than 15 millimeters) while through transmission measurements are performed on thinner samples.[79-80] Regardless of the signal capturing methods, the results are quantitative as the size of a defect present may or may not directly coincide with the mode of failure. This is especially true when monitoring smaller voids and delaminations within a composite.

X-ray radiography NDE methods use x-ray radiation to pass through composite samples where the signal is then received by a detector and the intensity plotted. This technique has been utilized in the medical industry for many years for examining bone structures. The difference in absorption coefficients between air and the surrounding polymeric matrix and inclusions cause differences in the intensities as air has a low extinction coefficient compared to polymers, glass, and carbon.[2] For polymeric matrices, the use of heavy metal salts as penetrants highlight cracks, voids, and delaminations with greater contrast than air. The emergence of charge coupling devices (CCDs) and the more portable x-ray sources have led to 3-D imaging of internal flaws within PMCs as the image can be captured in 180° and multiple CCD screens to produce an image which has been used for numerous applications.[81] The use of high-resolution X-ray computed tomography (i.e., microtomography) has provided an insight into a variety of polymer composites and even investigated small defects created during UV exposure of composites.[82] These methods are far more functional than the originally used photographic film to capture the material response.[83] Three dimensional imaging is a progressive technology, but a major concern is length of time required to capture an image which can take up to 10 hours to scan an entire sample.[82] Of note, x-rays have been known to cause serious health effects including mutagenic and cytogenic conditions.[84] Also, the emergence of polymeric fibers, which have similar densities to the matrix materials, would not be observed via x-ray radiography. These reasons have lead to x-ray not being widely utilized for NDE of PMCs.

Electrochemical Impedance Spectroscopy (EIS) is a NDE typically used on coated metals to determine the attributes of the coating system, coating-metal interface, and

metallic substrate and the coating performs when exposed to degrading stimuli.[5, 85] A potentiostatic EIS method is most often used to apply a "controlled" sinusoidal voltage between two electrodes and the current response is measured, as the frequency is swept, to determine the magnitude of the impedance. The results of EIS experimentation are depicted in graphs of impedance magnitude versus frequency, phase angle (i.e., the offset of current from voltage) versus frequency, and the real versus imaginary components of the impedance. From these plots of data, circuit modeling with resistors, capacitors, and constant phase elements can be performed to produce a better understanding of the physical characteristics. The circuit elements, when placed in combinations of series and parallel, can replicate the results obtained during EIS measurements. Of more interest, each element can be monitored over time and compared to other systems. For instance, the delamination of a coating from substrate can be monitored over exposure time by the modeled capacitive elements within a spectra.[86] The resistive elements of the spectra can be an indicator of coating degradation as pore development can affect the barrier function of the coating system.[87] EIS is typically reserved for coatings with metallic substrates where one electrode of the experimentation is the conductive substrate, but more recently the use of non-conductive substrates has also been investigated.

By using a two electrode technique, displayed in Figure 1.1, the current measured is between the same two electrodes which apply the voltage making EIS measurements possible on non-conductive materials and in various configurations.[88] The quantitative measurement leads to statistical analysis of the results and correlation to various properties. Likewise, the repeatable measurements which are performed rather quickly make this technique a plausible method to be incorporated with the other NDE previously mentioned.

## 1.5 Electrochemical Impedance Spectroscopy of Polymer Matrix Composites

Both conductive and non-conductive composites can be measured by EIS via the three electrode and two electrode EIS techniques, respectively. With conductive samples, either the conductive element (i.e., usually a conductive fiber) may act as an electrode, or if a loading above the percolation threshold is present, a setup similar to coated metals can be used. To clarify the distinction, this section will be divided into the two different types of composites, conductive and non-conductive, and then sorted by the mode of void and delamination creation as many possible types of degradation exists including: mechanical stressing, absorption of various solutions, application of overpotentials, galvanic coupling to metallic alloys, and even microbial attack.

### *1.5.1 Investigation of Conductive Fiber PMCs Containing Carbon/Graphite Fiber via EIS*

Carbon and graphite fiber containing composites have been studied longer than the non-conductive composites as the electrode setup is more closely related to the traditional methods used for coated metals. A three electrode technique can be accomplished via the attachment of the working electrode to one of the conductive fibers, or the entire composite structure acting as the working electrode if intimate contact can be made with the conductive species. The entire structure is used as a working electrode with EIS of carbon fiber reinforced plastics (CFRPs) used to wrap concrete columns, but this will not be covered as only large area delaminations, in the magnitude of inches squared, are detected in this type of experimentation.[89-91] Also, these delaminations are not from the composite structures but rather from the delamination of the composite from the concrete.

The delamination of these structures undoubtedly occur from fatigue stressing of the concrete columns, but of more concern is the fatigue process in the actual composite

which has been researched by Glass and co-authors. Fatigue stresses are known to cause fiber failure, delaminations, fiber debonding, and matrix cracking in polymer matrix composites.[92] Glass et al. monitored the double layer capacitance in circuit modeled results of the electrochemical impedance spectra to determine the extent of delamination of a carbon fiber/epoxy matrix composite after significant flexural fatigue had been administered to the sample.[93] This three electrode configuration used a Luggin probe for the saturated calomel electrode (SCE) reference electrode to promote low resistance effects between the conductive solution, deaerated sodium sulfate solution, and sample. The counter electrode material was also made of carbon which acts as one of the electrodes measuring the current flow. Many fatigue cycles (i.e., 100,000 cycles) were then administered to the epoxy matrix/carbon fiber composite to induce voids throughout the PMC sample. The modeled double layer capacitor exhibited a major difference from that of the original values. This change can be attributed to the decrease in the active electrode area, more than likely, from the fiber breakage that occurred during the fatigue experimentation. Likewise, the absorption of solution in fatigued samples was observed to increase with increasing amount of fatigue cycles as void creation allows for more solution uptake.[94] This increase in solution absorption would also increase the solution resistance typically, but the decrease in area effect outweighed that of the permittivity effect. Equation 1.4 displays the calculation of capacitance for two electrodes separated by a less conductive material than that of the electrodes.

$$C = \varepsilon_r \varepsilon_o A/d \qquad (1.4)$$

In Equation 1.4, $\varepsilon_o$ is the permittivity of free space, $\varepsilon_r$ is the dielectric constant, $A$ is the active area, and $d$ is the distance between the two conductive electrodes. As fiber breakage

occurs, the fiber area decreases resulting in a smaller capacitance. However, the absorption of the dilute solutions increase the capacitance values as the relative permittivity of water is between 76.6 and 80 while polymer has a dielectric constant between 2.0 and 12.2.[95] A dilute salt solution does not affect the relative permittivity of the solution as the mixed media theory states that the volume fractions of each constituent are of utmost importance.[96] Likewise, the volume fraction of solution present in the polymer was outweighed by the area effect causing the capacitance variance. Another interesting aspect came from the research of the carbon fiber/epoxy matrix composite as the capacitance values were observed to decrease after completion of flexural fatiguing. This trend was attributed to atmospheric moisture causing further penetration of the solution to promoting swelling deeper within the matrix material and possibly causing fiber breakage. Again, the fiber breakage corresponds to less area causing a decrease in capacitance. The fiber breakage also led to higher resistance values as the longer pathway, from the fiber to counter electrode, through a more resistive media (i.e., polymeric matrix) increases the resistance. This work demonstrated that the fiber breakage mechanism was the main mode of degradation in this composite system and it could be monitored with EIS.

Glass et al. also investigated the immersion of the carbon fiber/epoxy matrix composites in different solutions, with intermittent dry cycles, to determine the influences on the EIS spectra.[93] The solutions used were distilled water and the sodium sulfate solution previously mentioned. A comparison was made between the as-received composite EIS spectra and that of composites dried at 140°C for 48 hours, composites immersed in sodium sulfate solution for 30 days at room temperature, composite immersed in distilled water for 4 days at 100°C, and composites dried after immersion in solution.

Both solutions displayed a decrease in the capacitance compared to the original values. The capacitance rose compared to initial values after drying the immersed samples. This observation can be credited to the increased electrolyte absorption due to matrix microcracking, void formation, and delaminations due to the swelling/unswelling cycle caused with wet and dry cycling. Void creation between fibers can cause electrical bridging with an electrolyte medium causing an increase in the surface area and, thus, an increased capacitance. Taylor et al. reinforced this claim by studying composite systems containing unsized graphite fiber in an epoxy matrix via EIS on a specimen that had been subjected to 90°C temperatures.[97] The 90°C environment was maintained until the samples were removed and then immediately measured with EIS. Thermal coefficients of expansion differences between the fiber and matrix caused delaminations and voids which caused an increase in the measured capacitance. Lastly, Glass et al. correlated the values of capacitance to the shear strengths of these composites as observed in Figure 1.10.[93]

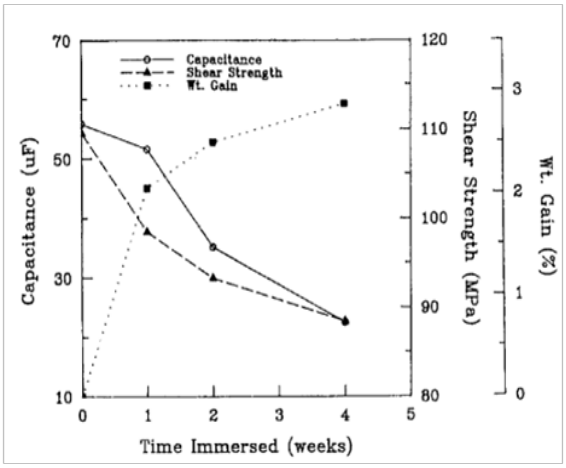


**Figure 1.10 - Relationship between capacitance, shear strength, and weight gain of samples immersed in 90°C distilled water**

**[Reproduced with kind permission from Springer Science+Business Media: Journal of Nondestructive Evaluation, Electrochemical impedance spectroscopy as a method to nondestructively monitor simulated in -service damage in a carbon fiber reinforced plastic, 6, 1987, 187, R. Glass, S. Taylor, G. Cahen, Jr., and G. Stoner, Figure 8.]**

The results displayed a positive correlation between capacitance and shear strength. An increase in water uptake further supports the postulation that with fiber breakage, from the polymeric swelling, decreased mechanical properties can be observed. This work was an initial contribution in the area of correlating the mechanical properties with circuit modeled elements.

Taylor et al. investigated the use of a solution containing hydroxyl ($OH^-$) ions as the hydroxyl ion is the anion which is believed to cause delaminations in bismaleimide matrix/graphite fiber composites.[98] Sodium hydroxide solutions, in various concentrations, were used as the source of the hydroxyl ions which are believed to be produced during cathodic polarization of PMCs. The results from the solution immersed samples did not demonstrate similar trends compared to the results obtained during the cathodic overpotentials applied in the same study. The Bode phase plots of the sodium hydroxide solution did not exhibit the same behavior of a "porous electrode" which is formed when delaminations occur along the fiber edge to create a crevice over the exposure time. The porous electrode effect was observed at the fiber/matrix interface within the bulk of the PMC. However, the only noticeable change from the dissolution of bismaleimide was observed at the surface of the PMC. This observation led to a further investigation as to which species were causing the delamination of the fiber from matrix when overpotentials were imposed upon the sample.

It has been observed, repeatedly, that carbon/graphite cross woven with glass fibers in polymer matrices display significant blistering at the surface when attached to anodic metals.[99-100] Literature states the blister formation is from evolved species at the carbon fiber/polymer matrix interface as cathodic overpotentials are induced and an

electrochemical process occurs. Circuit modeling was utilized by Kaushik and colleagues to investigate the effects of cathodic overpotentials on carbon and glass fiber weaves in a vinyl ester matrix.[101] Voltages of 0 volts, -0.65 volts, and -1.20 volts (versus saturated calomel electrode (SCE)) for various exposure times were applied. The model used to determine the circuit constituents was initially used by Mansfeld and Kendig of coated metals displaying corrosion initiation.[102-103] This circuitry displays two time constants, or two resistor-capacitor (RC) circuits in parallel, which includes a solution resistance, $R_s$, "coating" capacitance, $C_c$, pore resistance, $R_{po}$, a charge transfer resistance, $R_{ct}$, and a double layer capacitor, $C_{dl}$. Figure 1.11 reveals the commonly used circuit model utilized in this study.

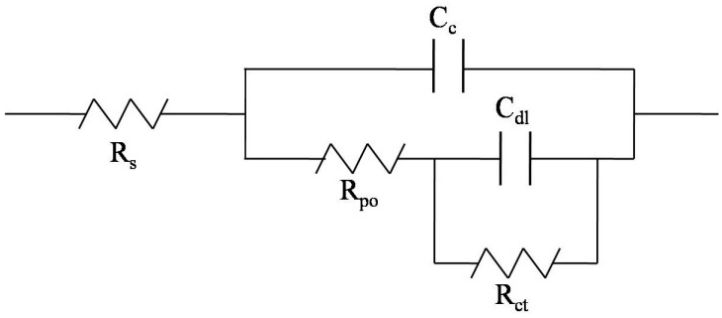


**Figure 1.11 – Two time constant circuitry utilized for circuit modeling**

Similarly, a constant phase element (CPE) can also be used for substitution of the capacitors as CPEs are thought of as "leaky" capacitors where the response is not entirely in a capacitive fashion. The pore resistance was of most importance when studying the blister formation as electrolyte penetration would be more pronounced with time. The results founded by Kaushik suggest that the blister formation does indeed occur at the fiber/matrix interface and migrates toward a surface. The results were visually confirmed by utilizing SEM to investigate the fiber/matrix interface. EIS results also exhibited a decrease in the pore resistance which results from the easier electron and ion paths between

the fiber (working electrode) and counter electrode. The pH, in the blisters, increased from the formation of hydroxyl ions which was the proposed degradation species created from cathodic overpotentials. As mentioned earlier, Taylor et al. believed hydroxyl ions were not the key ion or radical creating the delaminations and void creation at the fiber/matrix interface.[98]

Alias and Brown studied the topic of cathodic overpotentials on carbon and glass woven fiber/vinyl ester matrix and epoxy matrix in a similar fashion to the aforementioned work by Kaushik and colleagues.[104-105] Vinyl ester matrix composites displayed the formation of blisters and a black product on the composite surface while the epoxy matrix displayed a white deposit formed on the surface. From the circuit modeling results, it was observed that the pore resistance was negligible as the values approached zero which suggests that a "short circuit" was present. This can be caused when macro voids are present which was only the case with the epoxy based composites at cathodic potentials of -300 millivolt (versus SCE) or more negative. On the other hand, when the potentials were more positive than -300 millivolt (versus SCE), the pore resistance was still measurable and was greater in the epoxy composites than the vinyl ester composites. Both electrochemical impedance and visual assessment of these composites displayed greater damage to the structure with an increase in the cathodic potential applied. The impedance results displayed a decrease in magnitude with increasing exposure time. Phase angle shifts to lower frequencies were also observed with increasing exposure time. This work suggested that the hydrogen evolution was occurring at -1200 millivolt (versus SCE) which was the degradation species, but another hypothesis stated the possible direct reduction of the polymer matrix due to the high magnitude potentials.

Taylor's published research in 1994 sought to determine the damage instituted by cathodic overpotentials via a "crevice" geometry calculation to determine the area of delamination of the electrode (graphite fiber) from the matrix.[106] The derivation of this electrode geometry was initially proposed by de Levie to monitor surface roughening of electrodes over exposure to scratches during fast electrochemical measurements.[6] However, Taylor's derivation noticed that the only constituent required to monitor this effect was the phase angle at low frequencies in EIS experimentation. This discovery was unique as phase angle is a quantity that is independent of electrode size and area unlike traditional impedance magnitude, but could be used to determine crevice width and depth. The experimentation was conducted on composites consisting of a bismaleimide matrix and unidirectional graphite fiber. Three electrodes were again used in this study with a graphite fiber acting as the working electrode and the electrolyte was a 3.5% (weight percent) sodium chloride solution. One distinct advantage of having graphite as the working electrode is its non-Faradaic region near the open circuit potential which creates more accuracy in the measurement. Also, the polymeric matrix causes the main constituent of the impedance to be derived from the double layer capacitance formed from electrolyte solution penetration which was an assumption of the electrode geometry to monitor crevice width and depth. The degradation was accomplished by subjecting the samples to cathodic potentials of -1.2 volt, -1.4 volt, and -1.73 volt (versus SCE) for varying amounts of time. It should be mentioned that these potentials were not maintained during EIS experimentation as that would be far away from the open circuit potential which is needed for steady-state measurements. Figure 1.12 displays the depth of penetration for the three cathodic potentials for various exposure times.[98]

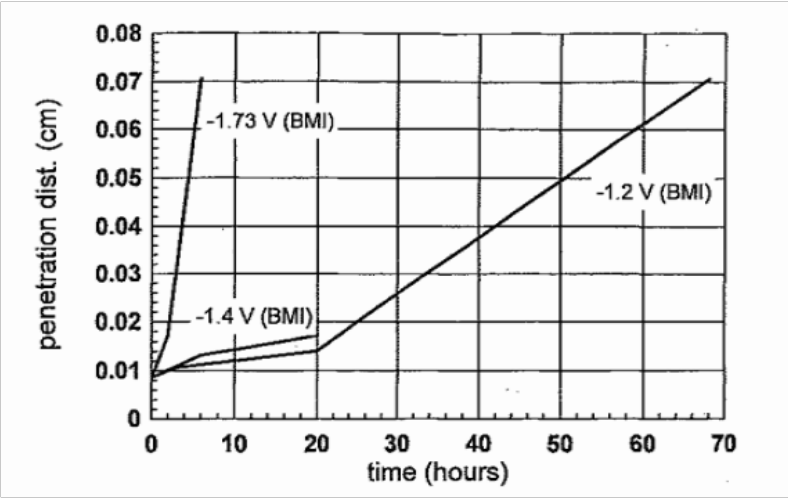


**Figure 1.12 - Penetration depth of delaminations as calculated by the EIS phase angle data for three cathodic potentials**

**[Reproduced by permission of The Electrochemical Society: Journal of The Electrochemical Society, The detection and analysis of electrochemical damage in bismaleimide/graphite fiber composites, 143, 1996, 451, S. Taylor, F. Wall, and G. Cahen, Jr., Figure 5.]**

The depth of penetration calculation had many assumptions which were not necessarily met during experimentation. For instance, the opening of the crevice (i.e., distance from the fiber edge to the surface of polymer) was held constant even though it was expected to change over time from the delamination effect. The double layer capacitance was approximated from the suggested values of the basal plane of graphite and crystal edges, but these values from the actual configuration were not calculated during this study. Even with the assumptions made, the extrapolated data correlated well with composite samples coupled to magnesium in seawater. This was promising as the crevice geometry of delamination could be very beneficial in understanding mechanical damage over exposure time in service conditions where coupling to a metal was present.

This work was continued by Taylor et al. in work published in 1996.[98] Bismaleimide matrix/graphite fiber composites were studied with the same setup and potentials mentioned in the 1994 work. In this research, a closer investigation of the phase

angle was proposed as not only could the depth of delamination be determined, but with shifts in the phase angle, other interfacial characteristics could be explored. The results revealed that with an increasing cathodic potential the corresponding changes in the phase angle were more pronounced. It was determined, by potentiodynamic polarization, that both the -1.2 volts and -1.4 volts (versus SCE) applied voltages should be limited by diffusion processes, but it was observed in the results for -1.4 volts a larger change in the phase angle was measured. This was not expected as the imposed voltages in both cases were of the same magnitude, therefore the reactions and evolved species should be the same or very similar. Smaller overpotentials were applied and investigated for their effect on the phase angle and other EIS data. Potentials of 0 volts to -100 millivolts (versus SCE) demonstrated the phenomenon was not observed at the other potentials, but once the potential was change in the range of -200 millivolts to -300 millivolts, the capacitance values increased as expected. The inhomogeneity of the samples and a constant assumed open circuit potential was the suggested reason for the discrepancies in the low potentials. The discrepancies could also be accounted for by the slight reduction of certain functional groups at these low potentials. The reduction of functional groups can possibly produce electrostatic debonding at the fiber/matrix interface. The major contribution from this work came from a proposed degradation species present when the composites were subjected to the overpotentials. As mentioned previously, the hydroxyl ion did not produce the same type or extent of degradation, when applied as a solution, as that of cathodic overpotentials. This was further reinforced by curvature observed in the low frequency phase angles. The new proposed species were peroxide, superoxide radicals, and potentially hydroperoxyl radicals. Cleavage of the carbon-carbon bonds, along with

various other mechanisms, to produce the aforementioned species has been well documented from the breakdown of polymer matrices.[107-109] The species were not chemically determined within this study, but it was assumed that the type of degradation species would vary from polymer to polymer.

Anodic overpotentials were also studied by Taylor et al. in the work mentioned previously.[98] The instance where a graphite fiber would be subjected to an anodic overpotential is very rare in an industrial sense as graphite is one of the noblest materials used today. However, stray currents could produce this type of potential which was why a large over potential of +1.5 volts (versus SCE) was applied to the composites for a 20 hour duration. After exposure, EIS was performed in the traditional three electrode technique. The results displayed a decrease in the magnitude of impedance, a shift in the capacitive regions toward lower frequencies, but no significant changes were observed in the phase angle peak. This did not lead to noticeable changes in the delamination effects. Also, the impedance magnitude decreased with time which was explained by the solution ingression which was not accompanied by a delamination.

Galvanic coupling of two conductive materials is similar in nature to cathodic overpotentials but more typically found in industrial settings. Taylor studied graphite fiber composites galvanically coupled to a more active metal in the presence of an electrolyte.[98] Coupling of the bismaleimide matrix/graphite fiber composites to aluminum, steel, copper, and titanium was performed and the EIS behavior monitored over exposure time. The results obtained during this study were similar, but not identical, to that of what was observed during the cathodic overpotential study. A decrease in the impedance magnitude, phase angle depression, and slope of the Nyquist plot decreasing

were all commonly observed during the cathodic overpotential study but not to the same extent for all samples. As expected, the change in impedance magnitude correlated with the difference in electrochemical potentials of the composite and metal. In this study, the aluminum coupled composites displayed the most damage. Aluminum has a potential of -0.81 volts (versus SCE), low carbon steel has a potential of -0.70 volts (versus SCE), copper has a potential of -0.20 volts (versus SCE), and lastly titanium has a potential of -0.05 volts (versus SCE) in a saltwater solution which was very similar to the sodium chloride solution used during this experimentation.[110] The porous electrode effect, or crevice geometry, calculations were most pronounced in the aluminum as the assumed peroxide radicals were being formed more readily to cause more degradation reactions.

Delaminations caused by microbial attack of the matrix material, at the interface of the matrix and fiber, is the last mode of delamination studied. Gu studied the extent of microbial growth at the interface of carbon fiber composites as microbe growth is known to occur at additive (i.e., sizings, plasticizers, flame retardant, etc.) sites within PMCs as supported by SEM.[111] It was hypothesized that EIS would be the proper experimental method to determine the growth of the microbes at the consequence of the graphite fiber/matrix interface leading to delamination.[112-113] Graphite cross woven with glass fibers was impregnated with an epoxy matrix to produce a PMC that was inoculated with a fungal mixture. The consortium of fungi was then allowed to incubate for a period of 179 days and characterization via EIS and SEM was performed. EIS results revealed that the impedance magnitude decreased from values collected from non-microbe administered samples. In fact, the impedance increased slightly in the non-microbe containing samples but then stabilized. The impedance data suggested a decrease in both the real and

imaginary portions of the impedance. Real impedance is the resistive elements where the decrease in the real portion being attributed to the pore formation and expansion with increased microbe deterioration. The capacitive elements account for the imaginary portion of the impedance which can be accounted for with an increased electrode area from electrical bridging between newly exposed fibers. Both of these results were visually verified with the investigation of scanning electron micrographs.

*1.5.2 Investigation of Non-Conductive PMCs via EIS*

Non-conductive fiber in a non-conductive matrix is a completely insulative material which cannot have EIS experimentation conducted upon it in the traditional three electrode fashion. This has led to very little investigation of this class of composite in an electrochemical sense. However, non-conductive fiber usage is at the forefront of research due to the exceptional properties which rival and exceed the properties present within carbon and graphite fibers. One fiber type that is inexpensive and has been engineered to perform in specialized ways, depending upon its composition, is glass fiber. The emergence of S Glass®, M Glass® and C Glass® ,from the traditional E Glass®, display increases in many properties ranging from strength to chemical resistance.[114] Therefore, a quantitative methodology for determining the extent of damage is needed and has been investigated by EIS in a very limited fashion. The typical setup is a two electrode configuration which was displayed in Figure 1.1. Again, this setup leads to the reference acting as a quasi-reference without comparison to a standard reference electrode.

Fazzino et al. used this form of EIS methodology to investigate the effects of fatigue cycles on the impedance data.[115-116] The composite of interest was a halogenated epoxy matrix/E Glass® which was subjected to cyclic compression where

voids and delaminations were expected to occur. First, the effects of immersion and drying were studied to determine the overall influence on the impedance characteristics. After 48 hours of immersion and drying, the initial circuitry was observed to contain both resistive and capacitive effects. Once the sample was sufficiently dried, a capacitive dominated circuitry transpired. This is expected behavior as a completely non-conductive media (i.e., composite) sandwiched between two conductive plates should behave in a predominantly capacitive nature. Wet samples have solution ingression in pre-existing voids, which are inherent in composites, creating resistive pathways. It was also determined that higher concentrations of the sodium chloride solution decreased the impedance as easier electron and ion movement is possible with more chlorine anions present. After initial studies, the samples were then fatigued and the EIS spectra monitored. As the fatigue cycles increased, it was found that the impedance correspondingly decreased due to increased absorption of the three molar sodium chloride solution which created shorter resistive pathways from increased penetration of the electrolyte. Interestingly, even though small amounts of damage, only 20% of the needed cycles to failure, were administered to the sample, visual assessment displayed no noticeable damage while EIS detected drastic changes in the impedance.

Fazzino et al. also investigated the dependence of the fatigue direction with respect to the fiber alignment. Composites were produced using a stacked plain weave 0° and 90° (with respect to the warp fiber direction) orientation to obtain a thickness of one millimeter. Composite samples where then cut at 0°, 90°, and 45° for examination. As expected, the 0° and 90° cut samples revealed similar results as a plain weave exhibits isotropic characteristics in both the weft and warp fiber directions. The 45° cut specimen displayed

drastically different qualities compared to 0° and 90° cut samples. For instance, the low frequency impedance was lower in the 45° cut sample by two orders of magnitude and the high frequency impedance was changed in the 45° sample, but remained unchanged in the 0° and 90° specimens. These effects can be attributed to the 45° sample having matrix driven degradation causing significantly more voids and microcracking than the other configurations. As mentioned, lower impedance insinuates further electrolyte penetration with more hydration sites for easier electron and ion flow. The large shift in high frequency impedance suggests that not only were the resistive qualities changing but also the capacitive properties were modified. Further examination found that relationships were present between the impedance spectra, area of damage, strain to break, and the fraction of fatigue life conducted. The impedance magnitude at 1000 Hertz and the initial slope of the Nyquist plot correlated with the mechanical strain at break after normalizing these values to their initial value. This was very important because it proves the mechanical behavior of a non-conductive composite could be predicted based on EIS results.

**1.6 Conclusions**

PMCs exhibit low density and high strength which is why this class of material is becoming more acceptable for use in high-profile applications in many sectors. One of the major drawbacks is that these materials undergo degradation reactions in the environment where they are utilized. UV exposure is present in all areas of the world and it can cause significant damage to PMCs if allowed to degrade for extended periods of time. Therefore, EIS is proposed to be a quantitative methodology suitable for non-destructive evaluation of polymeric composites which have undergone various degradation mechanisms. This method provides quick measurements, repeatable results, and quantitative data leading to a

better understanding of correlation to other mechanical, thermal, and electrical properties of the composite. Several EIS studies have been performed in the area of conductive fiber composites which can monitor delamination progression from a variety of stimuli. However, literature available in the realm of non-conducting PMCs is scarce, but the literature in existence demonstrates that EIS results correlated with mechanical properties.

### 1.7 References


1. Strong, A., *Fundamentals of composites manufacturing: materials, methods and applications*. 2nd ed. 2008, Dearborn, MI: Society of Manufacturing Engineers.
2. Agarwal, B., L. Broutman, and K. Chandrashekhara, *Analysis and performance of fiber composites*. 3rd Edition ed. 2006, New York, NY: Wiley.
3. Wicks Jr., Z., *Organic coatings: science and technology*. 3rd Edition ed. 2007, New York, NY: Wiley-Interscience.
4. Lee, S., *Handbook of composite reinforcements*. 1992, New York, NY: Wiley-VCH.
5. Mansfeld, F., *Electrochemical impedance spectroscopy (EIS) as a new tool for investigating methods of corrosion protection.* Electrochimica Acta, 1990. **35**(10): p. 1533-1544.
6. De Levie, R., *The influence of surface roughness of solid electrodes on electrochemical measurements.* Electrochimica Acta, 1965. **10**(2): p. 113-130.
7. Watson, J. *Preliminary design development AV-8B forward fuselage composite structure*. in *Fourth Conference on Fibrous Composites in Structural Design*. 1978. San Diego, CA, USA: Plenum Press.
8. Pilato, L. and M. Michno, *Advanced composite materials*. 1994: Springer-Verlag.
9. Brosius, D., *Boeing 787 update.* Composites World, 2007. **May 2007**.
10. GangaRao, H., N. Taly, and P. Vijay, *Reinforced concrete design with FRP composites*. 2006, Boca Raton, FL: CRC.
11. Dolan, C., S. Rizkalla, and A. Nanni, eds. *Fourth International Symposium: Fiber Reinforced Polymer Reinforcement for Reinforced Concrete Structures*. 1999, ACI International: Farmington Hills, MI.
12. Buyukozturk, O. and B. Hearing, *Failure behavior of precracked concrete beams retrofitted with FRP*. Journal of Composites for Construction, 1998. **2**(3): p. 138-144.
13. Lau, K., L. Zhou, P. Tse, and L. Yuan, *Applications of composites, optical fibre sensors and smart composites for concrete rehabilitation: an overview.* Applied Composite Materials, 2002. **9**(4): p. 221-247.
14. Tang, B. and W. Podolny, *A successful beginning for fiber reinforced polymer (FRP) composite materials in bridge applications.* FHWA Proceedings, 1998.
15. Zaera, R., *Ballistic Impacts on Polymer Matrix Composites, Composite Armor, Personal Armor.* Impact Engineering of Composite Structures, 2011: p. 305-403.
16. Jacobs, M. and J. Van Dingenen, *Ballistic protection mechanisms in personal*

*armour*. Journal of Material Science, 2001. **36**(13): p. 3137-3142.
17. Strong, A., *Plastics: materials and processing*. 3rd Edition ed. 2000: Prentice Hall.
18. Gutowski, T., *Advanced composites manufacturing*. 1997: Wiley New York.
19. Abraham, D., S. Matthews, and R. McIlhagger, *A comparison of physical properties of glass fibre epoxy composites produced by wet lay-up with autoclave consolidation and resin transfer moulding.* Composites Part A, 1998. **29**(7): p. 795-801.
20. Brandt, J., K. Drechsler, and F. Arendts, *Mechanical performance of composites based on various three-dimensional woven-fibre preforms.* Composite Science and Technology, 1996. **56**(3): p. 381-386.
21. Pospíšil, J. and S. Nešpurek, *Photostabilization of coatings. Mechanisms and performance.* Progress in Polymer Science, 2000. **25**(9): p. 1261-1335.
22. Day, R., *The role of titanium dioxide pigments in the degradation and stabilisation of polymers in the plastics industry.* Polymer Degradation and Stability, 1990. **29**(1): p. 73-92.
23. Pritchard, G., *Reinforced plastics durability*. 1999, Boca Raton, FL: CRC Press LLC.
24. Bank, L., T. Gentry, and A. Barkatt, *Accelerated test methods to determine the long-term behavior of FRP composite structures: environmental effects.* Journal of Reinforced Plastics and Composites, 1995. **14**(6): p. 559.
25. Pillay, S., U.K. Vaidya, and G.M. Janowski, *Effects of moisture and UV exposure on liquid molded carbon fabric reinforced nylon 6 composite laminates.* Composite Science and Technology, 2009. **69**(6): p. 839-846.
26. Shokrieh, M. and A. Bayat, *Effects of ultraviolet radiation on mechanical properties of glass/polyester composites.* Journal of Composite Materials, 2007. **41**(20): p. 2443.
27. Falk, R., C. Felton, and T. Lundin. *Effects of weathering on color loss of natural fiber thermoplastic composites*. in *3rd International Symposium on Natural Polymers and Composites*. 2001. Sao Pedro, Brazil: ISNaPol.
28. Kumar, B., R. Singh, and T. Nakamura, *Degradation of carbon fiber-reinforced epoxy composites by ultraviolet radiation and condensation.* Journal of Composite Materials, 2002. **36**(24): p. 2713.
29. Hammami, A. and N. Al Ghuilani, *Durability and environmental degradation of glass vinylester composites.* Polymer Composites, 2004. **25**(6): p. 609-616.
30. Pimentel Real, L., A. Ferraria, and A. Botelho do Rego, *The influence of weathering conditions on the properties of poly (vinyl chloride) for outdoor applications. An analytical study using surface analysis techniques.* Polymer testing, 2007. **26**(1): p. 77-87.
31. Ito, M. and K. Nagai, *Evaluation of degradation on Nylon 6 and Nylon 6/montmorillonite nanocomposite by color measurement.* Journal of Applied Polymer Science, 2008. **108**(6): p. 3487-3494.
32. Boyle, D. and B. Gesner, *Aging of polyblends.* Journal of Applied Polymer Science, 1968. **12**(5): p. 1193-1197.
33. Berns, R., *Billmeyer and Saltzman's Principles of Color Technology*. 3rd Edition ed. 2000, New York, NY: Wiley
34. Carlson, N., L. Blackwood, L. Torres, J. Rodriguez, and T. Yoder. *Accelerated*

*aging of polymer composite bridge materials*. in *6th International Symposium on Smart Structures and Materials*. 1999. Newport Beach, CA.
35. Wypych, G., *Handbook of material weathering*. 3rd. Edition ed. 2003, New York, NY: William Andrew Inc.
36. Ahmad Thirmizir, M., Z. Mohd Ishak, R. Mat Taib, S. Rahim, and S. Mohamad Jani, *Natural Weathering of Kenaf Bast Fibre-Filled Poly (Butylene Succinate) Composites: Effect of Fibre Loading and Compatibiliser Addition.* Journal of Polymers and the Environment, 2001: p. 1-11.
37. Yew, G., W. Chow, Z. Mohd Ishak, and A. Mohd Yusof, *Natural weathering of poly (Lactic Acid): Effects of rice starch and epoxidized natural rubber.* Journal of Elastomers and Plastics, 2009. **41**(4): p. 369.
38. Correia, J., S. Cabral-Fonseca, F. Branco, J. Ferreira, M. Eusebio, and M. Rodrigues, *Durability of pultruded glass-fiber-reinforced polyester profiles for structural applications.* Mechanics of Composite Materials, 2006. **42**(4): p. 325-338.
39. Toporets, A., *Specular reflection from a rough surface.* Optics and spectroscopy, 1964. **16**: p. 102-111.
40. Aldajah, S., A. Al-omari, and A. Biddah, *Accelerated weathering effects on the mechanical and surface properties of CFRP composites.* Materials and Design, 2009. **30**(3): p. 833-837.
41. Mouzakis, D., H. Zoga, and C. Galiotis, *Accelerated environmental ageing study of polyester/glass fiber reinforced composites (GFRPCs).* Composites Part B: Engineering, 2008. **39**(3): p. 467-475.
42. Huang, G., *Degradation of glass fibre/polyester composites after ultraviolet radiation.* Materials and Design, 2008. **29**(7): p. 1476-1479.
43. Paillous, A. and C. Pailler, *Degradation of multiply polymer-matrix composites induced by space environment.* Composites, 1994. **25**(4): p. 287-295.
44. Joseph, P., M. Rabello, L. Mattoso, K. Joseph, and S. Thomas, *Environmental effects on the degradation behaviour of sisal fibre reinforced polypropylene composites.* Composite Science and Technology, 2002. **62**(10-11): p. 1357-1372.
45. Liau, W. and F. Tseng, *The effect of long term ultraviolet light irradiation on polymer matrix composites.* Polymer Composites, 1998. **19**(4): p. 440-445.
46. Rabello, M., R. Tocchetto, L. Barros, J. DAlmeida, and J. White, *Weathering of polypropylene composites containing weldlines.* Plastics, rubber and composites, 2001. **30**(3): p. 132-140.
47. O'Donnell, B. and J. White, *Stress-accelerated photo-oxidation of polypropylene and glass-fibre-reinforced polypropylene.* Polymer Degradation and Stability, 1994. **44**(2): p. 211-222.
48. Lundin, T., S. Cramer, R. Falk, and C. Felton, *Accelerated weathering of natural fiber-filled polyethylene composites.* Journal of Materials in Civil Engineering, 2004. **16**: p. 547.
49. Lundin, T., R. Falk, and C. Felton. *Accelerated weathering of natural fiber-thermoplastic composites: effects of ultraviolet exposure on bending strength and stiffness*. in *6th Internation Conference on Woodfiber-Plastic Composites*. 2001. Madison, WI.
50. Lee, B. and D. Lee, *Surface degradation properties of ultraviolet treated*

*epoxy/glass fiber.* Dielectrics and Electrical Insulation, IEEE Transactions on, 1999. **6**(6): p. 907-912.
51. Khan, R., M. Khan, A. Khan, and M. Hossain, *Effect of gamma radiation on the performance of jute fabrics-reinforced polypropylene composites.* Radiation Physics and Chemistry, 2009. **78**(11): p. 986-993.
52. Micelli, F. and A. Nanni, *Durability of FRP rods for concrete structures.* Construction and Building materials, 2004. **18**(7): p. 491-503.
53. Chin, J., T. Nguyen, and K. Aouadl, *Effects of environmental exposure on fiber-reinforced plastic (FRP) materials used in construction.* Journal of Composites Technology and Research, 1997. **19**: p. 205-213.
54. Sharma, S., M. Krishna, and H. Narasimhamurthy, *Studies on the weathering behavior of glass coir polypropylene composites.* Journal of Reinforced Plastics and Composites, 2006. **25**(9): p. 925.
55. Bakar, A., A. Hassan, and A. Yusof, *Effect of accelerated weathering on the mechanical properties of oil palm empty fruit bunch filled UPVC composites.* Iranian Polymer Journal, 2005. **14**(7): p. 627-635.
56. Singh, B., M. Gupta, and A. Verma, *The durability of jute fibre-reinforced phenolic composites.* Composite Science and Technology, 2000. **60**(4): p. 581-589.
57. Roylance, D. and M. Roylance, *Weathering of fiber reinforced epoxy composites.* Polymer Engineering & Science, 1978. **18**(4): p. 249-254.
58. George, P. and H. Dursch, *Low earth orbit effects on organic composites flown on the long duration exposure facility.* Journal of advanced materials, 1994. **25**(3): p. 10-19.
59. Han, J. and C. Kim, *Low earth orbit space environment simulation and its effects on graphite/epoxy composites.* Composite Structures, 2006. **72**(2): p. 218-226.
60. Monney, L., C. Dubois, D. Perreux, A. Burtheret, and A. Chambaudet, *Mechanical behaviour of an epoxy-glass composite under photo-oxidation.* Polymer Degradation and Stability, 1999. **63**(2): p. 219-224.
61. Sookay, N., C. Von Klemperer, and V. Verijenko, *Environmental testing of advanced epoxy composites.* Composite Structures, 2003. **62**(3-4): p. 429-433.
62. Abu-Sharkh, B. and H. Hamid, *Degradation study of date palm fibre/polypropylene composites in natural and artificial weathering: mechanical and thermal analysis* 1.* Polymer Degradation and Stability, 2004. **85**(3): p. 967-973.
63. Shubhra, Q., M. Saha, A. Alam, M. Beg, and M. Khan, *Effect of matrix modification by natural rubber on the performance of silk-reinforced polypropylene composites.* Journal of Reinforced Plastics and Composites, 2010. **29**(22): p. 3338.
64. Shubhra, Q., A. Alam, M. Beg, M. Khan, and M. Gafur, *Mechanical and degradation characteristics of natural silk and synthetic phosphate glass fiber reinforced polypropylene composites.* Journal of Composite Materials, 2011. **45**(12): p. 1305.
65. Jana, S. and W. Zhong, *Effects of Hygrothermal Conditions and UV Radiation on UHMWPE Fibers/Nanofiber—Epoxy Composites.* Journal of Composite Materials, 2007. **41**(24): p. 2897.
66. Segovia, F., C. Ferrer, M. Salvador, and V. Amigo, *Influence of processing variables on mechanical characteristics of sunlight aged polyester-glass fibre composites.* Polymer Degradation and Stability, 2000. **71**(1): p. 179-184.

67. Chevali, V., D. Dean, and G. Janowski, *Effect of environmental weathering on flexural creep behavior of long fiber-reinforced thermoplastic composites.* Polymer Degradation and Stability, 2010.
68. Summerscales, J., *Non-destructive testing of fibre-reinforced plastics composites*. 1987, New York, NY: Springer.
69. Avdelidis, N., B. Hawtin, and D. Almond, *Transient thermography in the assessment of defects of aircraft composites.* NDT & E International, 2003. **36**(6): p. 433-439.
70. Bates, D., G. Smith, D. Lu, and J. Hewitt, *Rapid thermal non-destructive testing of aircraft components.* Composites Part B: Engineering, 2000. **31**(3): p. 175-185.
71. Reynolds, W., *Inspection of laminates and adhesive bonds by pulse-video thermography.* NDT International, 1988. **21**(4): p. 229-232.
72. Meola, C., G. Carlomagno, and L. Giorleo, *Geometrical limitations to detection of defects in composites by means of infrared thermography.* Journal of Nondestructive Evaluation, 2004. **23**(4): p. 125-132.
73. de Groot, P., P. Wijnen, and R. Janssen, *Real-time frequency determination of acoustic emission for different fracture mechanisms in carbon/epoxy composites.* Composite Science and Technology, 1995. **55**(4): p. 405-412.
74. Prosser, W., K. Jackson, S. Kellas, B. Smith, J. McKeon, and A. Friedman, *Advanced waveform-based acoustic emission detection of matrix cracking in composites.* Materials evaluation, 1995. **53**(9): p. 1052-1058.
75. Grandia, W. and C. Fortunko. *NDE applications of air-coupled ultrasonic transducers*. in *Ultrasonics Symposium*. 1995. Seattle, Wa: IEEE.
76. Rogovsky, A., *Development and application of ultrasonic dry-contact and air-contact C-scan systems for nondestructive evaluation of aerospace composites.* Materials evaluation, 1991. **49**(12): p. 1491-1497.
77. Imielińska, K., M. Castaings, R. Wojtyra, J. Haras, E. Clezio, and B. Hosten, *Air-coupled ultrasonic C-scan technique in impact response testing of carbon fibre and hybrid: glass, carbon and Kevlar/epoxy composites.* Journal of Materials Processing Technology, 2004. **157-158**(0): p. 513-522.
78. Mouritz, A., C. Townsend, and M. Shah Khan, *Non-destructive detection of fatigue damage in thick composites by pulse-echo ultrasonics.* Composite Science and Technology, 2000. **60**(1): p. 23-32.
79. Schuster, J. and K. Friedrich, *Fatigue testing of thermoformed bidirectional LDF™-composites.* Applied Composite Materials, 1994. **1**(1): p. 55-68.
80. Shoup, T., J. Miller, J. Heyman, and W. Illg. *Ultrasonic Characterization of Fatigue and Impact Damage in Graphite Epoxy Composite Laminates*. in *Ultrasonics Symposium*. 1982. San Diego, Ca: IEEE.
81. Stock, S., *X-ray microtomography of materials.* International Materials Reviews, 1999. **44**(4): p. 141-164.
82. Awaja, F., M. Nguyen, S. Zhang, and B. Arhatari, *The investigation of inner structural damage of UV and heat degraded polymer composites using X-ray micro CT.* Composites Part A: Applied Science and Manufacturing, 2010.
83. Baidya, K., S. Ramakrishna, M. Rahman, and A. Ritchie, *Quantitative radiographic analysis of fiber reinforced polymer composites.* Journal of Biomaterials Applications, 2001. **15**(3): p. 279.

84. Little, J., H. Nagasawa, T. Pfenning, and H. Vetrovs, *Radiation-induced genomic instability: Delayed mutagenic and cytogenetic effects of X rays and alpha particles.* Radiation Research, 1997. **148**(4): p. 299-307.
85. Amirudin, A. and D. Thieny, *Application of electrochemical impedance spectroscopy to study the degradation of polymer-coated metals.* Progress in Organic Coatings, 1995. **26**(1): p. 1-28.
86. Scully, J., D. Silverman, and M. Kendig, *Electrochemical impedance: analysis and interpretation*. 1993, West Conshohocken, PA: ASTM International.
87. Lavaert, V., M. De Cock, M. Moors, and E. Wettinck, *Influence of pores on the quality of a silicon polyester coated galvanised steel system.* Progress In Organic Coatings, 2000. **38**(3-4): p. 213-221.
88. Qi, X., *Organic Coatings for Corrosion Protection. Thesis.* North Dakota State Universtiy, Coatings and Polymeric Materials, 2009.
89. Davis, G., M. Rich, and L. Drzal, *Monitoring Moisture Uptake and Delamination in CFRP-Reinforced Concrete Structures with Electrochemical Impedance Sensors.* Journal of Nondestructive Evaluation, 2004. **23**(1): p. 1-9.
90. Hong, S., R. Harichandran, and F. Pe, *Sensors to monitor CFRP/concrete bond in beams using electrochemical impedance spectroscopy.* Journal of Composites for Construction, 2005. **9**: p. 515.
91. Kim, S., C. In, K. Cronin, H. Sohn, and K. Harries, *Reference-Free NDT Technique for Debonding Detection in CFRP-Strengthened RC Structures.* Journal of Structural Engineering, 2007. **133**(8): p. 1080-1091.
92. Kelly, A. and C. Zweben, *Comprehensive composite materials: Volume 2 Polymer Matrix Composites*. 2000, Oxford, UK: Elsevier.
93. Glass, R., S. Taylor, G. Cahen, and G. Stoner, *Electrochemical impedance spectroscopy as a method to nondestructively monitor simulated in-service damage in a carbon fiber reinforced plastic.* Journal of Nondestructive Evaluation, 1987. **6**(4): p. 181-188.
94. Callinan, R., *Environmental Effects on the Static and Fatigue Strength of Graphite/Epoxy Structures.* A.D.o. Defense, Austrailian Aeronautical Research Labs. Melbourne, Australia, AD-A170 927. 1985.
95. Lide, D., *Handbook of chemistry and physics*. 84th Edition ed. 2003: CRC Press LLC.
96. Iglesias, T. and J. Peón Fernández, *A new approach for prediction of the permittivity of mixtures.* The Journal of Chemical Thermodynamics, 2001. **33**(10): p. 1375-1381.
97. Taylor, S., L. Melvin, T. Mangiacapre, G. Cahen Jr., and G. Stoner, *Non-Destructive Method for Environmental Breakdown of Graphite Fiber Reinforced Polymer Composites.* U.S.A.R. Office, University of Virginia. AD-A223 729. 1990.
98. Taylor, S., F. Wall, and G. Cahen Jr, *The detection and analysis of electrochemical damage in bismaleimide/graphite fiber composites.* Journal of The Electrochemical Society, 1996. **143**(2): p. 449-458.
99. Tucker, W., R. Brown, and L. Russell, *Corrosion between a graphite/polymer composite and metals.* Journal of Composite Materials, 1990. **24**(1): p. 92.
100. Sloan, F. and J. Talbot, *Corrosion of Graphite-Fiber-Reinforced Composites I Galvanic Coupling Damage.* Corrosion, 1992. **48**(10).

101. Kaushik, D., M. Alias, and R. Brown, *An impedance study of a carbon fiber/vinyl ester composite.* Corrosion, 1991. **47**(11): p. 859-867.
102. Mansfeld, F., M. Kendig, and S. Tsai, *Evaluation of corrosion behavior of coated metals with AC impedance measurements.* Corrosion, 1982. **38**(9): p. 478-485.
103. Kendig, M., F. Mansfeld, and S. Tsai, *Determination of the long term corrosion behavior of coated steel with AC impedance measurements.* Corrosion Science, 1983. **23**(4): p. 317-329.
104. Alias, M. and R. Brown, *Damage to composites from electrochemical processes.* Corrosion, 1992. **48**(05).
105. Alias, M. and R. Brown, *Corrosion behavior of carbon fiber composites in the marine environment.* Corrosion Science, 1993. **35**(1-4): p. 395-402.
106. Taylor, S., *A Nondestructive Electrochemical Method to Detect and Quantify Graphite Fiber/Polymer Matrix Disbondment in Aqueous and Cathodically Polarized Conditions.* Composite Interfaces, 1994. **2**(6): p. 403-217.
107. Song, J. and C. Fischer, *Thermal oxidative degradation of poly (methyl methacrylate).* Polymer Degradation and Stability, 1992. **36**(3): p. 261-266.
108. Braun, D., S. Richter, G. Hellmann, and M. Rätzsch, *Peroxy-initiated chain degradation, crosslinking, and grafting in PP-PE blends.* Journal of Applied Polymer Science, 1998. **68**(12): p. 2019-2028.
109. Cao, H., J. Yuan, R. Zhang, C. Huang, Y. He, T. Sandreczki, Y. Jean, B. Nielsen, R. Suzuki, and T. Ohdaira, *Degradation of polymer coating systems studied by positron annihilation spectroscopy. 3. Wavelength dependence of UV irradiation effect.* Macromolecules, 1999. **32**(18): p. 5925-5933.
110. Jones, D., *Principles and Prevention of Corrosion*. 2nd ed. 1992, Upper Saddle River, NJ: Prentice-Hall.
111. Gu, J., *Microbiological deterioration and degradation of synthetic polymeric materials: recent research advances.* International Biodeterioration & Biodegradation, 2003. **52**(2): p. 69-91.
112. Gu, J., A. Crasto, K. Thorp, C. Lu, and R. Mitchell, *Fungal Degradation of Fiber-Reinforced Composites Materials.* Corrosion, 1996.
113. Gu, J., C. Lu, K. Thorp, A. Crasto, and R. Mitchell, *Fiber-reinforced polymeric composites are susceptible to microbial degradation.* Journal of Industrial Microbiology & Biotechnology, 1997. **18**(6): p. 364-369.
114. Wallenberger, F. and P. Bingham, *Fiberglass and Glass Technology: Energy-friendly compositions and applications*. 2010, New York, NY: Springer Science.
115. Fazzino, P. and K. Reifsnider, *Electrochemical Impedance Spectroscopy Detection of Damage in Out of Plane Fatigued Fiber Reinforced Composite Materials.* Applied Composite Materials, 2008. **15**(3): p. 127-138.
116. Fazzino, P., K. Reifsnider, and P. Majumdar, *Impedance spectroscopy for progressive damage analysis in woven composites*. Composites Science and Technology, 2009. **69**(11-12): p. 2008-2014.

# CHAPTER 2. MATERIALS AND METHODOLOGIES

## 2.1 Materials

The materials used during this study consisted of polymer matrix composites, which were integral to the research, as well as materials used in the measurement of impedance via electrochemical impedance spectroscopy (EIS). The materials for EIS measurement consisted of ultra-pure water and a conductive gel. The conductive gel was utilized to provide a defined surface area of the electrode during EIS measurements.

### *2.1.1 Polymer Matrix Composites*

The composites studied were produced by Sioux Manufacturing Corporation of Fort Totten, North Dakota. Four different sample sizes consisting of two material systems were studied. A phenolic matrix plasticized with polyvinyl butyral (PVB) was used for all samples with either S2 Glass® fiber or Kevlar® fiber. In order to produce balanced and symmetric laminates, plain woven fiber plies were "laid up" in an alternating scheme of 0° and 90° (with respect to warp fiber or longitudinal direction) until the desired thickness was achieved. To adhere to ASTM standard D 2344, the composite specimens manufactured for determination of interlaminar shear strength had the final dimensions of 6 inches long by 2 inches wide by 1 inch thick (or 15.24 centimeters long by 5.08 centimeters wide by 2.54 centimeters thick). This thickness was accomplished with 50 fiber plies in the case of the S2 Glass® composite and 45 plies in the Kevlar® composites. The tensile properties were also investigated in accordance with ASTM D3039 with the ideal sample dimensions being 6 inches long by 0.6 inches wide by 0.06 inches thick (or 15.24 centimeters long by 1.52 centimeters wide by 0.15 centimeters thick). However, the minimal thickness along with the symmetric nature required at least three fiber plies be

used, so the thickness was altered slightly from the ideal dimension. The Kevlar® composite had a final nominal thickness of 0.087 inches (or 0.22 centimeters) while the S2 Glass® composite had a nominal thickness of 0.059 inches (0.15 centimeters).

*2.1.2 Materials for EIS Measurements*

The ultrapure water was produced from a Millipore Milli-Q® water purification system to produce water with a resistivity of 18.2 MΩ·centimeter. The conductive gel used for the EIS measurements was Spectra 360® which is produced by Parker Laboratories. This gel is designed specifically for electrode use, predominantly in the medical industry, but contains a salt which promotes both electrode health and minimal skin irritation.

**2.2 Electrochemical Impedance Spectroscopy: Principles and Circuit Modeling**

EIS is an electrochemical technique that has been used extensively in monitoring the durability of coatings in the corrosion sector. In potentiostatic EIS, a sinusoidal voltage is applied and the resulting current response is measured over a frequency range. To maintain a non-destructive nature, only a small perturbation is applied about the open circuit potential which is usually on the order of millivolts. The equation for determination of the modulus is a slight manipulation of Ohm's Law which states the direct current voltage is related to the current by the magnitude of the resistance. Equation 2.1 demonstrates this relationship with an alternating current.

$$V_{OCP} + V_{pert}\sin(\omega t) = I\sin(\omega t + \theta) \bullet Z(\omega) \qquad (2.1)$$

In Equation 2.1, $V_{OCP}$ is the open circuit potential, $V_{pert}$ is the perturbation voltage, $\omega$ is the angular frequency, $t$ is time, $I$ is the magnitude of the current, $\theta$ is the phase between current and potential response, and $Z$ is the impedance magnitude. The current responses, both in magnitude and phase, allow for a calculation of the impedance versus

frequency and phase angle versus frequency which are known as the Bode impedance and Bode phase plots, respectively. The phase between the current and voltage lead to responses both in-phase and out-of-phase over the frequency range sweep. This phenomenon leads to a complex impedance with real and imaginary parts where the overall magnitude of the impedance can be calculated from Equation 2.2.

$$|Z| = \sqrt{(Z')^2 + (Z'')^2} \qquad (2.2)$$

*Z'* denotes the real portion of the impedance and *Z''* denotes the imaginary response. In the two ideal cases, and cases most often observed in EIS literature, the ideal real impedance response is solely resistive while the ideal imaginary response is completely capacitive. Nyquist plots show the relationship between the imaginary and real portions of impedance.

The results of electrochemical impedance spectra can be modeled as a combination of resistors and capacitors in series and parallel. This process is known as circuit modeling of impedance data. Common models are used for systems and processes occurring in coating systems upon exposure. The most commonly observed model in literature for ideal coating systems, and thus composite systems, is known as a Randle's cell.[1] A diagram of the circuitry is displayed in Figure 2.1.

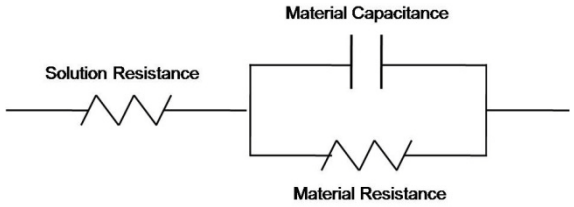


**Figure 2.1 - Randle's cell configuration of circuit elements**

The solution resistance is the inherent uncompensated resistance of the electrolyte used during EIS experimentation while the material resistance is usually a measure of pore

resistance which tends to be present even in ideal systems. Lastly, the material capacitance is attributed to the out-of-phase response between the voltage and current. The classical definition of a capacitor is the response of current between two conductive species (i.e., electrodes) separated by a non-conductive species (i.e., coating or composite). An ideal Randle's cell would display the characteristic Bode plots displayed in Figure 2.2.

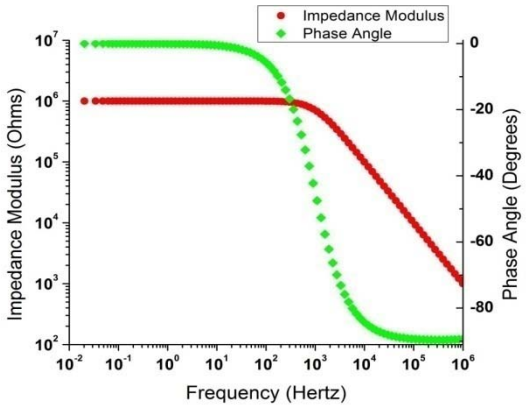


**Figure 2.2 - Ideal Randle's cell response**

It should be noted that in the mid to low frequencies, the response is completely resistive as the impedance is independent of frequency and the phase shift between voltage and current is non-existent (i.e., 0°). Conversely, the high frequency response is completely capacitive which can be observed by the -90° difference between current and voltage (i.e., voltage lags the current). By monitoring these circuit constituents over exposure time, a better understanding of which degradation mechanism is occurring may be obtained. For instance, if the pore resistance decreases, it can be assumed that either the pores are becoming larger or more numerous in quantity causing easier electron and ion mobility. Also, capacitance effects can be observed to change due to water or electrolyte penetration into the coating or composite which changes the dielectric properties with dependence on the volume fraction of each constituent present.

## 2.3 Methodologies

Several methodologies were utilized for characterization of the weathered PMCs including: EIS, surface characterization, mechanical, and ballistic experimentation. The methodology for weathering the composites will also be covered in this section.

*2.3.1 Ultraviolet Exposure Criterion*

The accelerated weathering of composite samples was conducted within a QUV Accelerated Weathering Tester manufactured by Q-Panel Lab products. The lamps utilized in this study were equipped with UVA-340 fluorescent bulbs. These bulbs emit a power spectrum displayed in Figure 2.3 which is compared with that of sunlight.[2]

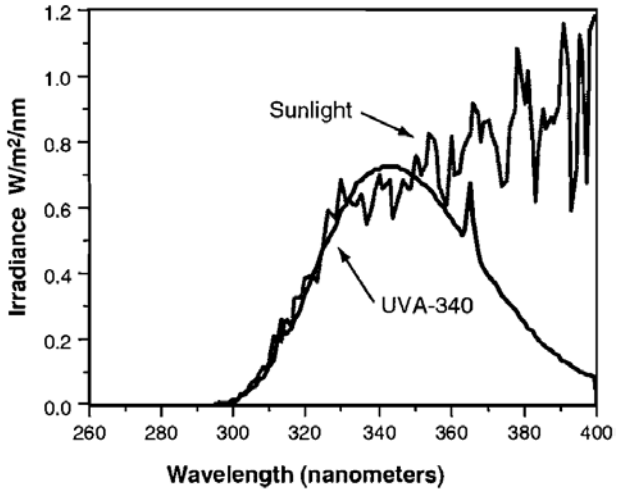


**Figure 2.3 – Spectral power distribution of the UVA-340 lamps compared to sunlight (figure extracted from Q-Panel Lab Products Technical Bulletin LU-0822)**

The irradiance was increased for the composite samples to a value of 1.35 watts/square meter at the 340 nanometer wavelength. This intensity was held for six hours at a temperature of 60°C. The second cycle was a wet cycle containing distilled water vapor for a duration of two hours at 50°C. In the second cycle, no ultraviolet radiation was subjected to the sample. The “large” composite samples were subjected to a maximum of

6000 hours of the ultraviolet cycle in 1200 hour increments while the “thin” samples were subjected to a maximum of 3000 hours of ultraviolet exposure in 600 hour increments. To promote even weathering, the samples were flipped in the QUV chamber at the median weathering increment. For example, the “thin” samples with 600 hours of exposure would have 300 hours of ultraviolet exposure on each side of the composite specimen.

*2.3.2 Methods for EIS measurement, Circuit Modeling, and Data Exclusion*

EIS was the main methodology utilized during the course of all experimentation because the core investigation was to relate impedance data to mechanical properties. Modeling of the impedance data, via circuit modeling, was accomplished for better understanding of the degradation processes and characteristics. For a better mathematical understanding, Thompson’s tau analysis was performed on the circuit elements to discard outliers that could appear from testing variation.

For flexural samples, both a “short” and “long” immersion time were used where the “short” immersion time was six minutes and the “long” immersion period was sixty minutes. In each instance, the mass of the composite was weighed before and after immersion in ultrapure water with a Mettler Toledo New Classic MF balance with model number MS1003S-1200g. The balance can weigh samples up to 1200 grams with a resolution of 0.001 grams. The composite samples used in flexural measurements (i.e., “thick” samples of 1 inch thickness) used a novel electrode system which had platinum coated niobium mesh acting as the electrode with a rubber suction cup surround to promote connection to the composite sample throughout the duration of the experimentation. The coated mesh electrode had a surface area of approximately 0.75 square inches or 4.84 square centimeters. EIS was performed in a transmission configuration where the current

and ion motion would be through the bulk material as opposed to a surface measurement. Four milliliters of Spectra 360® electrode gel was applied directly to each suction electrode before attachment to the composite sample producing a complete electrode area of 1.61 square inches or 11.40 square centimeters. Figure 2.4 displays the electrode configuration of the "thick" samples.

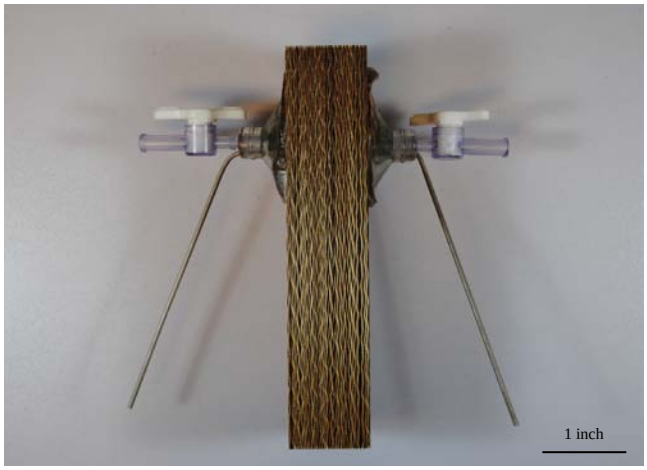


**Figure 2.4 – Electrode configuration for "thick" composite specimens**

Before electrode placement, the adsorbed layer of water present on the surface of the composite was removed by laying the composite onto two plies of paper towel, supplied by Georgia Pacific, and rolling on each side allowing only the weight of the composite to remove the water. A nominal time of 45 seconds was observed between removal of the sample from ultrapure water to beginning the EIS experimentation. For flexural samples, EIS was performed between 100,000 Hertz and 0.001 Hertz. The low frequency, of 0.01 Hertz, was utilized as it was hypothesized that low frequency influences may be observed in the "thick" samples. Five points per decade were measured with an AC perturbation of 30 millivolt about the open circuit potential. Initial studies determined the 30 millivolt root-mean-square perturbation yielded the most stable impedance spectra at low frequencies. EIS was performed with Gamry PC4 model potentiostats or femtostats.

"Thin" tensile samples were also studied via EIS. The immersion times were slightly altered from the "thick" samples, as the "thin" samples were subjected to a "short" immersion of ten minutes and "long" immersion of sixty minutes. A different "short" immersion period was utilized in the "thin" samples as it provided the most repeatable impedance spectra. As before, the mass was measured on the Mettler Toledo scale before and after immersion. The adsorbed water was removed with two Kimwipes, supplied by VWR Scientific, placed in a sandwich configuration. By placing an aluminum panel above the sample and drawing down with a hammer, a constant mass of 300 grams was administered repeatedly to the specimens. The electrodes were then attached in transmission configuration utilizing a stainless steel shim as the electrode with a surface are of 0.197 square inches or 1.70 square centimeters. A volume of 0.1 milliliters of Spectra 360® electrode gel was also administered to the stainless steel surface to promote a constant surface area regardless of surface topography. Maintaining a constant surface area was very important as both the capacitive and resistive elements, utilized in circuit modeling, are dependent on the surface area. A period of 45 seconds between removal of the sample from the ultrapure water to the onset of EIS experimentation was adhered to for each measurement. EIS for the "thin" composite samples were performed from 100,000 Hertz to 0.01 Hertz with an AC perturbation of 10 millivolts about the open circuit potential. The decrease in perturbation voltage from the "thick" samples was utilized as 10 millivolts provided a stable measurement for the "thin" samples without the possibility of degradation from the larger potential. Figure 2.5 represents a schematic drawing and image of the "thin" composite electrode configuration.

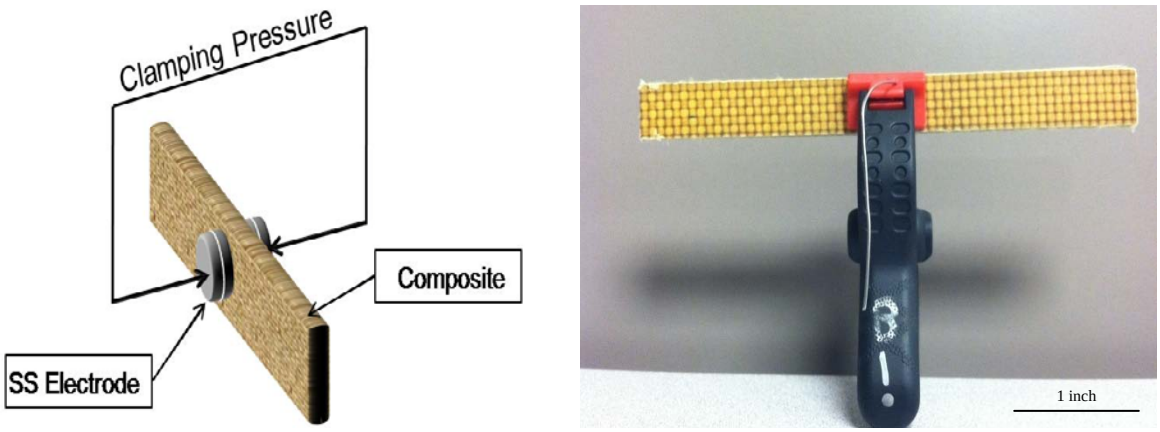


**Figure 2.5 - Electrode configuration for "thin" composite specimens with schematic (left) and actual (right)**

Data collection was acquired in a logarithmic fashion with ten points per decade. Again, EIS measurements were conducted with Gamry potentiostats. To clarify the measurement attributes, Table 2.1 summarizes the EIS experimental differences between the two composite sample dimensions.

**Table 2.1 – Summary of EIS Methods and Characteristics**

| Quantity | "Thick" Composites | "Thin" Composites |
|---|---|---|
| Configuration | Transmission | Transmission |
| "Short" Immersion Length | 6 minutes | 10 minutes |
| "Long" Immersion Length | 1 hour | 1 hour |
| Electrode Surface Area | 11.40 square centimeters | 1.70 square centimeters |
| Initial Frequency | 100,000 Hertz | 100,000 Hertz |
| Final Frequency | 0.001 Hertz | 0.01 Hertz |
| AC Perturbation | 30 millivolts | 10 millivolts |
| Points per Decade | 5 | 10 |

Once EIS spectra were obtained, circuit modeling was performed utilizing ZVIEW circuit modeling software. A modified Randle's cell, which has a constant phase element (CPE) instead of a capacitor, was used to acquire data for analysis and interpretations. A CPE accounts for variation within the system associated with stray currents,

inhomogeneous surface geometry, etc.[3-4] It was observed that more electrode gel and a larger surface area present in the "thick" samples resulted in a lower solution resistance, 25 ohms, compared to the small amount used in the "thin" sample which had a solution resistance of 25,000 ohms. Circuit modeling revealed three circuit elements which were measured and monitored over the weathering periods. These modeling constituents were the composite resistance, or pore resistance, composite CPE-T value (i.e., capacitance magnitude), and composite CPE-P value (attribute which explains degree of capacitive nature).

To ensure the data obtained was void of numerical outliers (i.e., values not statistically within the natural variation of experimentation), Thompson's tau analysis was performed on the three circuit modeled elements. This data exclusion principle utilizes the sample set average, standard deviation, and a tau value to present a range of statistically significant values. Thompson's tau analysis is a commonly used analytical technique within the industrial sector.[5] Equation 2.3 demonstrates the range of acceptable values from a data set.

$$X_{bounds} = \lambda \pm \sigma\tau \qquad (2.3)$$

$\lambda$ is the mathematical average, $\sigma$ is the standard deviation, and $\tau$ is a numerical value dependent on the number of samples within the set. The bounds of this range are determined by either the additive and subtractive mathematical property. After an exclusion of an outlier occurs, the new average, standard deviation, and tau value are recalculated to investigate the remaining values until all data is free of outliers. In terms of the circuit modeled elements, Thompson's tau analysis was performed on each element individually. If one circuit constituent was deemed to be an outlier, the other two

parameters obtained during that test were also rejected. A sample set of ten measurements was used for the "thin" composites and seven measurements for the "thick" composites. A smaller sample set was used for the "thick" composites as the time required for the "thick" composite EIS measurement was significantly longer than the "thin" composites. Both sample sets provided large data matrices which were utilized to minimize the range by decreasing the standard deviation.

*2.3.3 Methods for Measurements of Surface Characteristics*

Typically, ultraviolet degradation of polymers and PMCs results in several changes in the surface characteristics. One of the most notable changes is in the color. To monitor color change, a spectrophotometer can be used to monitor the absorption of visible wavelength radiation. In this study, a Macbeth Color-Eye 7000 was utilized to measure the "thick" composite samples with the software ProPalette used to analyze results. The "thin" composite color was monitored with a Datacolor International Microflash model of spectrophotometer which had a smaller measurement port for the smaller samples. Both instruments supplied a D65 light source, and the CIE (i.e., Commission Internationale de L'éclairage ) L*a*b* color coordinate system was used for monitoring the color changes in each of the L*, a*, and b* coordinates. The L*a*b* coordinate system displays a point in three dimensions in the color space. The L* value dictates the lightness of the color with a whiter color being a more positive number and darker color being more negative. The a* value demonstrates the color on a red to green scale with red being positive and green being negative. The b* value is a measure of the yellow to blue scale with yellow being positive and blue being a more negative coordinate. As the space is Euclidean (i.e., real numbers define the position in three dimensions) in nature, a total color change can be

calculated by simply applying vector mathematics in a Pythagorean metric. Each sample had a data set of six measurements per exposure time with three measurements per side.

Gloss measurements were performed on the composites with three different measurement angles. A Novo-Gloss Trio goniophotometer manufactured by Rhopoint Instruments Ltd. measures the gloss value at 20°, 60°, and 85°. The data output is a percentage of the highest theoretical intensity at the angle of light present. The highest theoretical value is determined by Fresnel's equation for an optically smooth surface in combination with Snell's Law. The combination of these principles can be combined to form equations for both the parallel (Equation 2.4) and perpendicular (Equation 2.5) polarized light.[6]

$$R_s = \left(\frac{\cos\theta_1 - (n^2 - sin^2\theta_1)^{1/2}}{\cos\theta_1 + (n^2 - sin^2\theta_1)^{1/2}}\right)^2 \quad (2.4)$$

$$R_p = \left(\frac{n^2\cos\theta_1 - (n^2 - sin^2\theta_1)^{1/2}}{n^2\cos\theta_1 + (n^2 - sin^2\theta_1)^{1/2}}\right)^2 \quad (2.5)$$

These equations assume air is the first medium through which the light passes through before coming into contact with a second medium, with a refractive index of n, at an angle of incidence of $\theta_1$. The arithmetic average of these two values is the theoretical gloss value at an angle of $\theta_1$. Typically, for polymeric materials, the three aforementioned angles are used for high gloss, semi-gloss, and low gloss surfaces, respectively. Each specimen had six measurements performed with the average and deviation reported.

Surface profilometry was utilized to measure the surface roughness accounted for by polymer degradation over exposure time. These measurements were performed by the Princeton Applied Research Electrochemical Suite in Optical Scan Profilometry mode. The scan size was 7500 micrometer by 7500 micrometer at a scan rate of 1000

micrometer/second. Data was collected at every 10 micrometer with a step of 10 micrometer between each line scan. The experiments were performed on the "thin" composite samples as the large z-direction limited experimentation on the "thick" samples. Area surface roughness was observed for both the arithmetic average and root-mean square average. As the measurements were approximately five hours in length, only one measurement was made for each specimen at the final exposure time.

Water contact angle is an indication of the surface energy for various materials. The angle formed at the substrate-water interface can give insight to the surface roughness and many other surface composition properties. The water utilized for measurement was from the ultra-pure source, and the camera used to capture images was a 60 Hertz V2-RS170 manufactured by North American NTSC. Side imaging was also captured with this camera to display surface aspects as a function of accelerated exposure. To analyze the contact angle captured by the camera, FTA32 Video software was employed. The contact angle data was collected with six measurements per sample with three measurements conducted on both sides.

*2.3.4 Mechanical and Ballistic Measurement Methodologies*

Tensile mechanical measurements were conducted in two separate methodologies as the two fiber systems exhibited drastically different behavior. The Kevlar® fiber composites needed very little sample preparation as 100 grit sandpaper was wrapped around the composite clamping area for little slippage and failure within the gage section. The higher strength S2 Glass® fiber composites needed 10° composite taper tabs to induce failure within the gage sections. Tabs were adhered to the composite samples with a high strength epoxy "Plastic Bonder" produced by Loctite®. Both composites were subjected to

tensile experimentation in accordance with ASTM D3039.[7] This guideline was followed to produce the correct composite dimensions and the proper layup mentioned previously. A displacement rate of 2 millimeter/minute was used in accordance with the standard. The tensile modulus was calculated as the change in stress over the change in strain for small strains (i.e., less than 0.2%). Ultimate tensile strength, strain at break, and energy at ultimate tensile strength were also monitored during tensile measurements. All measurements were performed on an Instron 5567 model with MTS Sintech clamping fixtures. A MTS extensometer (model 632.25B-20) was utilized for accurate strain measurements in low stress (i.e., 0 – 100 megapascal (MPa)) regimes. The load cell was also manufactured by MTS and had a rating of 30 kilonewton (kN). A total of five measurements were performed at each weathering period. From these experiments, only the samples which demonstrated failure within the gage section were recorded for data analysis.

Flexural property assessment was administered in a three point bending configuration. ASTM D 2344 for short beam strength of polymer matrix composite laminates was followed for measurement protocol and sample preparation for both the "thick" S2 Glass® fiber and Kevlar® fiber composite samples.[8] A displacement of 1 millimeter/minute was administered to the samples. The loading nose had a diameter of 6 millimeters and the loading supports a diameter of 3 millimeters. Short beam strength was also calculated by Equation 2.6 which was observed in ASTM D2344.[8]

$$F^{sbs} = 0.75\frac{P_m}{bh} \qquad (2.6)$$

The short beam strength, or $F^{sbs}$, is dependent on the maximum load ($P_m$), width ($b$), and thickness ($h$) of the composite sample. Interlaminar shearing is observed within the

mid-section of the composites usually within a matrix rich region. With consideration to the ASTM standard, the span length was nominally set to four times the composite thickness. To apply a large enough load, a MTS load cell, model number 661.23A-01, of 250 kN capacity was utilized. The MTS system, model number 312.31, was operated from a FlexTest SE platform. Hydraulic wedge grips were employed, model 647, with a max pressure rating of 69 MPa. The hydraulic wedge grips were utilized to maintain proper position of both the bottom and top flexural fixtures. North Dakota State University manufactured the flexural fixtures used in this experimentation. A total of three samples per weathering period were measured for both composite systems. Of these measurements, only the samples which failed in an interlaminar shearing fashion were utilized in the interlaminar shear strength values. However, flexural modulus could not be obtained for these samples as the span to composite thickness ratio yielded interlaminar shear stresses which are not truly indicative of elastic deformations.

Ballistic resistances of the composites were measured at North Dakota State University. The gas gun apparatus consisted of a high pressure chamber, a firing cylinder, and a capture chamber containing two infrared chronographs. The high pressure chamber manufactured with AISI 1045 steel was produced at North Dakota State University. The chamber was pressurized with Helium gas to a nominal value of 150 pounds/square (psi) inch. A pneumatic actuator and ball valve produced by Novospect, Inc. was utilized for releasing the pressure to the firing chamber in less than one second. A solenoid was utilized for remote firing of the actuator. The 150 psi pressure produced high velocity ($\geq$ 100 meters/second) projectiles for impacting the composite specimens. The actuator opens a valve which allows the release of gas to push the sabot with the mounted projectile. A

polyurethane foam sabot was used to carry the fragment simulating projectile (FSP) toward the sabot stripper which removes the sabot immediately before the impact chamber. After sabot removal, an infrared CED Millenium chronograph captures the velocity of the projectile before and after interacting with the composite. However, the projectile form and velocities used in this ballistic study were not conducive for the FSP to proceed through the composites. Accordingly, the exit velocity was not observed during this study. The composite structures allowed for a more accurate representation of the cross sections utilized for up-armoring of military vehicles, but the "thick" cross sections were not conducive for traditional ballistic limit measurements.

A fragment simulating projectile (FSP) comprised of AISI 1019 carbon steel (Rockwell B hardness of 73) was utilized in this experimentation to produce damage.[9] The FSP had a nominal weight of 17.3 grams (or 267 grains). Figure 2.6 exhibits the projectile dimensions utilized for ballistic characterization.

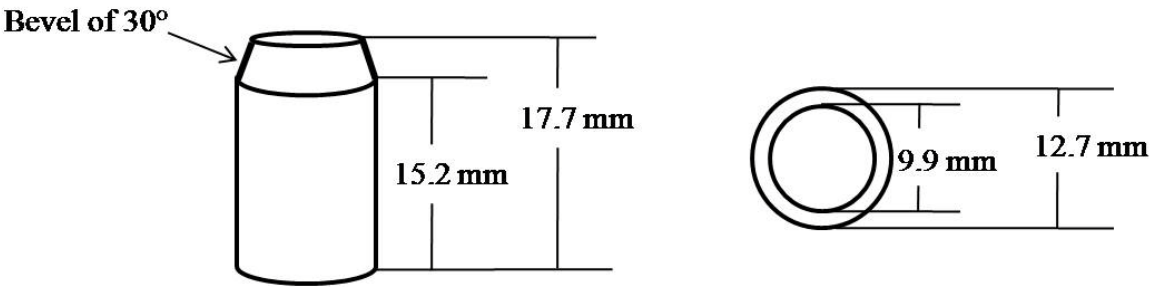


**Figure 2.6 – Characteristic dimensions of fragment simulating projectile**

The projectile consisted of a necked structure to produce an impact which would cause interlaminar delaminations, transverse shear failure, and fibrous tensile failure along with the expected projectile penetration.[10] Since ballistic limit experimentation could not be conducted, a comparative study was administered with visual cross section examination of the FSP penetration depth. Two measurements of the penetration depth

were utilized. Surface penetration was measured immediately above the impact area to the depth of the penetration. Cross-sectional penetration measured the depth of the penetration with respect to the unaffected composite surface. Cross-sectional measurements were performed after cutting the affected zone with a wet saw.

## 2.4 References


1. Hinderliter, B. and S. Croll, *Simulations of nanoscale and macroscopic property changes on coatings with weathering.* Journal of Coatings Technology and Research, 2006. **3**(3): p. 203-212.
2. Brennan, P. and C. Fedor, *Sunlight, UV and Accelerated Weathering.* Technical Bulletin LU-0822, 1994.
3. Schiller, C.A. and W. Strunz, *The evaluation of experimental dielectric data of barrier coatings by means of different models.* Electrochimica Acta, 2001. **46**(24-25): p. 3619-3625.
4. Jorcin, J.-B., M.E. Orazem, N. Pébère, and B. Tribollet, *CPE analysis by local electrochemical impedance spectroscopy.* Electrochimica Acta, 2006. **51**(8-9): p. 1473-1479.
5. Dieck, R.H., *Measurement uncertainty: methods and applications*. 2006, Research Triangle Park, NC: The Instrumentation, Systems and Automation Society.
6. Trezza, T. and J. Krochta, *Specular reflection, gloss, roughness and surface heterogeneity of biopolymer coatings.* Journal of Applied Polymer Science, 2001. **79**(12): p. 2221-2229.
7. ASTM D3039, 2008, "Standard Test Method for Tensile Properties of Polymer Matrix Composite Materials," ASTM International,West Conshohocken, PA, 10.1520/D3039_D3039M-08
8. ASTM Standard D2344, 2006, "Standard Test Method for Short-Beam Strength of Polymer Matrix Composite Materials and Their Laminates," ASTM International,West Conshohocken, PA, 10.1520/D2344_D2344M-00R06
9. Matweb, L. *AISI 1019 Cold-Drawn Steel*. [Material Property Data] 2011 [cited 2011 November 22, 2011]; Available from: http://www.matweb.com/search/DataSheet.aspx?MatGUID=1f2a8cfb89f241949c94b360958d8592&ckck=1.
10. Iremonger, M. and A. Went, *Ballistic impact of fibre composite armours by fragment-simulating projectiles.* Composites Part A: Applied Science and Manufacturing, 1996. **27**(7): p. 575-581.

# CHAPTER 3. ELECTROCHEMICAL IMPEDANCE SPECTROSCOPY INVESTIGATION OF BALLISTIC RESISTANT POLYMER MATRIX COMPOSITES

## 3.1 Introduction

Electrochemical impedance spectroscopy (EIS) investigation of non-conducting polymer matrix composites (PMCs) was conducted to determine if ultraviolet degradation would change the characteristic spectra. It was hypothesized that the wetted composite would produce conductive pathways for ion and electron flow and display spectra similar to that of polymeric coatings. Initial investigation of the ballistic resistant composites reaffirmed this assumption, but another result displayed a phenomenon not observed in literature. This effect was determined to be caused by evaporation that occurred when the samples were exposed to the ambient conditions of the experimental chamber. Two different immersion times were also studied to determine if the circuit modeled constituents would exhibit a statistically significant change. Lastly, the circuit modeled constituents were examined after several accelerated exposure durations for both "thin" and "thick" configurations.

## 3.2 Initial EIS Investigation of Ballistic Resistant PMCs

Two composite systems (i.e., phenolic matrix/S2 Glass® fiber and phenolic matrix/Kevlar® fiber) were used in this study along with two different sample dimensions. Therefore, each section in this chapter will divide the results based on the sample dimensions of "thin" or "thick".

### *3.2.1 Initial EIS Investigation of the "thin" Ballistic Resistant PMCs*

Initial investigations of the "thin" composite samples exhibited a difference of the

two composite systems in terms of the impedance magnitudes in the mid and low frequencies. It was also observed that changing the immersion time between 10 minutes and 60 minutes had an influence on several characteristics of the impedance spectra. Figure 3.1 displays the differences between the two composite systems for the two immersion times of the S2 Glass® fiber and Kevlar® fiber composites.

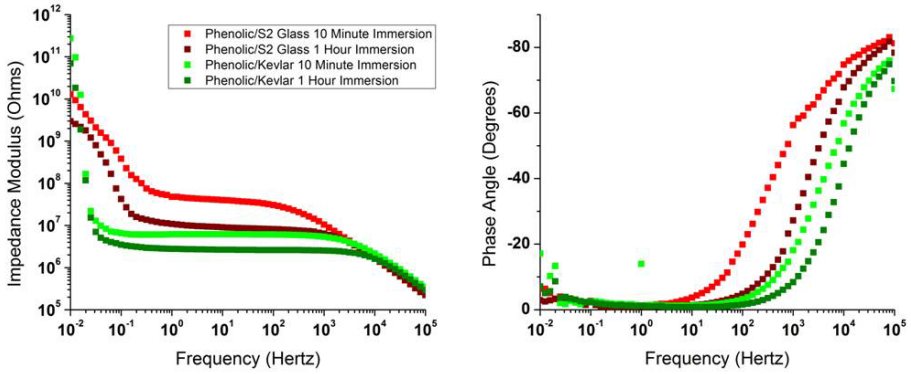


**Figure 3.1 - Typical EIS results for the thin composite samples displaying the Bode impedance modulus plot (left) and Bode phase angle plot (right)**

The most interesting phenomenon associated with the initial EIS investigation was observed in the low frequencies. As the impedance increases with lower frequencies, substantial change from 0° cannot be observed in the Bode phase plot. However, the low frequency data of the Kevlar® fiber composites demonstrated noisy results associated with the potentiostat measurement capabilities. The 0° phase angle was indicative of the system maintaining a resistive nature. Typically, the increase in impedance at the lower frequencies is accompanied with an increase in the phase angle toward -90° as the system is displaying capacitive effects in the low frequency. In this case, the increasing impedance was explained by an evaporation process occurring from the experimental conditions associated with the Faraday cage utilized for measurements. To reinforce these claims, a

single frequency impedance measurement was measured at 0.1 Hertz. The frequency was selected because it is in the evaporation affected regime for both immersion times and both composite systems. Figure 3.2 displays the impedance magnitude of the unweathered "thin" composite specimens, phenolic matrix/S2 Glass® fiber composite and phenolic matrix/Kevlar® fiber composite, at 0.1 Hertz for a period of three hours.

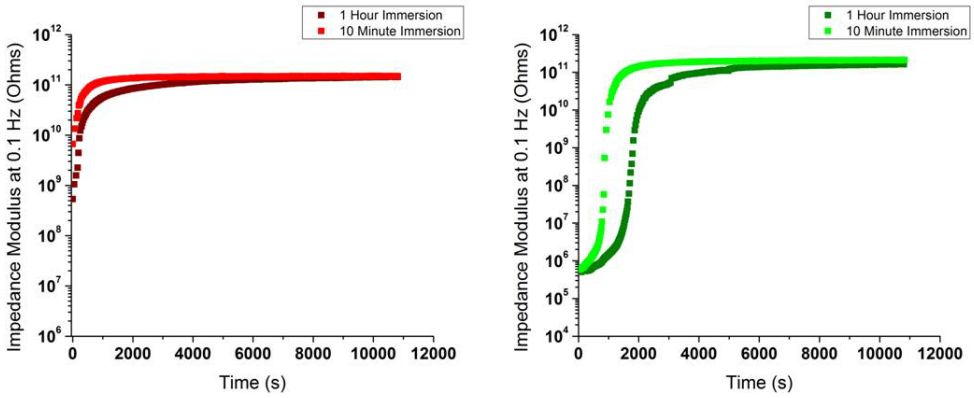


**Figure 3.2 - Impedance modulus at 0.1 Hertz versus time for phenolic matrix/S2 Glass® fiber composite (left) and phenolic matrix/Kevlar® fiber composite (right)**

Figure 3.2 reveals increasing impedance with experiment time. The measurements were conducted for approximately 10,800 seconds, which was longer than the original experiment, but was conducted to prove a convergence of the modulus toward a steady value. In each case, the impedance displays an increase with time from evaporation causing longer pathways through a less conductive material resulting in higher impedance. Figure 3.2 also reveals that the large increase in impedance occurs later in the samples immersed for one hour as opposed to ten minutes. At the beginning of the measurement, the impedance was larger for the ten minute immersed samples which was also displayed in Figure 3.1. Likewise, the S2 Glass® fiber composites expressed a larger impedance than the Kevlar® fiber composites. The lofty nature of the Kevlar® fiber composites allowed the evaporation to take place more slowly compared to the S2 Glass® fiber composites.

Another study regarding the evaporation influence examined the dependence of the increasing modulus on water weight loss. Figure 3.3 displays the impedance at 0.1 Hertz for a length of 3,600 seconds with simultaneous weight loss measurements on Kevlar® fiber composites.

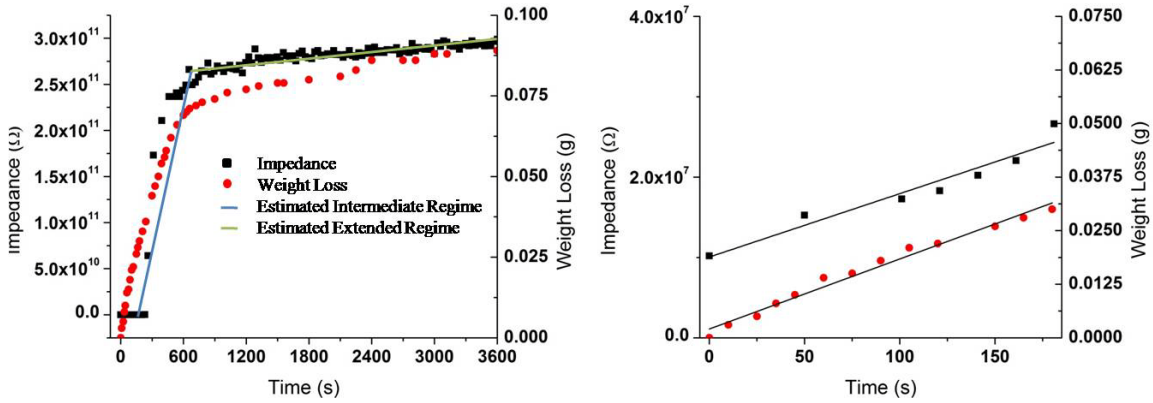


**Figure 3.3 – Single frequency EIS of Kevlar® fiber composites with corresponding weight loss (left) and inset to demonstrate initial linear increase of the impedance modulus (right)**

Three regimes of the single frequency impedance were observed including: a slow initial (0 – 200 seconds) increase, fast intermediate increase, and a slowly increasing final regime. The blue and green lines provide a visual estimation of the intermediate and long evaporation regimes. The initial linear increase was also observed in the amount of water weight loss during the weight measurement. When comparing the EIS and weight loss at times between 200 and 600 seconds, a rapid increase in the impedance was observed while the water weight loss rate remained unchanged. At times exceeding 600 seconds, both the impedance and water weight loss displayed a slowly increasing linear trend. Again, the impedance increased due to longer resistive pathways as the water evaporated from the composite. By linear fitting of the data, it was observed that the three regimes exhibited a different impedance change per weight loss. The initial regime exhibited a slow 0.48 MΩ/

milligram of water loss, the intermediate regime displayed a fast changing regime of 6711 MΩ/milligram of water loss, and the final regime exhibited 1837 MΩ/ milligram of water loss. The final value is larger than expected due to the low value of weight change observed in this regime, effectively increasing the ratio.

The circuit modeled elements, which consisted of constant phase element (CPE) attributes and composite resistance, data values were obtained for the initial spectra. After Thompson's tau analysis was performed, the averages were plotted to observe the differences incurred with an increase in the immersion time. Figure 3.4 reveals the averages of the three circuit modeled elements for the phenolic matrix/S2 Glass® fiber composites with one standard deviation.

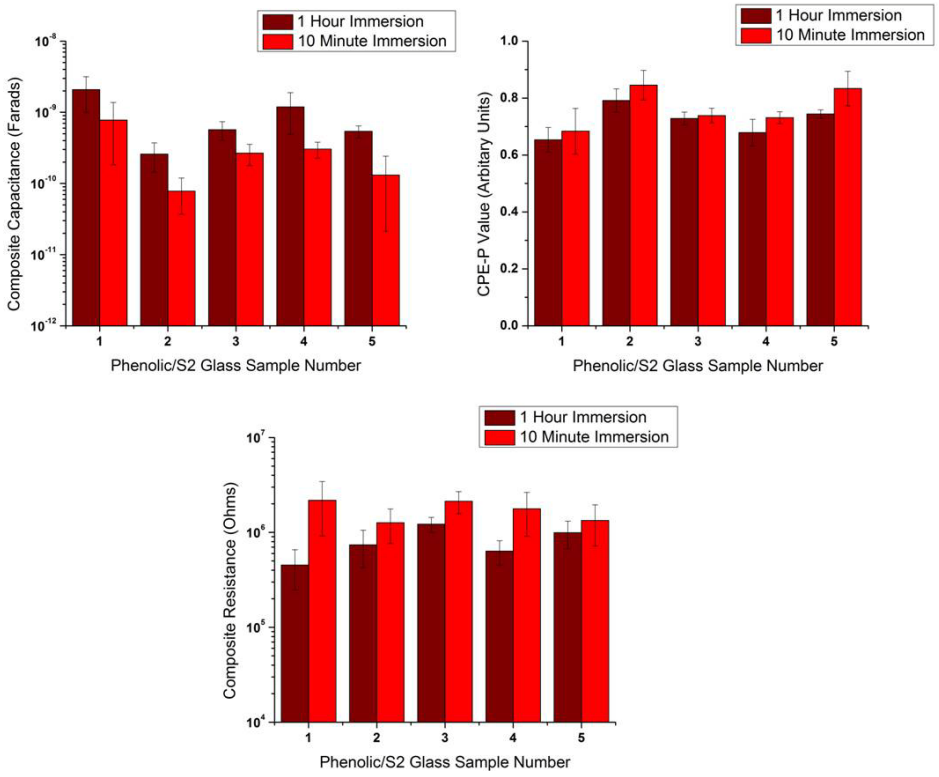


**Figure 3.4 - Phenolic matrix/S2 Glass® fiber composite circuit modeled constituents including composite capacitance (upper left), CPE-P value (upper right), and composite resistance (bottom)**

The CPE-T value (i.e., magnitude of capacitance) exhibits a statistically significant difference in four instances for these five samples and was also observed a majority of the time with the other samples. This trend was attributed to the capacitive nature increasing with an increase in water absorption which is typically observed in coating studies.[1-3] The increased amount of water absorbed in the one hour immersion increases the bulk dielectric as the dielectric constant of water is 80 and for common polymers is between 2 and 5.[4] Also, the increase in depth of penetration reduces the distance between electrodes to further increase the capacitance.

The CPE-P value represents the extent of the CPE-T element acting as a perfect capacitor. A purely capacitive element would exhibit a CPE-P value of one. The values range from approximately 0.65 to 0.85 in the S2 Glass® fiber composite measurements. On average, the one hour immersion specimens have a higher CPE-P value, but the large deviations demonstrate low statistical confidence in the difference.

The last value of concern is the composite resistance which directly relates to the pore resistance of the composite system. For S2 Glass® fiber composites, the value of the pore resistance is usually higher for the 10 minute immersion as water had not ingressed as far into the matrix leading to longer pathways of electrons and ions through a higher impedance material. This is further supported by the diffusion depth which is related to the diffusion coefficient and the square of immersion time.[5] The differences between the 10 minute and 60 minute immersions, in terms of the square root of immersion time, was not distinguished significantly (i.e., only by a factor of approximately 2.45 times) to be measured by EIS. Theoretically, this would be a measurable difference with the EIS capabilities, but the composite surface variability caused large deviations in the data.

The phenolic matrix/Kevlar® composites displayed different behavior when the circuit modeled element analysis was conducted. Figure 3.5 reveals the circuit modeled elements of the aforementioned polymer matrix composite and the differences of these values for the two immersion times.

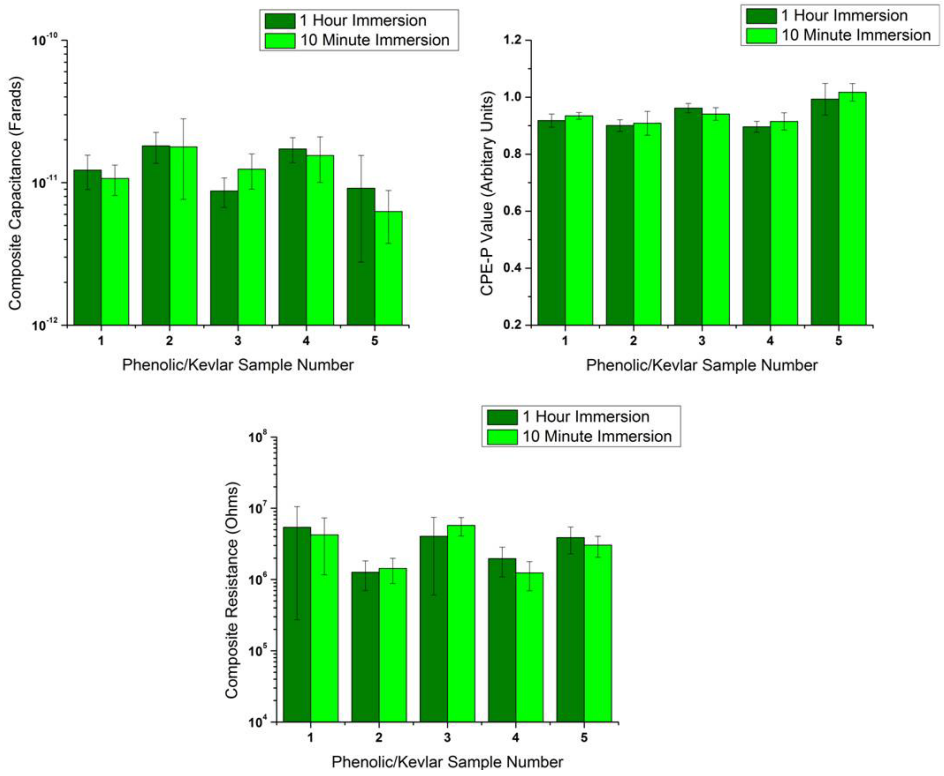


**Figure 3.5 -Phenolic matrix /Kevlar® fiber composite circuit modeled constituents including composite capacitance (upper left), CPE-P value (upper right), and composite resistance (bottom)**

The CPE-T values are approximately the same value regardless of immersion time. This was accounted for by the porous structure of the composites which is also accompanied by porous peel ply. The fiber ends and the intact peel ply caused increased absorption of water. Also, the voids being instantaneously filled with water during immersion creates a composite which has a majority of the water uptake occurring in the first stage of immersion which is supported by Figure 3.6. Figure 3.6 displays the weight

change for the initial testing of the composites systems for both 10 and 60 minute immersion durations. It should be noted that only one standard deviation of error is displayed in Figure 3.6.

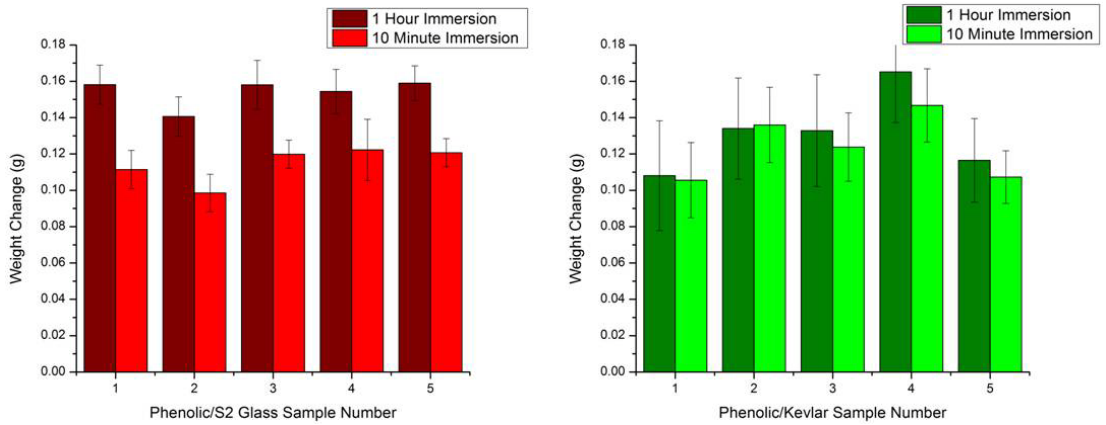


**Figure 3.6 - Weight Change from water immersion of phenolic/S2 Glass® composite (left) and phenolic/Kevlar® composite (right)**

The phenolic matrix/S2 Glass® composites exhibited a more uniform trend, from sample to sample, in water uptake during the immersion periods. There was also more confidence of the difference in weight gain between the different immersion durations in the S2 Glass® fiber composites. The small deviations caused the composite capacitances to be statistically different as was observed in Figure 3.4. The phenolic matrix/Kevlar® fiber composites demonstrated little difference in the different immersion periods. This led to a CPE-T value with a similar magnitude in both immersion times. These explanations also describe the similarities in both the CPE-P value and pore resistance for the "thin" Kevlar® fiber composites.

Differences between the composite systems were observed predominantly in the capacitive effects, specifically in the CPE-T value. The phenolic matrix/Kevlar® fiber had a lower capacitive magnitude by roughly a factor of 10. This was accounted for by the

difference in the dielectric constants of the two fibers as S2 Glass® has a higher value of dielectric at 5.2-5.3 while Kevlar® can range between 3.5 and 4.5 with experimental results favoring the smaller value.[6-7] Another attribute is the difference in thickness as the Kevlar® composite samples were thicker at 2.23 millimeters ± 0.06 millimeters while the S2 Glass® fiber composites were approximately 1.45 millimeters ± 0.01 millimeters. The Kevlar® fiber composites also exhibited a more capacitive behavior as the CPE-P demonstrates. The CPE-P has been known to account for stray currents associated with a "leaky" capacitor type situation as well as non-uniform thicknesses and currents.[8-9] In the case of the Kevlar® fiber, both the resistivity and dielectric are more similar to the encapsulating phenolic matrix which may lead to a lower probability of stray current occurring from an incomplete circuit pathway. Both composites do possess uneven thicknesses from a surface roughness inherent with high fiber volume fraction. Lastly, the resistances are slightly higher in the phenolic matrix/S2 Glass® fiber composites. This was attributed to the high resistivity of the S2 Glass® fiber which again causes longer pathways as the resistivity is approximately $9.1 \times 10^{12}$ ohm·centimeter.[6] The S2 Glass® volume resistivity is almost an order of magnitude higher than the phenolic polymer that surrounds these fibers which has a volume resistivity of $1.0 \times 10^{12}$ ohm·centimeter.[10] Kevlar® fiber also has a low volume resistivity compared to S2 Glass® which is shown to be $0.5 \times 10^{12}$ ohm·centimeter.[11] This leads to longer paths for the electrons and ions as the higher impedance glass fiber acts as a disturbance which needs to be circumnavigated.

*3.2.2 Initial EIS Investigation of the "thick" Ballistic Resistant PMCs*

Initial investigations of "thick", 1 inch or 2.54 centimeter, composite samples were also conducted to study the applicability of performing EIS on these composites. Literature

reported is often performed on relatively thin composite samples as polymers are high impedance materials which cannot easily be measured with most common potentiostats. Figure 3.7 displays the impedance spectra difference between a “dry” sample and that of a sample immersed for six minutes.

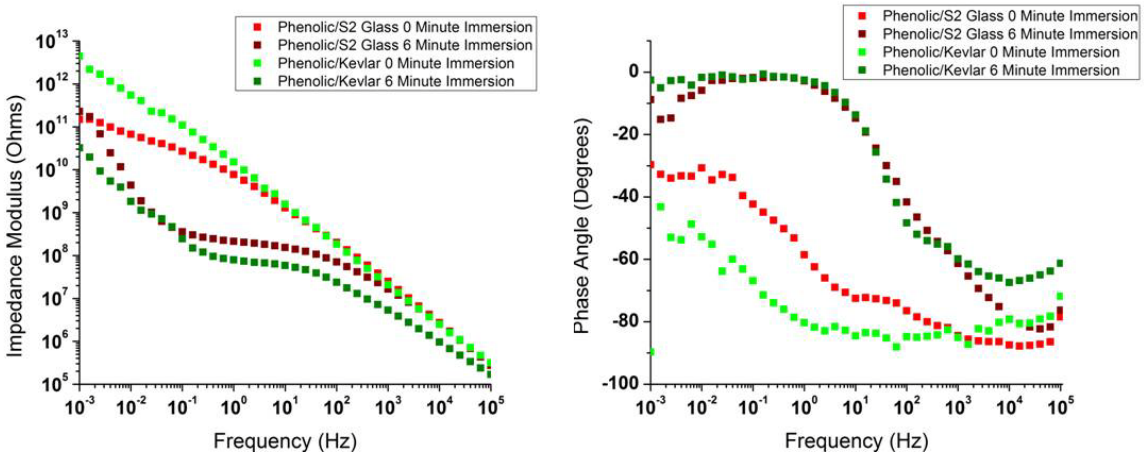


**Figure 3.7 - Typical impedance spectra differences observed for the two composites systems in the Bode impedance plot (left) and Bode phase angle plot (right)**

It was observed that in both cases the “dry” samples demonstrated a more capacitive manner, as the phase angle is around -90° until the low frequencies. The low frequency range scatter may be from a non-steady state measurement as the low frequency decade, last five frequencies, could take up to 3 hours to measure. However, it was deduced that even a small immersion time can change the impedance magnitude. The immersed samples revealed the same trend as the “thin” samples where the resistive portion of the response was higher for the S2 Glass® fiber composites. Also, the capacitive portion of the response was greater in the Kevlar® fiber composites. The total impedance is inversely affected by the capacitance, thus, smaller capacitances have higher impedance. Lastly, the evaporation effect was also observed in this study which, again, contributed to the ambient conditions observed by the composite during the EIS measurement.

### 3.3 Ultraviolet Exposure Effects on Ballistic Resistant PMCs

Both the "thin" and "thick" composites were exposed to accelerated weathering conditions possessing an ultraviolet irradiation intensity of 1.35 watts/square meter at 340 nanometers. EIS was explored as a possible mean to monitor changes in the ballistic resistant composites.

*3.3.1 EIS Investigation of Exposure on "thin" Ballistic Resistant PMCs*

The "thin" composite samples were measured by EIS after defined accelerated exposure durations. Circuit modeled element values were then subjected to data exclusion methodologies. Figure 3.8 displays the values observed for the three circuit modeled elements for S2 Glass® fiber composites after a ten minute immersion.

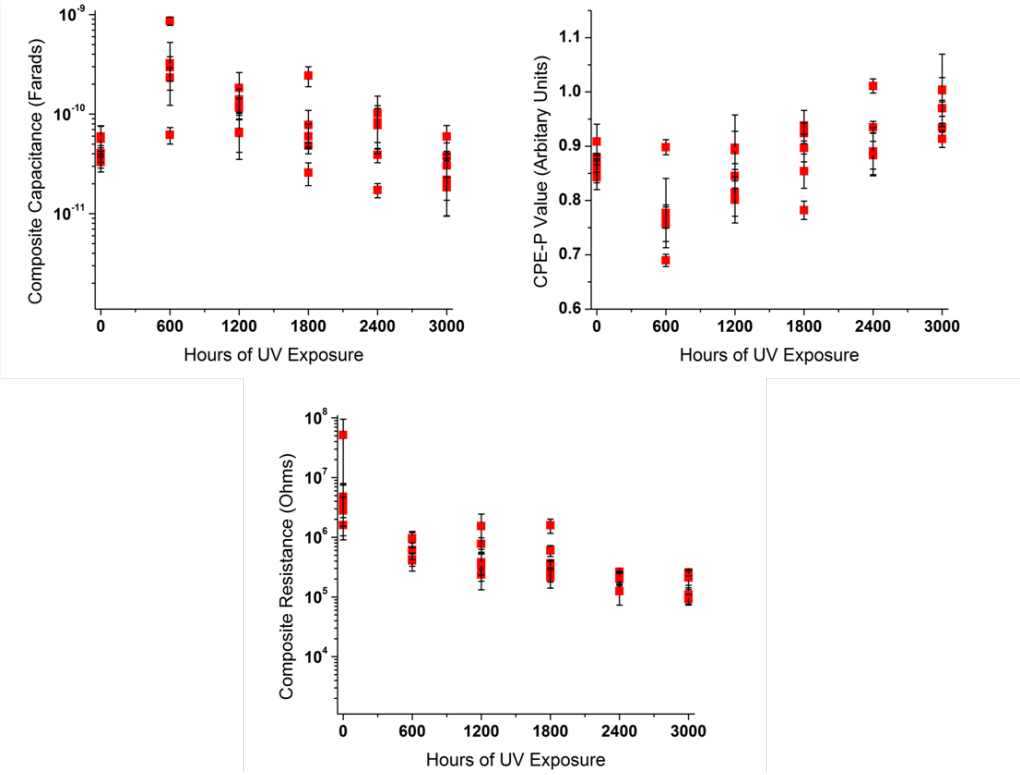


**Figure 3.8 - Composite circuit modeled constituent values as a function of weathering time including the composite capacitance (upper left), CPE-P value (upper right), and composite resistance (bottom) for "thin" S2 Glass® composites**

The trends observed were identical between the ten minute and one hour immersions; however, the magnitudes of the responses shifted in a similar manner as was observed in the initial "thin" composite immersion study. It was observed that large variations were present which was displayed by the averages at each exposure time. Four of the five samples demonstrated an initial increase of capacitance at 600 hours before decreasing at 1200 hours back toward the original capacitance value. This is counter intuitive as the capacitance should increase with the increased water absorption from pore creation and water entrapment. Figure 3.9 depicts the increase in water absorption for the six weathering periods of the "thin" S2 Glass® fiber composites.

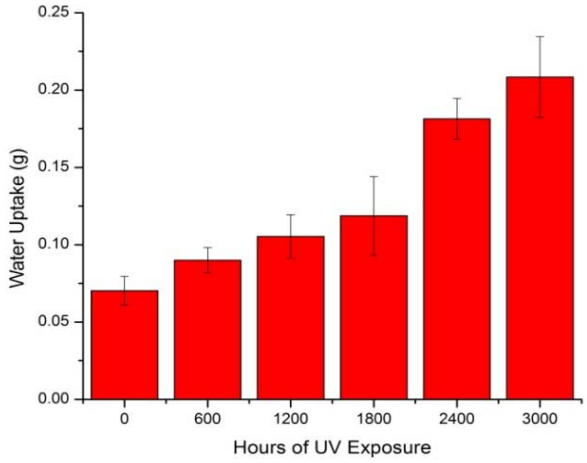


**Figure 3.9 - Water absorption during 10 minute immersion for the phenolic matrix/S2 Glass® fiber composites**

As this data suggests, the capacitance should be increasing with exposure time. However, the area effect may be far exceeding the relative permittivity effect as more fiber bridging, or fiber protrusion from the bulk composite, leads to smaller electrode area because a more resistive material comes to the surface. Another reason for decreased capacitance may come from the increased measurement thickness as the fiber protrusion effectively increases the distance between the two electrodes. Also, a swelling effect from

water ingression into the matrix may be occurring. Both the swelling and increased thickness effects have been observed in composite literature for possible decreasing capacitive trends with increased water absorption.[12] The water uptake data also exhibits a noticeable change at 2400 and 3000 hours. The composite resistance exhibited the most notable trend with confidence of a significant change after 2400 hours of ultraviolet exposure which was explained by the increase in porosity. At 2400 hours, fiber bridging was observed on all samples while only a few samples displayed the fiber bridging before 2400 hours. Figure 3.10 displays the normalized, final value to initial value, circuit modeled elements.

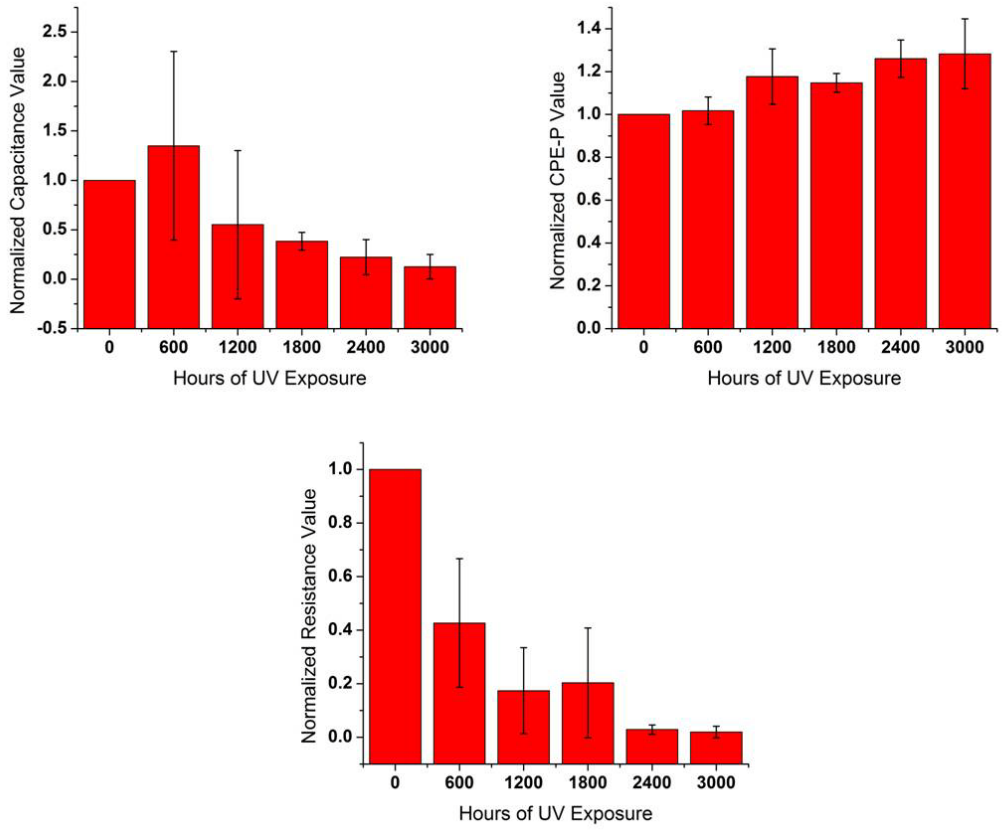


**Figure 3.10 - Normalized data for the phenolic matrix/S2 Glass® composites including the composite capacitance (upper left), CPE-P value (upper right), and composite resistance (bottom)**

A trend of three distinct regimes is present within the pore resistance measurements. The trend observed signifies that the 0 hour measurement is a pristine sample, 600 to 1800 hours of exposure demonstrate some porosity and minimal fiber bridging, and 2400 to 3000 hours demonstrate much porosity due to complete removal of the polymer top layer. These characteristics are similar to those observed within the absolute results; however, Figure 3.9 was presented to verify both the changes observed and the uniformity of the measurement. Again, it should be noted that the 2400 hour and 3000 hour weathered samples exhibited the least amount of variation from sample to sample as the weathering had uniformly removed the top most polymeric layer in these composites.

Kevlar® fiber composites demonstrated less distinguishable results than those of the S2 Glass® fiber composites. This was attributed to the presence of an intact peel ply which caused a screening of the ultraviolet intensity. After removal of the peel ply, subsequent experimentation suggested that the peel ply was porous causing little statistical influence on the resistive values. The mean of the resistance values with the peel ply removed was within the natural variance measured with the peel ply intact. However, the water absorption of the peel ply caused the capacitive values to be altered from that of bulk Kevlar® fiber composite. Initially, the mean of the Kevlar® PMC capacitance, without the peel ply, was an order of magnitude larger than with the peel ply intact. At 3000 hours of accelerated ultraviolet exposure, the CPE-T and CPE-P mean values demonstrated little variation from the mean of the PMCs with the peel ply intact suggesting that the peel ply had been photodegraded. Figure 3.11 displays the circuit modeled results for the “thin” Kevlar® composites after 10 minutes of immersion with the peel ply attached.

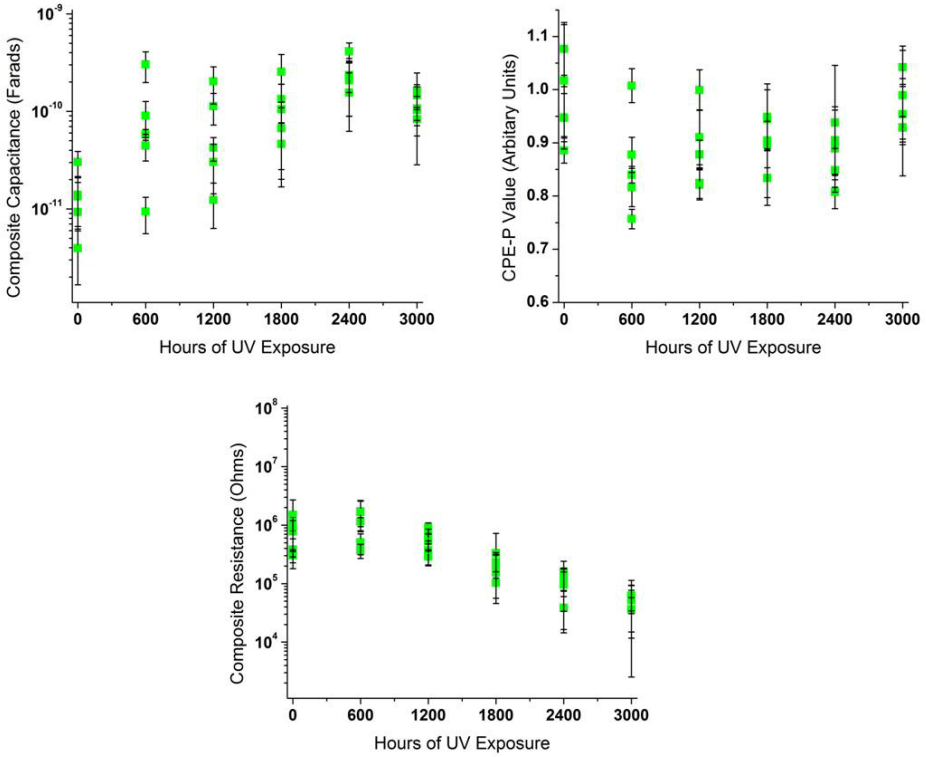


**Figure 3.11 - Composite circuit modeled constituent values as a function of weathering time including the composite capacitance (upper left), CPE-P value (upper right), and composite resistance (bottom) for "thin" Kevlar® composites**

The one hour immersion samples exhibited the same trends with shifts in capacitance and resistance similar to those of the initial results. As suggested earlier, the change in the capacitive elements was not completely due to the degradation of the PMC from ultraviolet exposure. However, the resistive changes in the "thin" Kevlar® fiber composites were deemed to be independent of the peel ply as it was highly porous. Therefore, the only circuit modeled element that was monitored for change was the composite resistance.

Both the matrix and fiber are polymers possessing aromatic nature in the chemical structure. Also, literature has shown that the major absorption of ultraviolet wavelengths of Kevlar® occurs at the wavelength supplied by the UVA 340 lamps.[13] The composite

resistance demonstrates a slight increase in porosity which effectively lowered the composite resistance. The increase in porosity suggests photodegradation occurred as a small fraction, ranging from 0.06 watts per square meter to 0.12 watts per square meter, of the ultraviolet radiation was able to proceed through the peel ply Figure 3.12 displays the normalized circuit modeled composite resistance for the 10 minute immersed phenolic matrix/Kevlar® fiber composites.

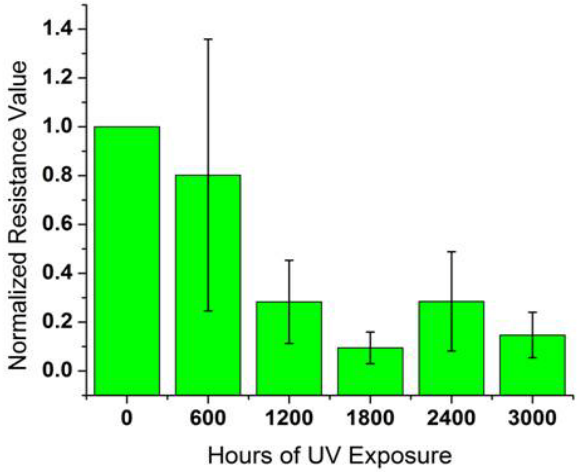


**Figure 3.12 - Normalized data for the phenolic matrix/Kevlar® fiber composite resistance**

The results from Figure 3.12 reveal that there was more variation in the Kevlar® fiber composite compared to the S2 Glass® fiber composites. Again, each specimen is realistically different when it is assumed to be theoretically the same, but the surface undulations and polymer thickness is different in each sample. Likewise, the one standard deviation demonstrates that the composite resistance has high variability. Also, a noticeable trend in the composite resistance was non-existent. This was attributed, again, to the presence of the peel ply which prohibited the amount of accelerated exposure needed to cause a distinguishable change.

*3.3.2 EIS Investigation of Exposure on "thick" Ballistic Resistant PMCs*

The "thick" composite specimens studied were of great interest as the literature reported in this area is non-existent. Additionally, the larger composite samples are more similar to the geometries used for ballistic resistant applications such as vehicle up-armoring. As the EIS methodology was suggested for use as an in-service NDE method, the results on the thicker samples were monitored to determine the applicability of using EIS on "thick" cross-sections. The experimental scheme allowed monitoring of the progression of decreased impedance over exposure time. Figure 3.13 displays the impedance spectra of the two composite specimens weathered for 6000 hours of ultraviolet exposure.

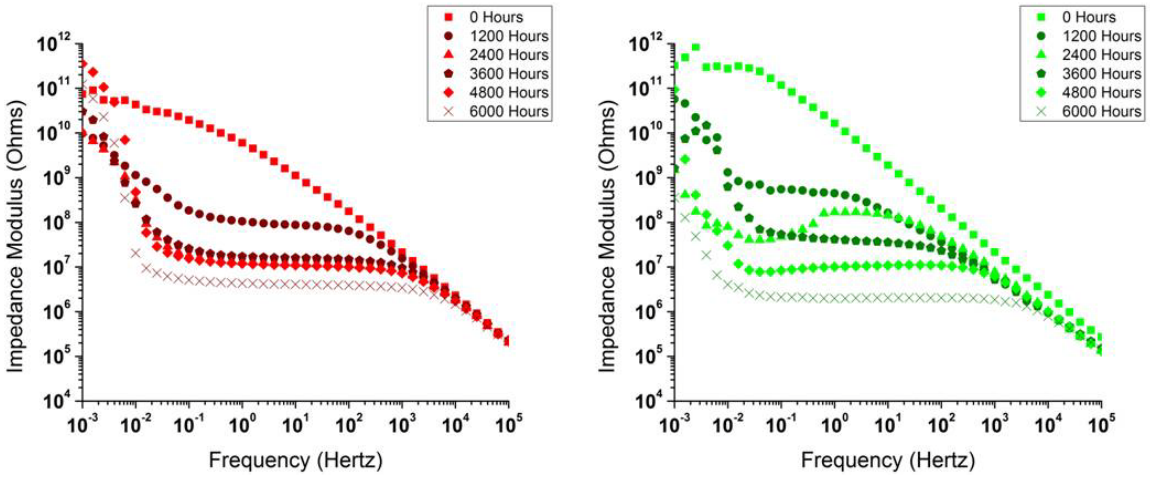


**Figure 3.13 –EIS spectra during exposure for an ideal "thick" samples of phenolic/S2 Glass® composite (left) and phenolic Kevlar® composite (right)**

Figure 3.13 demonstrates that impedance data obtained throughout the duration of exposure displayed expected results. The zero hour measurement is a "dry" measurement for both composite systems. It is observed that the modulus does not necessarily decrease accordingly during the exposure time. The EIS spectra demonstrate the significance of data exclusion principles for this specific experimentation. It was apparent in the S2

Glass® fiber composites that the impedance was slightly higher in 3600 hours experimentation than the 2400 hours experimentation. The Kevlar® fiber composites displayed two instances of decreasing modulus in the mid-frequencies, but this would not influence the circuit modeled element values as the range is from 100,000 to 10 Hertz. However, the decreasing impedance suggests that accelerated exposure durations did display noticeable changes between each exposure time. This is a promising attribute as only one measurement was required to display the differences in the spectra after accelerated exposure. Also, data presented displayed that the "thick" composites were measurable with the current capabilities of EIS.

Next, multiple EIS experiments were performed on each "thick" composite sample at the designated weathering times much like the "thin" composite measurements. Due to the "thick" cross-section, longer exposure times were required. Longer exposure times were required, compared to the "thin" samples, as a thicker polymeric top layer was observed in the "thick" composites, specifically the S2 Glass® composites. The longer duration would increase the probability of distinguishing the differences observed in the circuit modeled values.

Both six minute and one hour immersion times were subjected to the composites. Similar to the results obtained with the "thin" composites, the trends observed between the 10 minute and 60 minute immersion times were similar with slight changes in the magnitudes. Figure 3.14 displays the circuit modeled constituents versus the ultraviolet exposure time for the S2 Glass® fiber composites immersed for six minutes. It should be noted that each value observed is the average displayed with one standard deviation error bars.

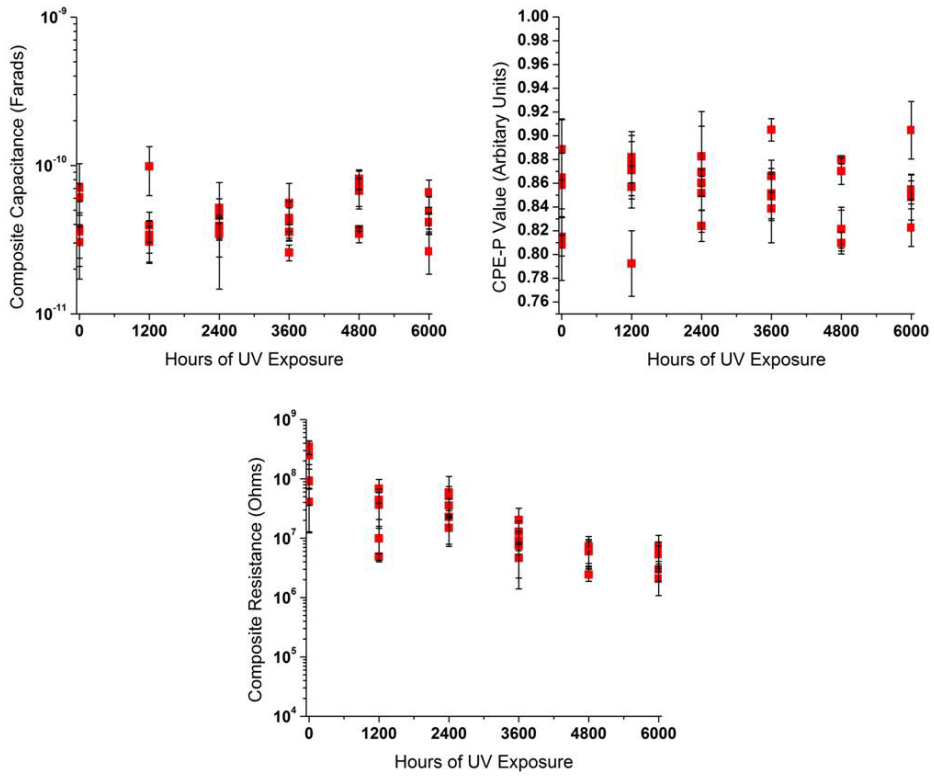


**Figure 3.14 - Composite circuit modeled constituent values as a function of weathering time for "thick" S2 Glass® fiber containing composites including the composite capacitance (upper left), CPE-P value (upper right), and composite resistance (bottom)**

The resistance of the composite does have a decreasing trend with exposure time as was observed for the "thin" S2 Glass® fiber composites. This decrease is accounted for by a more porous structure occurring as the matrix material is removed during ultraviolet exposure. The results indicate that the capacitive attributes (i.e., composite capacitance and CPE-P value) measured during EIS experimentation demonstrated undetectable changes. This was explained by the volume fraction of water present within the composite systems after immersion. The amount of water was too small to adequately change the permittivity and thus the capacitance magnitudes. Figure 3.15 displays the water uptake during the six minute immersion for the phenolic matrix/S2 Glass® fiber composites.

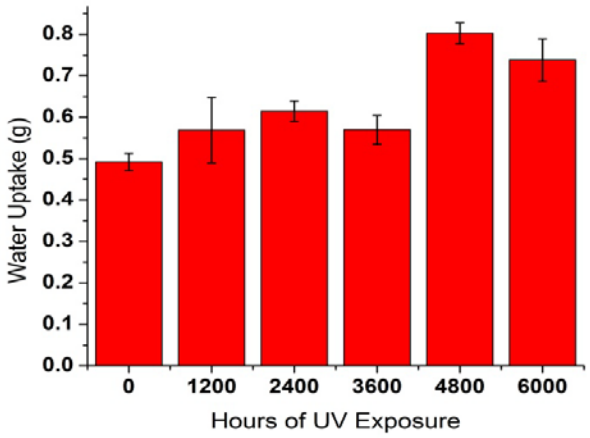


**Figure 3.15 – Water gain during immersion for "thick" S2 Glass® fiber composites**

The water uptake displays a large change from the previous values at 4800 and 6000 hour immersions. The observation also displays a high amount of confidence in the increase in water absorption. The increase in water absorption should demonstrate a noticeable change in the capacitance values; however, the volume fraction of water within the phenolic matrix/S2 Glass® fiber composite is much lower than the "thin" PMC. The slight change in the relative permittivity that may occur is not deducible within the measurement variability associated with the natural variation of the composites. Again, the surface area effect of the electrodes may be counteracting the increase which is expected to occur from increased water absorption.

The "thick" phenolic matrix/Kevlar® fiber composites were also investigated. Again, both 10 minute and 60 minute immersion times were performed on the Kevlar® fiber composites. However, only the 10 minute data is displayed as the trends between the two immersion periods displayed were similar with a shift in the magnitude. As before, the circuit modeled element values for these Kevlar® fiber composites is displayed with one standard deviation for each value in Figure 3.16.

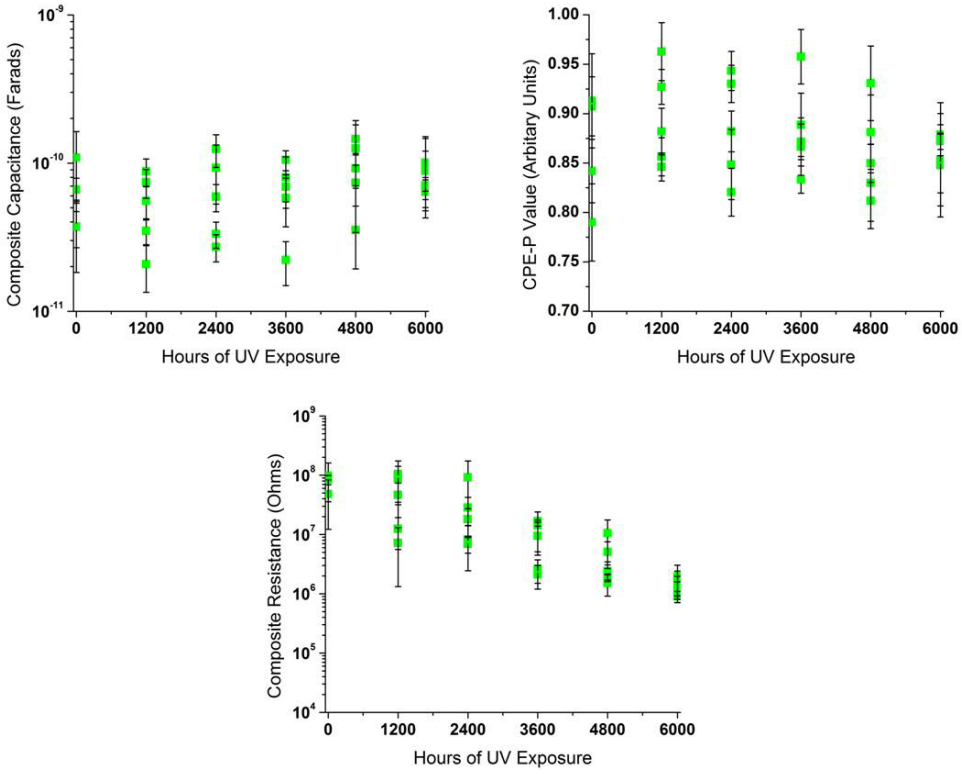


**Figure 3.16 - Composite circuit modeled constituent values as a function of weathering time for "thick" Kevlar® fiber containing composites including the composite capacitance (upper left), CPE-P value (upper right), and composite resistance (bottom)**

The results in Figure 3.16 demonstrate the same trend as the S2 Glass® fiber composites with statistically unchanged capacitive responses. However, CPE-P values of the Kevlar® composites were larger, on average, than the S2 Glass® composites. Again, this can be explained by the fiber and matrix possessing similar resistivity and dielectric properties. The similar properties allow for a more conducive path for electron and ion flow compared to the S2 Glass fiber composites. Increased water uptake is the reason for the unchanging capacitive trend as a discernable increase in water uptake was not observed for the six weathering periods. The weight gain during immersion was more uniform for the case of the Kevlar® fiber composites which is displayed in Figure 3.17.

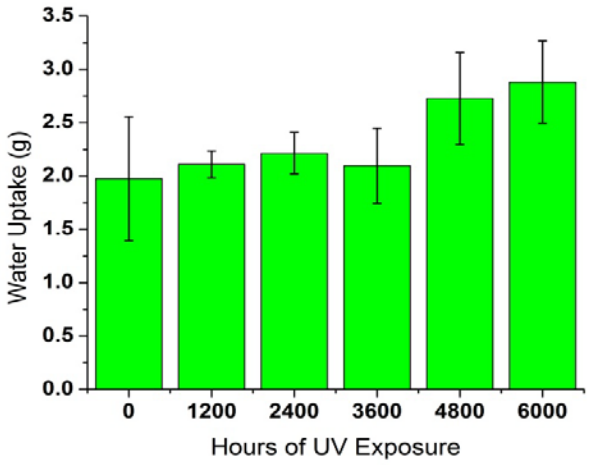


**Figure 3.17 - Water gain during immersion for "thick" Kevlar® fiber composites**

Figure 3.17 reveals an increase in the water uptake during immersion when observing the averages. However, the deviation associated with these measurements displays low confidence in the mean values increasing with accelerated exposure. On the other hand, the resistance displayed a trend of increasing porosity which corresponded to a decrease in impedance as the motion of ions and electrons occurred more freely with increased exposure.

### 3.4 Conclusions

Initial investigation conducted on both composite systems yielded an understanding of the variability of the EIS measurements. However, the capacitance magnitude for the S2 Glass® fiber composites demonstrated a substantial change with longer immersion time. This was not observed with the phenolic matrix/Kevlar® fiber as water uptake occurred quickly causing little difference in the volume fraction of water present. In both composites, the resistance did not display any noticeable changes with increased immersion times. The composite resistance is more closely related to the void content which would not have changed with increased immersion.

Another interesting aspect of the initial experimentation was the low frequency response. The low frequency response demonstrated an increase in impedance without a corresponding phase angle decrease toward a capacitive value. This effect was accounted for by evaporation which occurred as the sample was subjected to ambient conditions during EIS experimentation. Single frequency EIS measurements were conducted at a frequency of 0.1 Hertz to monitor the impedance modulus with time. Both composite systems displayed an increase of impedance with time as evaporation occurred. The composites also demonstrated that with more water present (i.e., one hour immersion as compared to ten minutes) the impedance modulus required longer lengths of time to reach a steady state of impedance.

Next, the influence of ultraviolet radiation on the circuit modeled elements was studied. It was determined that an anomaly occurred within the capacitive nature of the "thin" S2 Glass® composites. An increase in water absorption was observed, but the capacitance magnitude decreased with increased exposure time. This was attributed to possible changes in the electrode area of contact and thickness effects from fiber bridging and swelling of the matrix after immersion. The resistance of the pores in the composite exhibited a decreasing trend which is assumed to be occurring with larger pore formation during ultraviolet weathering. Larger pores cause less impeded flow of ions and electrons during EIS experimentation and thus lower impedance. "Thin" phenolic matrix/Kevlar® fiber composites were also subjected to accelerated ultraviolet weathering. The presence of a peel ply limited the ultraviolet exposure subjected to these samples. It was noted that the presence of the peel ply changed the capacitive values measured while not influencing the resistive values. Therefore, the resistive element was the only circuit element to produce

values which were consistent with the changes from ultraviolet exposure. The resistance was observed to decrease slightly in this composite system which was occurring from increased porosity.

Larger composite samples possessing a thicker cross-section were also studied as these geometries are more realistic for ballistic resistant applications. The thicker cross-sectional composites have not been studied via EIS in literature to-date making this aspect of this research novel. Initial investigation demonstrated that the composite could be analyzed with EIS experimentation if the samples were immersed before conducting the measurement. In fact, an ideal case revealed that each composite could be observed to produce results of decreasing impedance as a function of the weathering time. This is important in the realm of using this methodology as an in-service measurement as smaller sample sizes are more conducive for quick measurements. Likewise, final circuit modeling investigation for each composite at distinct weathering increments revealed trends when statistical evaluation was conducted. Both composite systems demonstrated little change in the capacitance magnitude and the degree to which the composite was acting capacitive. The volume fraction of water was not sufficient enough to change the relative permittivity to be measured with the current methodology. Water uptake displayed an increasing trend with exposure time in both cases which was more than likely from pore formation within the composites. This increase in pore formation is believed to be the reason for the decrease in the circuit modeled resistance. Again, the motion of ions and electrons are less hindered in larger pores making the pathway between the two electrodes less impeded.

Overall, the composite resistance decreased with exposure time in every instance which demonstrates a diminishing effect which may result in a loss of mechanical integrity.

The mechanical properties may be altered and the change in these properties may correspond with the changes observed in modeled resistance. The influence and the correlation of these values will be displayed in Chapter 5 of this thesis.

### 3.5 References


1. Lavaert, V., M. De Cock, M. Moors, and E. Wettinck, *Influence of pores on the quality of a silicon polyester coated galvanised steel system.* Progress In Organic Coatings, 2000. **38**(3-4): p. 213-221.
2. Park, J., G. Lee, H. Ooshige, A. Nishikata, and T. Tsuru, *Monitoring of water uptake in organic coatings under cyclic wet-dry condition.* Corrosion Science, 2003. **45**(8): p. 1881-1894.
3. Zhu, Y., J. Xiong, Y. Tang, and Y. Zuo, *EIS study on failure process of two polyurethane composite coatings.* Progress in Organic Coatings, 2010. **69**(1): p. 7-11.
4. Lide, D., *Handbook of chemistry and physics*. 84th Edition ed. 2003: CRC Press LLC.
5. Jones, R.A.L., *Soft Condensed Matter*. Oxford Master Series in Condensed Matter Physics. Vol. 6. 2002, New York, NY: Oxford University Press.
6. AGY, *High Strength Glass Fibers*. Technical Data, 2006
7. Yao, L., X. Wang, F. Liang, R. Wu, B. Hu, Y. Feng, and Y. Qiu, *Modeling and experimental verification of dielectric constants for three-dimensional woven composites.* Composite Science and Technology, 2008. **68**(7-8): p. 1794-1799.
8. Jorcin, J.-B., M.E. Orazem, N. Pébère, and B. Tribollet, *CPE analysis by local electrochemical impedance spectroscopy.* Electrochimica Acta, 2006. **51**(8-9): p. 1473-1479.
9. Schiller, C.A. and W. Strunz, *The evaluation of experimental dielectric data of barrier coatings by means of different models.* Electrochimica Acta, 2001. **46**(24-25): p. 3619-3625.
10. Matweb: Material Property Data, *Sumitomo Bakelite Durez® 153 Phenolic, Compression Grade* 2011, Matweb.
11. AGY, *Advanced Materials: Solutions for Demanding Applications.* Technical Data, 2004.
12. Glass, R., S. Taylor, G. Cahen, and G. Stoner, *Electrochemical impedance spectroscopy as a method to nondestructively monitor simulated in-service damage in a carbon fiber reinforced plastic.* Journal of Nondestructive Evaluation, 1987. **6**(4): p. 181-188.
13. DuPont, *Technical Guide Kevlar: Aramid Fiber.* Technical Data, 2011.

# CHAPTER 4. SURFACE CHARACTERISTICS OF BALLISTIC RESISTANT POLYMER MATRIX COMPOSITES UPON ULTRAVIOLET EXPOSURE

## 4.1 Introduction

Polymer matrix composites (PMCs) were subjected to accelerated ultraviolet conditions to increase the number of degradation reactions compared to ambient conditions. Ultraviolet conditions are known to change several physical properties associated with PMCs which include: color change, surface roughening, gloss loss, etc. The changes can be detrimental if the intended application serves an aesthetic purpose. Likewise, changes in surface porosity may allow larger amounts of water and salt solution absorption causing increased weight of the structure which offsets the advantageous nature of these materials. Color change of PMCs is a commonly used methodology to examine the extent of weathering as polymers tend to become more yellow with increased exposure. This study examines the changes in color, surface roughness, gloss, and contact angle during accelerated ultraviolet exposure of ballistic resistant PMCs.

## 4.2 Physical Appearance of PMCs Exposed to Ultraviolet Conditions

The changes in physical appearance were vastly different between the two composite systems. This is attributed to the difference between the fibers for the two PMCs as one composite had a S2 Glass® fiber and the other a Kevlar® fiber. S2 Glass® is transparent to the ultraviolet radiation used for exposure while Kevlar® has a large increase in absorption over the spectral distribution present from UVA 340 light source.[1-2] The absorption characteristics led to a more uniform degradation in the case of the Kevlar® fiber as both the matrix, a phenolic polymer plasticized with polyvinyl butyral (PVB), and the Kevlar® fiber contain aromatic groups. Meanwhile, the S2 Glass® fiber did not degrade

noticeably upon accelerated ultraviolet exposure. This led to fiber bridging or the presence of fiber protrusion at the surface of the S2 Glass® fiber composites. Figure 4.1 presents the two "thin" composite systems after six intervals of accelerated weathering.

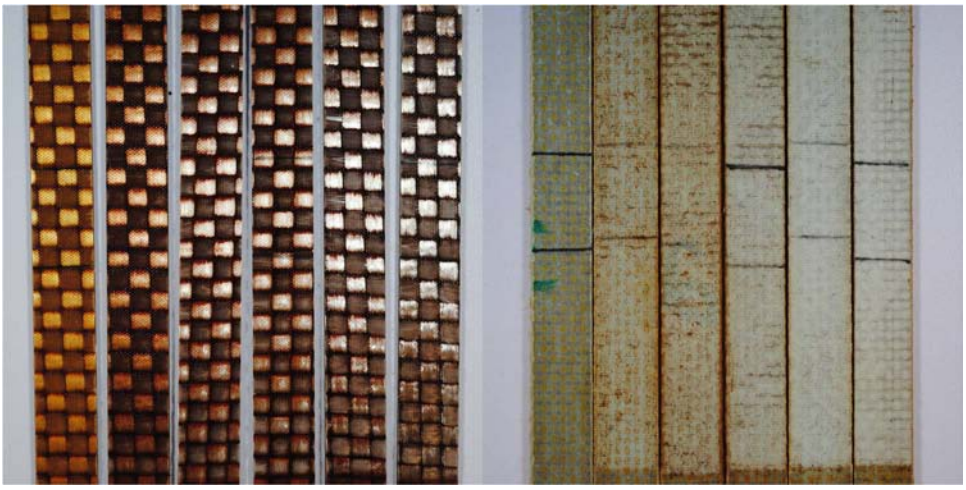

**Figure 4.1 - Physical appearance after accelerated exposure for "thin" phenolic matrix/S2 Glass® fiber composite (left) and phenolic matrix/Kevlar® fiber composite (right). Each set contains 0, 600, 1200, 1800, 2400, and 3000 hours of exposure starting at left and moving right**

It should be noted that the black lines present at the middle of the samples are marked for the EIS experimentation area. A substantial color change occurred for both composite systems when compared to the initial color. The phenolic matrix/S2 Glass® fiber composites tended to shift toward a darker color than the initial state as well as becoming more glossy with exposure time. On the other hand, the phenolic matrix/Kevlar® fiber composites shifted toward a brown color in the intermediate weathering periods and then to a lighter color after longer exposure times. However, the Kevlar® fiber composites had a well intact peel ply which served as a barrier to post-manufacturing handling which was mistakingly not removed prior to weathering. The color change observed was only

from the weathering of the peel ply. Fiber bridging could be observed at 1200 hours of accelerated ultraviolet exposure with promintent bridging occuring in the 2400 and 3000 hours sample sets for the phenolic matrix/S2 glass® composites. Figure 4.2 displays the surface of the "thin" S2 Glass® composites after the six weathering periods.

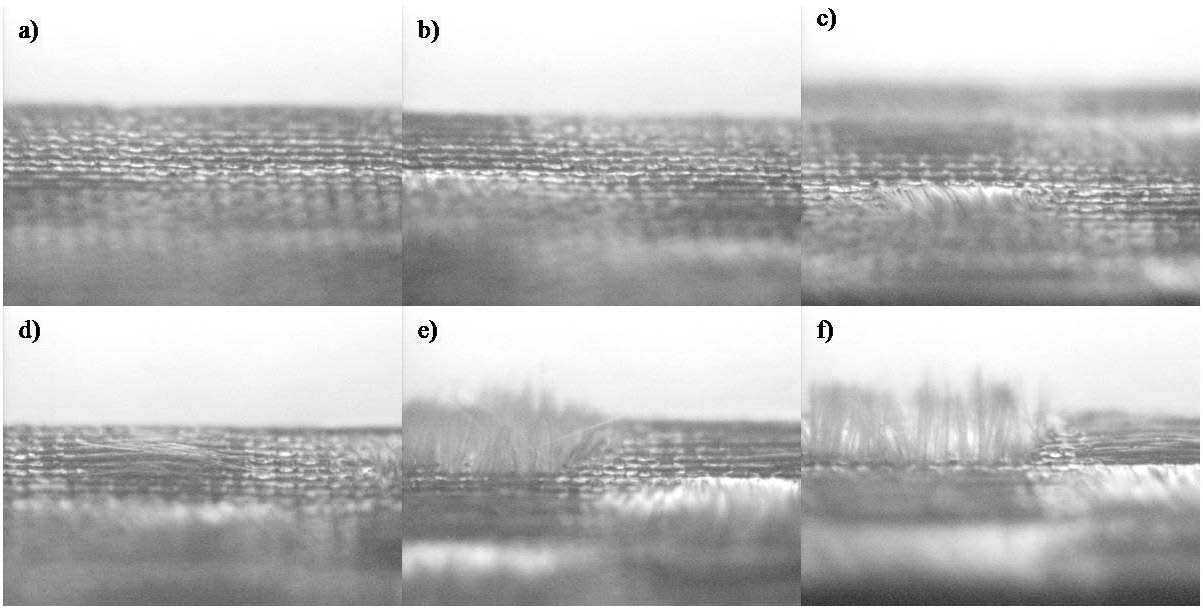


**Figure 4.2 - Phenolic matrix/S2 Glass® fiber composites after weathering a) 0 hours b) 600 hour c) 1200 hours d) 1800 hours e) 2400 hours and f) 3000 hours**

Initially, the surface pattern displays a phenolic matrix rich layer with no fiber bridging. As the exposure time increases, more fiber bridging is observed in the top most fiber weave. Fiber bridging was due to the fiber closest to the surface becoming exposed at this position. The degradation demonstrates fiber bridging in a checkered pattern with fiber bridging in one area, or square, and phenolic polymer in the other. Finally, at 3000 hours of accelerated exposure, enough matrix material has been degraded to expose fiber in both the weft and warp fiber directions which is observed in Figure 4.2f. There is still a small amount of polymer present between the fiber bridged regimes in the 3000 hour sample set as the thickest polymer region occurs at these points.

Fiber bridging was not apparent in the phenolic matrix/Kevlar® fiber composites as the peel ply prevented any fibers from coming to the surface. The lighter circles were present at 0, 600, and 1200 hours exhibiting regimes which were polymer rich as observed via visual microscopy making the initial removal of the peel ply very difficult. Figure 4.3 reveals the edge view of the Kevlar® fiber composite peel ply at the six weathering times.

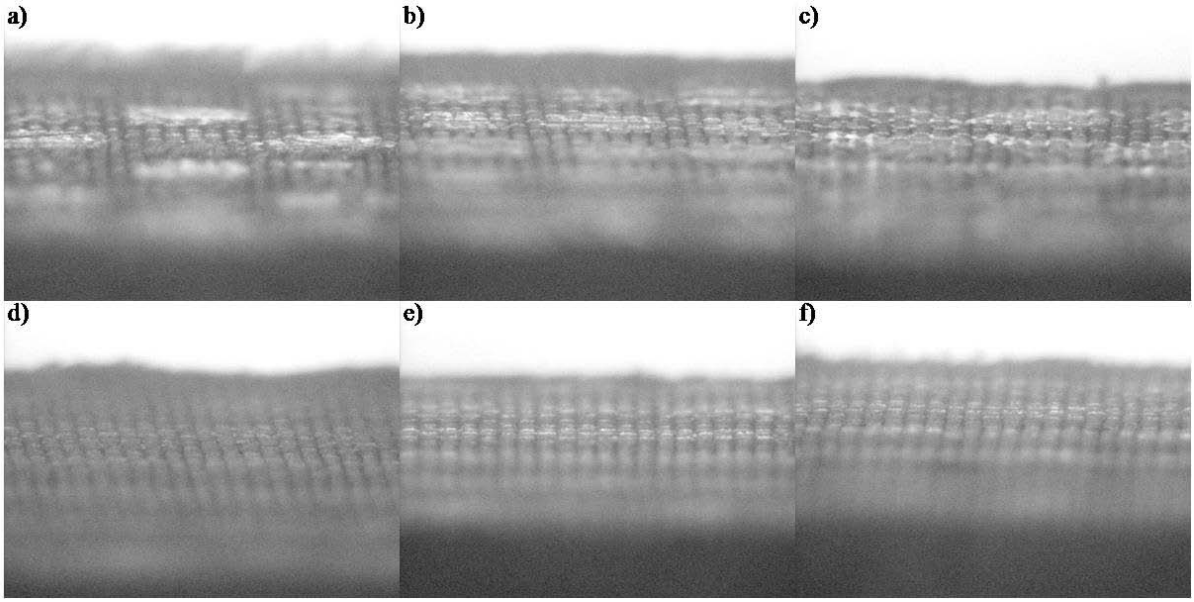


**Figure 4.3 - Phenolic matrix/Kevlar® fiber composites after weathering a) 0 hours b) 600 hour c) 1200 hours d) 1800 hours e) 2400 hours and f) 3000 hours**

After 1800 hours of accelerated exposure, it was observed that the polymer rich regimes are no longer apparent. Removal of the peel plies was easier at this time as the polymer was no longer present. Irradiation intensities were observed for the initial peel ply and after 3000 hours. It was observed that the irradiation increased from 0.06 watts per square meter initially to 0.12 watts per square meter at 340 nanometers which is attributed to the increase in porosity of the peel ply as a function of weathering.

Investigation of the "thick" composite samples demonstrated similar trends during exposure for the phenolic matrix/S2 Glass® fiber composites as the color became a darker

color with a glossier surface. However, the phenolic matrix/Kevlar® fiber composites demonstrated a noticeable difference in the color aspects of appearance. Figure 4.4 displays the physical appearance of the "thick" composite systems after the six exposure periods with the "thick" Kevlar® fiber composites demonstrating the color with the peel ply not present.

**Figure 4.4 - Physical appearance after accelerated exposure for "thick" phenolic matrix/S2 Glass® fiber composite (left) and phenolic matrix/Kevlar® fiber composite (right). Each set contains 0, 1200, 2400, 3600, 4800, and 6000 hours of exposure starting at left and moving right**

The Kevlar® fiber composites displayed a yellow initial color compared to the green colored composites present in the "thin" peel ply covered samples because the peel ply was removed after manufacturing. Upon removal of the peel ply, the initial color was similar. The weathering lengths were doubled in the case of the "thick" samples as compared to the "thin" samples. However, several physical characteristic trends in both thickness configurations remained similar over the duration of the accelerated exposure. The matrix removal during degradation is similar in both the "thin" and "thick" instances, but a thicker polymeric top layer was present in the "thick" composites allowing for greater weathering durations before fiber bridging was observed. The gloss was also similar as the 4800 and

6000 hour sample sets displayed a glossier appearance for the phenolic matrix/S2 Glass® fiber composites. The extent of gloss increase was not readily observed in the phenolic matrix/Kevlar® fiber composites, but was distinguished with quantitative analysis of gloss. The use of numerical methods for determining the changes in the surface characteristics are presented in the following sections to provide more insight into the trends observed.

### 4.3 Color of PMCs Exposed to Ultraviolet Conditions

Color changes in the CIE Lab color coordinate system were observed for each coordinate individually as well as the overall color change (i.e., ΔE). Figure 4.5 displays the three color coordinates as well as the overall change in color for the "thin" phenolic matrix/S2 Glass® fiber composites during the six weathering periods.

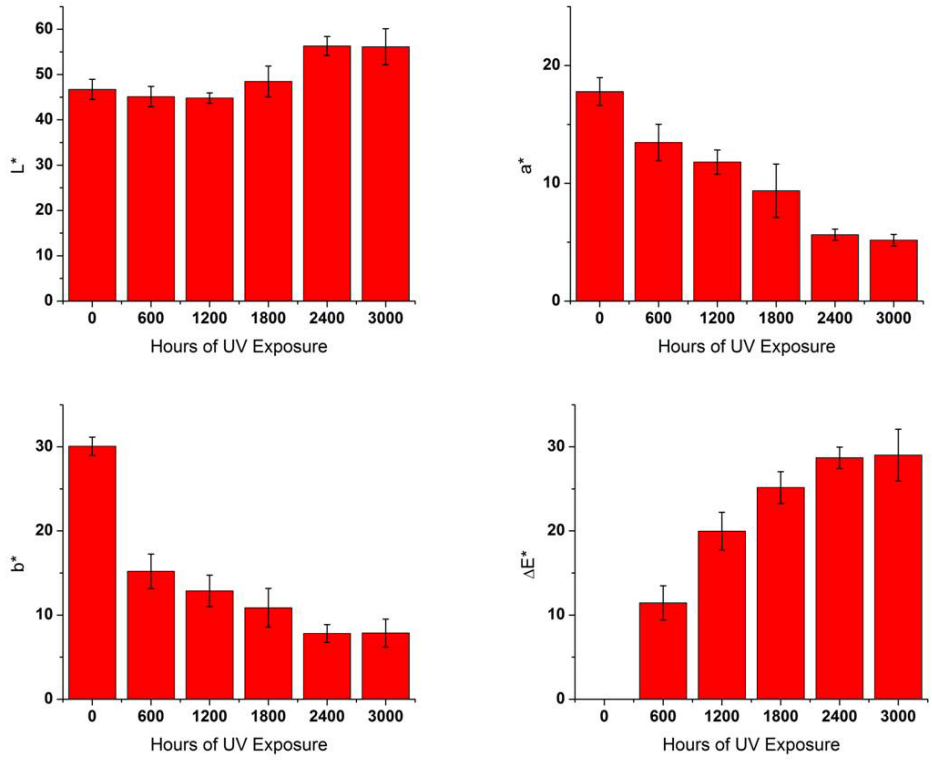


**Figure 4.5 - Numerical color results for the "thin" phenolic matrix/S2 Glass® fiber composites including L* (top left), a* (top right), b*(bottom left), and ΔE (bottom right)**

The L* color value drops slightly, on average, before increasing at the 2400 and 3000 hour time periods. This suggests that the S2 Glass® composites become slightly darker before changing to a lighter color. The predominance of fiber at the surface caused the 2400 and 3000 hour sample sets to appear lighter as light is reflected more easily. The a* value displayed a decrease over exposure time which demonstrates the composite shifting from a red color toward a green color. However, the shift may be toward the green, but the value is positive affirming it is more red than green. The b* value is a measure of the yellow to blue colors with yellow being on the positive axis. This value is considered the main indication of weathering degradation occurring in polymeric materials.[3-6] However, the common polymer binder systems monitored are either clear or white. The initial b* value for the phenolic matrix/S2 Glass® composites are far more yellow than blue, as Figure 4.5 suggests, but the shift in this instance is toward a blue value. An initial drop at 600 hours is observed before minor alterations in b* are observed. Lastly, the overall color change increased before remaining constant after 2400 hours.

Investigation of the "thin" Kevlar® fiber composites revealed that the lightness value (i.e., L*) displayed an increasing value with increasing exposure time which was observed visually. Little confidence is shown in the a* value changing in the first four time periods, but at the 2400 and 3000 ultraviolet exposure hours the a* become more green than the initial value. Similarly, the b* value showed little confidence in the initial increase, but overall the final time period suggests a more blue color. Finally, the color change increases with exposure time before a large increase in the 3000 exposure hour sample set. This data suggests that the peel ply layer was also undergoing photodegradation under the accelerated weathering conditions. Weathering of the peel ply

restricted the composite substrate from experiencing ultraviolet photodegradation. Figure 4.6 reveals the color characteristics of the "thin" Kevlar® fiber composites.

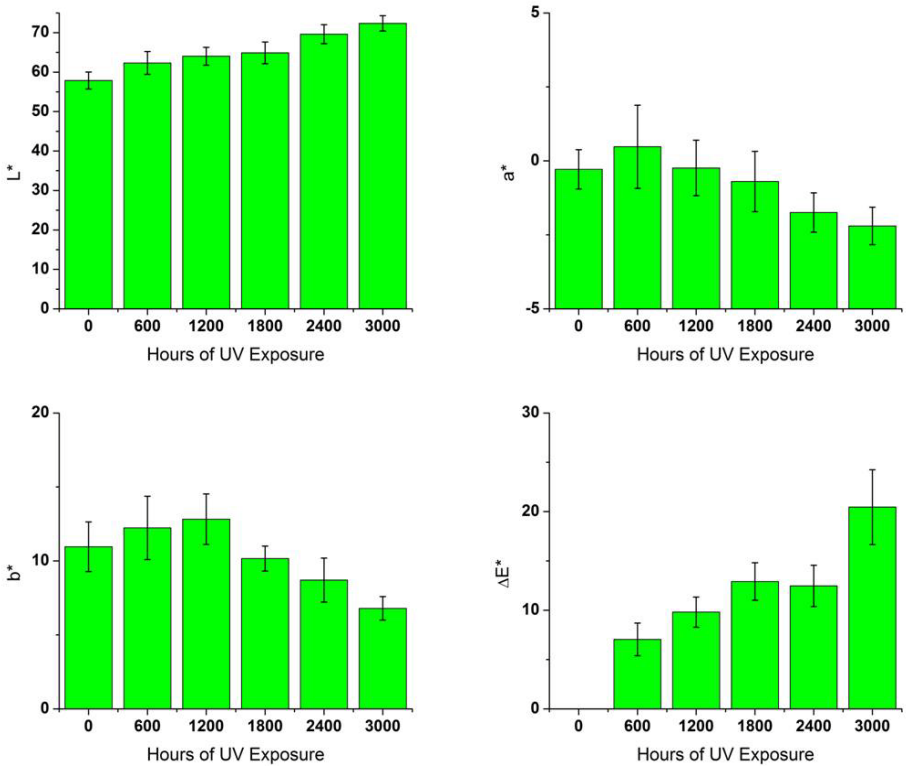


**Figure 4.6 - Numerical color results for the "thin" phenolic matrix/Kevlar® fiber composites including L* (top left), a* (top right), b*(bottom left), and ΔE (bottom right)**

Numerical color investigation of the "thick" S2 Glass® fiber composites was also examined. The trends observed in the L* and b* values are similar to that of the "thin" phenolic matrix/S2 Glass® composite samples. A larger change in the L* value after one period of exposure was accounted for by the "thick" samples being lighter at the onset of exposure which may be accredited to the composite manufacturing process. The high temperature associated with the autoclaving manufacturing process may have begun thermal oxidation processes which have been observed to cause a color change in phenolic compounds.[7] Differences in the lightness were observed upon initial investigation of the

samples. However, the lightness does increase with longer exposures because fiber bridging occurred in the thicker samples also. Initially the a* value was much lower in the "thick" samples, but the trend, once accelerated exposure was subjected to the samples, was similar in both sample geometries. The b* values were initially similar and the trends were similar in both the "thick" and "thin" samples. The overall color change exhibited a large increase at 1200 hours before remaining relatively stable. Figure 4.7 reveals the color values for the "thick" S2 Glass® fiber composites after exposure.

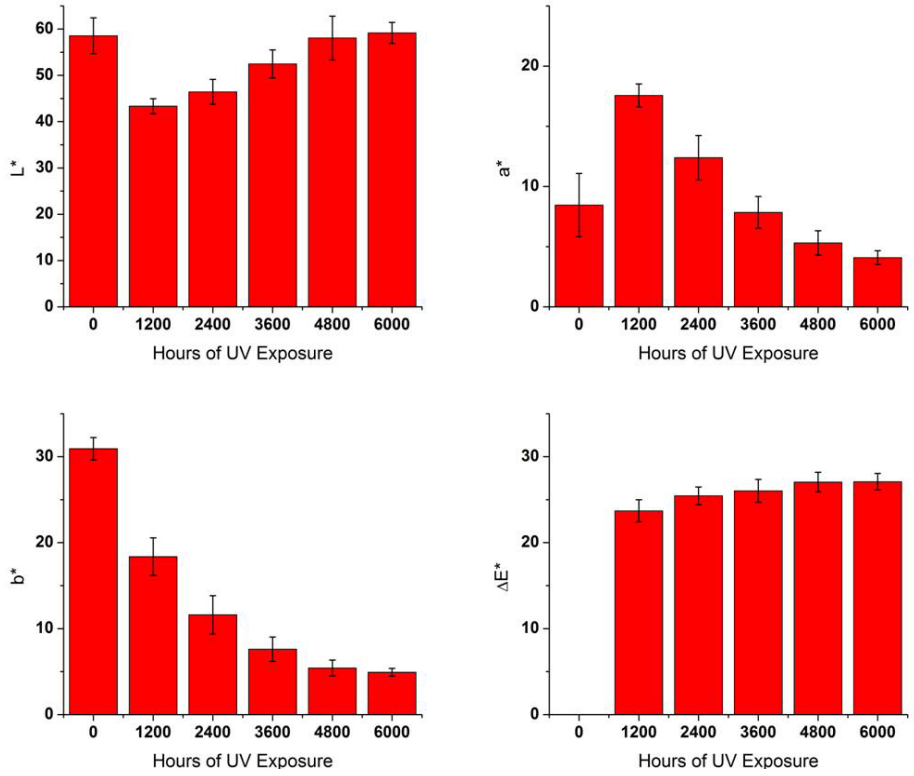


**Figure 4.7 - Numerical color results for the "thick" phenolic matrix/S2 Glass® fiber composites including L* (top left), a* (top right), b*(bottom left), and ΔE (bottom right)**

"Thick" composites containing Kevlar® fiber were also studied, with the peel ply removed, to determine the color characteristics. Many differences in the values and trends were observed due to the peel ply not being present on the "thick" samples. Figure 4.8

displays the color coordinates of the “thick” phenolic matrix/Kevlar® fiber composites for the six accelerated exposure times.

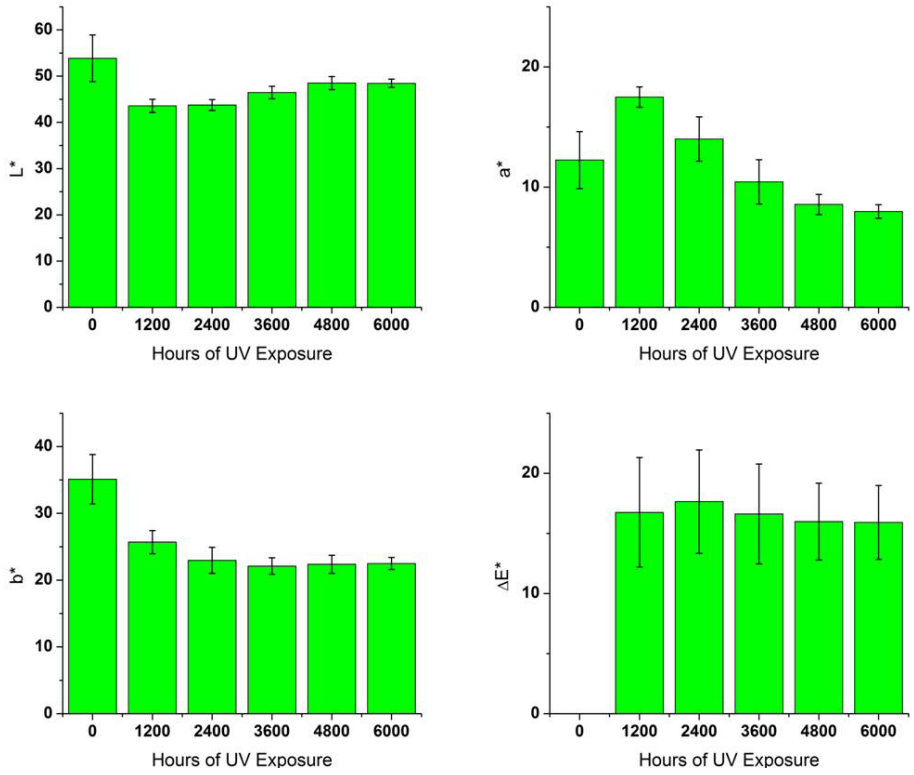


**Figure 4.8 - Numerical color results for the "thick" phenolic matrix/Kevlar® fiber composites including L* (top left), a* (top right), b*(bottom left), and ΔE (bottom right)**

As expected, there was a decrease of the L* value at 1200 hours of exposure before a gradual increase in lightness. The a* value increased in redness at 1200 hours before shifting toward a green value. The b* color values displayed a drop at 1200 hours of exposure before remaining unchanged for the final four time periods. Overall, the color change was large at 1200 hours, but remained approximately the same as both the L* and b* value deviated very small amounts in each of the last four exposure periods.

Even though the weathering time periods were different for the two geometries, the long exposure term trends were similar in the case of the S2 Glass® fiber composites. On

the other hand, the “thick” phenolic matrix/Kevlar® fiber composites demonstrated vastly different trends as the peel ply was removed causing a greater photodegradation to occur.

### 4.4 Surface Profile of PMCs Exposed to Ultraviolet Conditions

The surface changes incurred during weathering were also observed via optical profilometry. Figure 4.9 depicts the surface topography for the “thin” S2 Glass® fiber composites at the six exposure periods.

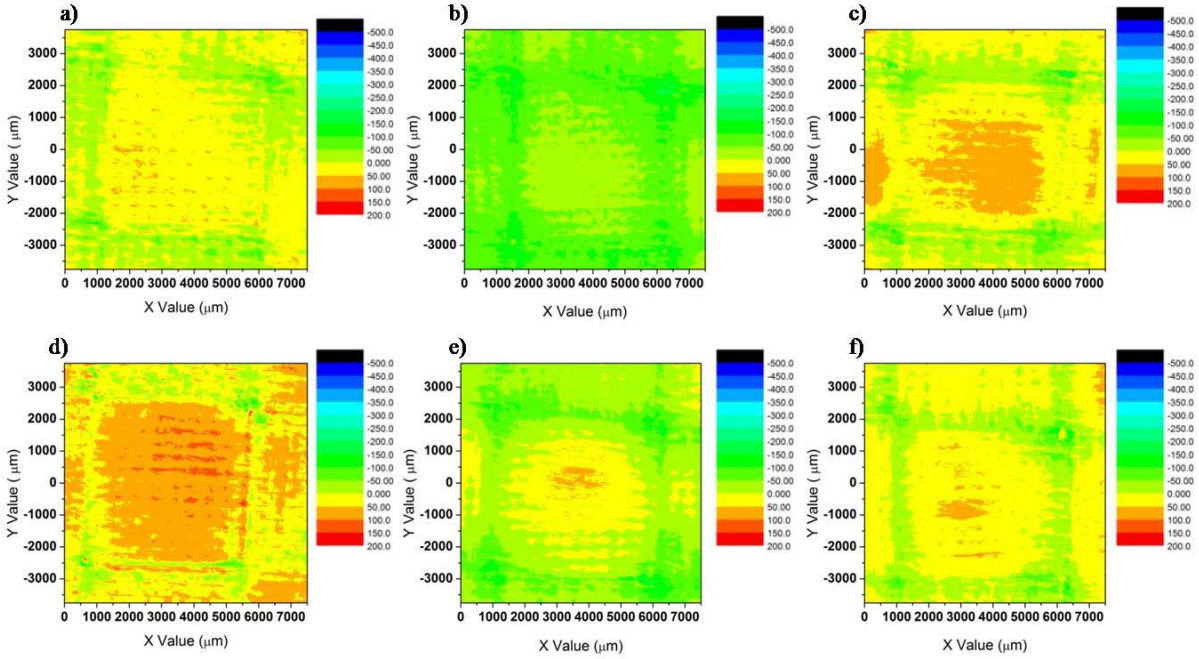


**Figure 4.9 – Surface topography for phenolic matrix/S2 Glass® fiber composite at a) 0 hours b) 600 hour c) 1200 hours d) 1800 hours e) 2400 hours and f) 3000 hours**

The square observed in the middle of each scan represents the area where the fiber weave comes close to the PMC surface which has also been observed in literature.[8] The over and under weaving of the fiber tows leaves a polymer rich zone around these squares which can also be observed in Figure 4.9. Profiles 4.9c and 4.9d suggest the breakthrough of fiber at the surface which was observed visually. Profiles 4.9e and 4.9f visually appear to have less fiber bridging occurring; however, this effect is observed visually and may be

diminished in the profiles as the polymer rich regimes become deeper from accelerated exposure. This statement is further reinforced when examining the surface roughness parameters of the area scan experiments. The emergence of fiber bridging began at 1200 hours of exposure which was also indicated with a noticeable surface roughness increase from the surface roughness characteristics. Figure 4.10 reveals the surface arithmetic and root-mean square (RMS) roughness for the six weathered "thin" S2 Glass® composite specimens.

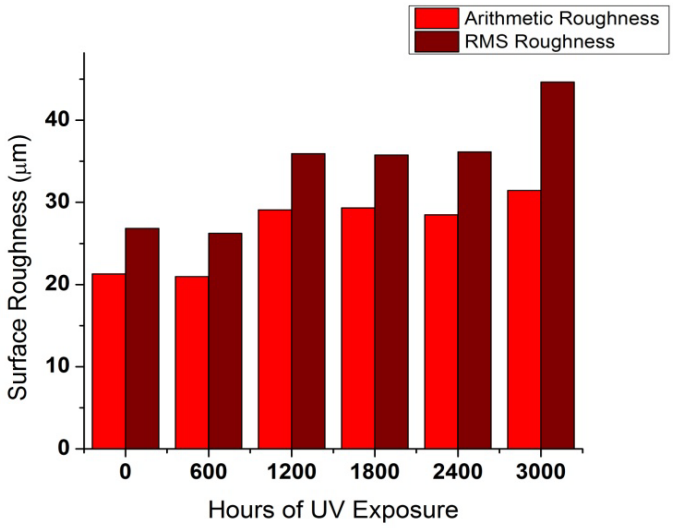


**Figure 4.10 – Surface roughness parameters for S2 Glass® fiber composites**

The surface roughness remained relatively stable until 3000 hours of accelerated ultraviolet exposure. An increase occurred in the both roughness parameters which may be indicative of the polymeric rich surround becoming more degraded (i.e., deeper) and the fiber surface remaining stable causing an increase in overall roughness.

The surface profile of the phenolic matrix/Kevlar® fiber composites was not studied as removal of the peel ply would cause significant mechanical damage to the composite. The weathering duration would not be correlated to the other composites as well due to the ultraviolet screening influence of the peel ply. Also, the "thick" samples could also not be

measured as the larger cross sections were not measurable due to the limitations of the optical profilometer.

### 4.5 Gloss of PMCs Exposed to Ultraviolet Conditions

Gloss values were measured throughout the ultraviolet exposure at three different angles. The three angles included 20°, 60°, and 85° with the last angle typically being utilized for rough surfaces as the near grazing angle allows a higher probability of the signal reaching the detector. Figure 4.11 reveals the gloss values of the three angles for the "thin" phenolic matrix/S2 Glass® composites.

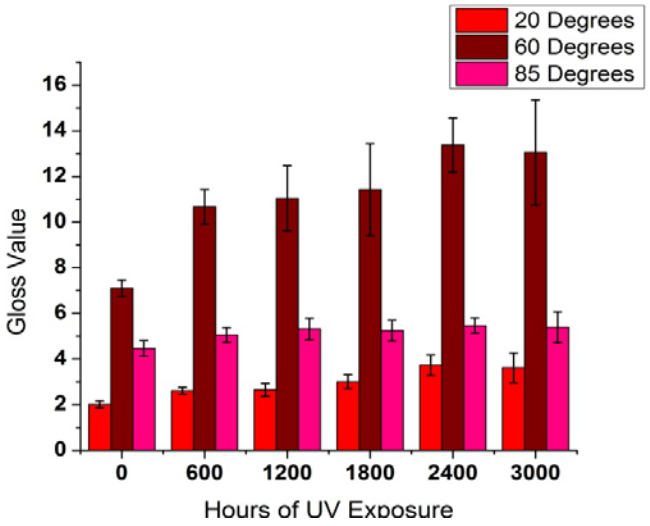


**Figure 4.11 – Gloss values of "thin" S2 Glass® fiber composites for the six weathering periods**

The results of Figure 4.11 demonstrate that the material is increasing in gloss with exposure time which has also been observed in literature for polymeric composites.[6] The 20° gloss measurement revealed a progression of increasing gloss, but the values were extremely low compared to traditional substrates. When measuring the 60° angle, the largest increases in gloss were observed with time. Between 600 and 1800 hours the surface increased in gloss by a combination of erosion of matrix and emergence of the S2

Glass® which reflects more light than the matrix material. At 2400 and 3000 hours another increase was observed, on average, as fiber bridging was observed visually. Lastly, the 85° angle demonstrated little change from the initial value. There was a slight increase at 600 and 1200 hours of exposure before stabilizing. This could be explained by a surface smoothing, on the macro scale, from erosion of matrix material before the long exposure times when fiber became exposed. After 1800 hours, fiber was present at the surface which does not degrade with increased exposure time creating a stable gloss value. Again, the gloss values of the "thin" Kevlar® fiber composites were measured, but the peel ply attached to the composite did not allow for an efficient measurement of gloss for the underlying composite system.

The larger composite specimens were also measured for gloss over the duration of the accelerated exposure. It was observed that all gloss angles demonstrated a significant change from the initial value at the longest exposure times. Figure 4.12 reveals the gloss values for the three gloss angles of the "thick" phenolic matrix/S2 Glass® fiber composites.

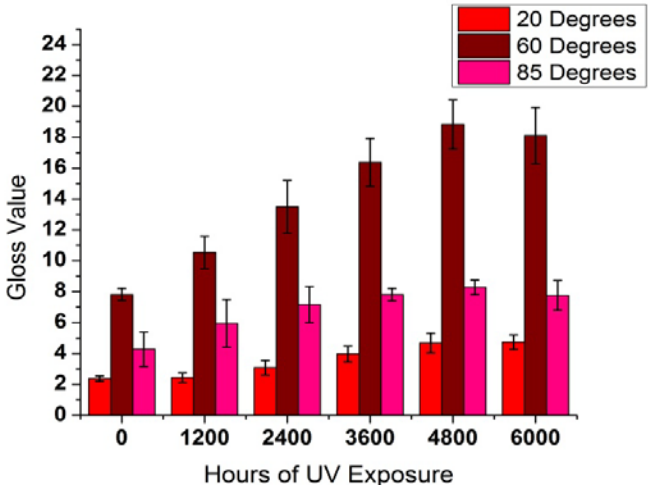


**Figure 4.12 - Gloss values of "thick" S2 Glass® fiber composites for the six weathering periods**

Again, the 60° gloss angle revealed the largest changes from the initial value. All angles exemplified the same gloss values as the "thin" composite specimens of the same composition. This verifies that the initial gloss values were dependent on the polymeric top layer, but upon exposure the values became slightly different as the thickness of the top layer is assumed to be different in each instance. The 20° and 60° gloss angles demonstrated noticeable changes during the exposure while the 85° did reveal a statistically significant change from the initial value at 3600 hours. At 3600 hours, the "thick" samples had fiber bridging beginning to occur which is responsible for the large change from the initial value before remaining stable for the last three weathering periods. Statistically, the last three weathering periods displayed stable values that were all significantly different than the initial value. Visually, this was observed as the fiber emergence became apparent at this exposure time. Figure 4.13 displays the gloss values of the phenolic matrix/Kevlar® fiber composites.

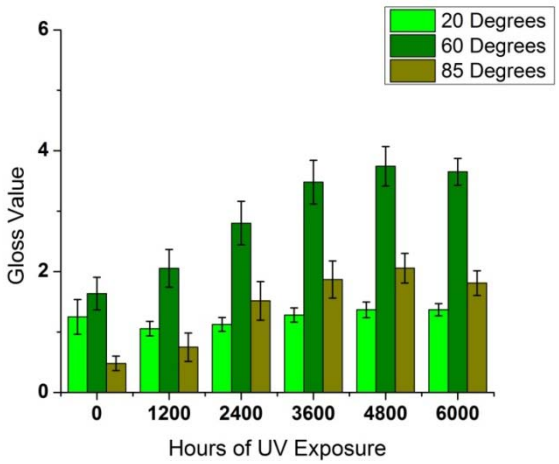


**Figure 4.13 - Gloss values of "thick" Kevlar® fiber composites for the six weathering periods**

As before, the 60° gloss angle revealed the largest change in gloss over the exposure time, but the gloss values are much lower than the S2 Glass® composites. The

20° gloss angle remained unchanged during exposure with a large variation initially. Much like the "thick" S2 Glass® composites at the 60° gloss value, the matrix erosion during weathering occurs to expose fiber which was glossier than the matrix material. This interpretation was visually observed with an increase of gloss after 3600 hours of exposure in Figure 4.4. Lastly, the surface also displayed a glossier finish at 85° as the incurred weathering increased, but after 2400 hours approximately the same gloss value was observed which may be accounted for the with the beginning of fiber protrusion. This again was accounted for by the emergence of fiber scattering which scatters more of the incident light.

### 4.6 Water Contact Angle of PMCs Exposed to Ultraviolet Conditions

Water contact angle is an indirect measure of a material's surface energy and is dictated by the angle formed at the water/material interface. The water contact angle can change over exposure time from a multitude of factors including both a surface energy change and a surface profile change. Figure 4.14 displays the water contact angle for the "thin" S2 Glass® composites.

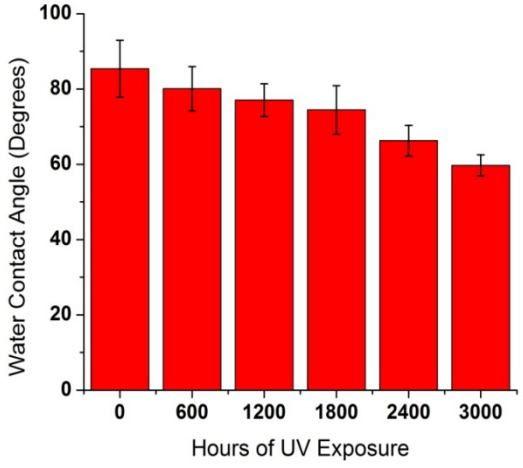


**Figure 4.14 – Water contact angle over exposure time for "thin" phenolic matrix/S2 Glass® fiber composites**

A decrease in the water contact angle was observed during the composite weathering. However, it was not until 2400 hours of ultraviolet exposure that the water contact angle was noticeably different. This could be due to the emergence of fiber at the surface. A wicking effect was noticed at later exposure times as the droplet of water would spread upon contact with the composite substrate. The constant volume of water was allowed to spread over a larger area reducing the angle of contact. The measurements after 3600 hours did not allow the system to achieve equilibrium, but a constant time of three seconds was used between water placement and measurement. Large variations in the samples were noted as the composite surfaces tended to have differences in surface structure initially. Also, fiber bridging did occur to some extent at 1200 hours, but was not observed in each sample leading to higher deviations from the average.

Unlike the "thin" samples of the same composition, the results of the "thick" S2 Glass fiber composites reveal no statistical change during the accelerated exposure. Figure 4.15 displays the water contact angle for the "thick" S2 Glass® fiber composites.

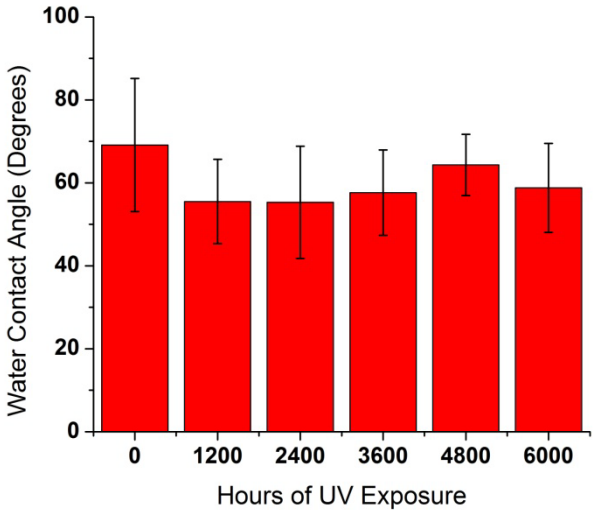


**Figure 4.15 – Water contact angle over exposure time for "thick" S2 Glass® fiber composites**

On average a decrease was observed, but very little significance was associated with this observation. The large variations are again due to the inconsistency of surface roughness at the local measurement level along with the difference from sample to sample in terms of when fiber bridging begins.

Contact angle measurements were also performed on the "thick" Kevlar fiber® composites. It was observed, on average, a trend of decreasing water contact angle was occurring. However, a statistically significant decrease, of one standard deviation difference, was observed from the 3600 hour water contact angle to the initial value. Figure 4.16 exhibits the values of water contact angle over exposure for the "thick" phenolic matrix/Kevlar® fiber composites.

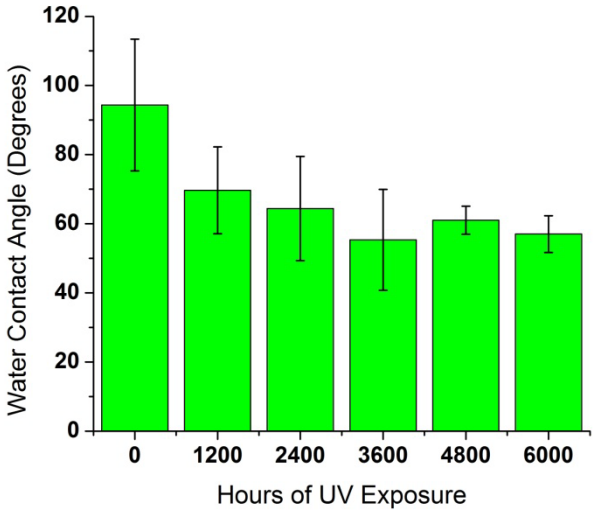


**Figure 4.16 - Water contact angle over exposure time for "thick" phenolic matrix/Kevlar® fiber composites**

At 3600 hours a relatively large deviation was observed, but smaller values were exhibited in 4800 and 6000 hours. This again was attributed to the emergence of fiber at these weathering periods as the 3600 hour value had a difference in value greater than one standard deviation. The Kevlar® fiber exhibited a more stable surface after the matrix

material was removed which led to smaller standard deviations. Water wicking still occurred, but to a lesser extent than the S2 Glass® fiber composites.

Overall, the S2 Glass® samples displayed little stability once fiber emerged at the surface as water wicking became a factor in the instability of the composite surface. This was especially evident in the "thick" S2 Glass® composites. Conversely, the Kevlar fiber composites demonstrated less wicking at the surface, but the results displayed larger deviations from the mean. It is assumed that the water contact changed in both composite systems due to changing surface roughness and increased fiber interaction.

**4.7 Conclusions**

The physical appearance of the composites was initially studied with visual assessment and edge profiles. It was observed that the "thin" and "thick" composites demonstrated similar characteristics except for the "thin" Kevlar® composites. A peel ply was attached to the composites because removal of the well intact protective layer might have caused significant mechanical damage. The matrix material in the Kevlar® fiber composites could be observed protruding through the peel ply in the edge view.

Color measurements were recorded over exposure time for both "thin" and "thick" composites. An overall color change was observed in for all samples. The "thin" S2 Glass® composites demonstrated an increase in lightness and a decrease in the a* and b* values suggesting the system becoming more green and blue, respectively. However, the S2 Glass® composite remained positive in both the a* and b* scales indicating the color was still more red than green and more yellow than blue. The peel ply attached to the "thin" Kevlar® fiber also displayed a color change, along with an increase in irradiation intensity which demonstrates peel ply weathering. In terms of the "thick" composites, a

large change in color was observed at 1200 hours before remaining relatively stable. Both systems exhibited a decrease in lightness before a gradual increase back toward the original value. The a* value demonstrated an increase at 1200 hours before gradually decreasing. Also, the b* value decreased a significant amount at 1200 hours before decreasing gradually. The major contribution to the color change was due to the large change in the b* value in both instances.

The surface roughness area scans were monitored for the "thin" S2 Glass® composites only as the "thin" Kevlar® fiber composites illustrated the deviation of the peel ply which was not of importance in this instance. The "thin" S2 Glass® composites revealed a surface roughening effect over the exposure times, and large values were obtained once the fiber began to emerge at the composite surface. The S2 Glass® is transparent to the ultraviolet light provided by the UVA lamps utilized during accelerated weathering. This led to the S2 Glass® fiber remaining visually unchanged while the matrix material degraded and created deeper crevices. Overall, the surface at 3000 hours revealed large amounts of fiber present with small regimes of phenolic polymer around the outside of the fiber tow squares.

Gloss was monitored with exposure time to observe the effect of matrix degradation and fiber bridging. A large increase in the 60° gloss value was observed in both the "thin" and "thick" composites for both material systems. The 20° gloss value revealed an increase in the S2 Glass® composites, but not in the Kevlar® fiber composites. The 85° gloss value may be an indication of when the fiber emergence becomes prominent after during accelerated exposure. The near grazing angle may have be an early indication of fiber protrusion because the value stabilizes after fiber exposure which was observed in the

S2 Glass® fiber composites. The stability in the gloss value at 85° stems from the S2 Glass® fiber not degrading with increased exposure making the gloss value only dependent on the fiber which does not degrade with increased exposure.

The water contact angle exhibited a decrease with exposure time for the "thin" S2 Glass® composites, but little change was observed in the "thick" S2 Glass® composites. The averages of the contact angle demonstrate an initial decrease at 1200 hours of exposure before remaining stable, but large deviations create little confidence in these finding. Large deviations are perhaps associated with local variations in the composite surfaces along with the change in when fiber bridging occurred. Lastly, at the 3600, 4800 and 6000 hour exposure periods, a change, of one standard deviation, could be observed from the initial value. This is again due to fiber emergence at the surface leading to water wicking which results in lower water contact angles. This methodology also provides insight to when the fiber bridging dominates the surface characteristics.

Overall, it was determined that the fiber protrusion occurs between 2400 and 3600 hours for the "thick" composite systems as multiple methods suggest. In the "thin" S2 Glass® composite systems fiber bridging dominates the surface properties after 2400 hours in the gloss and contact angle measurements, but fiber bridging was observed visually as early as 1200 hours. As a protective peel ply was adhered to the "thin" phenolic matrix/Kevlar® fiber composites, surface characteristics of the actual composite system were not monitored due to the changing amount of ultraviolet radiation subjected to the composites.

**4.8 References**

1. AGY, *S2 Glass Armor Systems.* Technical Data, 2004.
2. DuPont, *Kevlar: Aramid Fiber.* Technical Data, 2011.

3. Boyle, D. and B. Gesner, *Aging of polyblends.* Journal of Applied Polymer Science, 1968. **12**(5): p. 1193-1197.
4. Pimentel Real, L., A. Ferraria, and A. Botelho do Rego, *The influence of weathering conditions on the properties of poly (vinyl chloride) for outdoor applications. An analytical study using surface analysis techniques.* Polymer testing, 2007. **26**(1): p. 77-87.
5. Ito, M. and K. Nagai, *Evaluation of degradation on Nylon 6 and Nylon 6/montmorillonite nanocomposite by color measurement.* Journal of Applied Polymer Science, 2008. **108**(6): p. 3487-3494.
6. Correia, J.R., S. Cabral-Fonseca, F.A. Branco, J.G. Ferreira, M.I. Eusebio, and M.P. Rodrigues, *Durability of pultruded glass-fiber-reinforced polyester profiles for structural applications.* Mechanics of Composite Materials, 2006. **42**(4): p. 325-338.
7. Lochte, H.W., E.L. Strauss, and R.T. Conley, *The thermo-oxidative degradation of phenol–formaldehyde polycondensates: Thermogravimetric and elemental composition studies of char formation.* Journal of Applied Polymer Science, 1965. **9**(8): p. 2799-2810.
8. Kuhn, J. and P. Charalambides, *Modeling of plain weave fabric composite geometry.* Journal of Composite Materials, 1999. **33**(3): p. 188.

# CHAPTER 5. MECHANICAL AND BALLISTIC PROPERTIES OF BALLISTIC RESISTANT POLYMER MATRIX COMPOSITES UPON ULTRAVIOLET EXPOSURE

## 5.1 Introduction

Mechanical and ballistic properties of the weathered PMCs were obtained to quantify the degradation of these composites after accelerated ultraviolet exposure. Ultraviolet exposure is known to degrade polymers with aromatic structures which are within both the phenolic matrix and Kevlar® fibers. Tensile and flexural properties were obtained at six exposure periods of accelerated weathering. A comparative ballistic study was also performed on the two PMCs to determine the effect of ultraviolet exposure on the ability of the composite to resist ballistic penetration. In fibrous composites, the ballistic resistant capabilities are dependent on fiber's ability to transfer the absorbed energy away from the area of impact which may be comprised if long term continuity of the fiber is lost from ultraviolet exposure. The ultimate tensile strength of the S2 Glass® composites was compared to the EIS circuit modeled composite resistance. The correlation of the two material properties determines the applicability of utilizing EIS as a structural health monitoring technique.

## 5.2 Tensile Properties of PMCs Exposed to Ultraviolet Conditions

Mechanical integrity of composite materials is known to change under ultraviolet exposure as both the matrix and reinforcements can degrade. Each composite structure studied contains a phenolic matrix which is highly aromatic and is known to have a change in mechanical integrity after exposure to ultraviolet conditions.[1] A typical stress/strain curve is depicted in Figure 5.1, demonstrating several characteristics for each material.

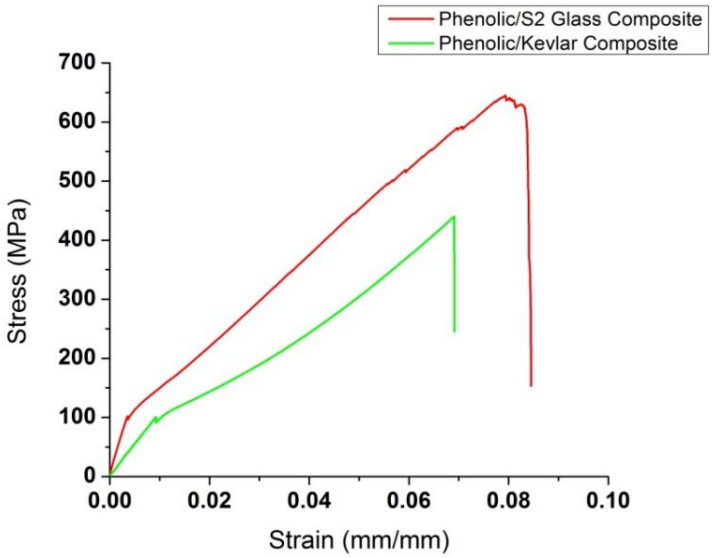


**Figure 5.1 – Stress/Strain curves for the two composite systems**

At 100 megapascal (MPa), there is a discontinuity observed which is attributed to the removal of the extensometer to avoid damage to the equipment. It was observed that the elastic modulus of the S2 Glass® fiber composites was larger than the Kevlar® composites as the slope in the linear region was larger. Also, the ultimate tensile strength of the S2 Glass® composites was higher than the Kevlar® composites. The S2 Glass® composites demonstrated similar sudden rises and depressions in higher stress responses. These sudden changes were due to the individual or multiple fiber filaments breaking at these stresses with the occurrence of this phenomenon occurring more frequently near failure. Finally, the mode of failure, as define by ASTM D 3039, was maintained throughout the experimentation as a combination of explosive and edge delamination were observed in the gage section of the composites for the S2 Glass® composites. Occasionally, longitudinal splitting was observed but these instances were also accompanied by explosive failure. In the case of the Kevlar® fiber composites, failure occurred from either a lateral or angled fracture. The individual fiber breakage was not

observed as frequently compared to the S2 Glass® fiber composites. However, the manner of failure was still brittle in nature as the ultimate tensile strength and strain at failure occurred simultaneously.

From the stress/strain curves, the tensile modulus, ultimate tensile strength, strains at break, and energy at ultimate tensile strength were properties obtained for analysis. Figure 5.2 displays the aforementioned properties for the "thin" phenolic matrix/S2 Glass® fiber composites after the six weathering periods.

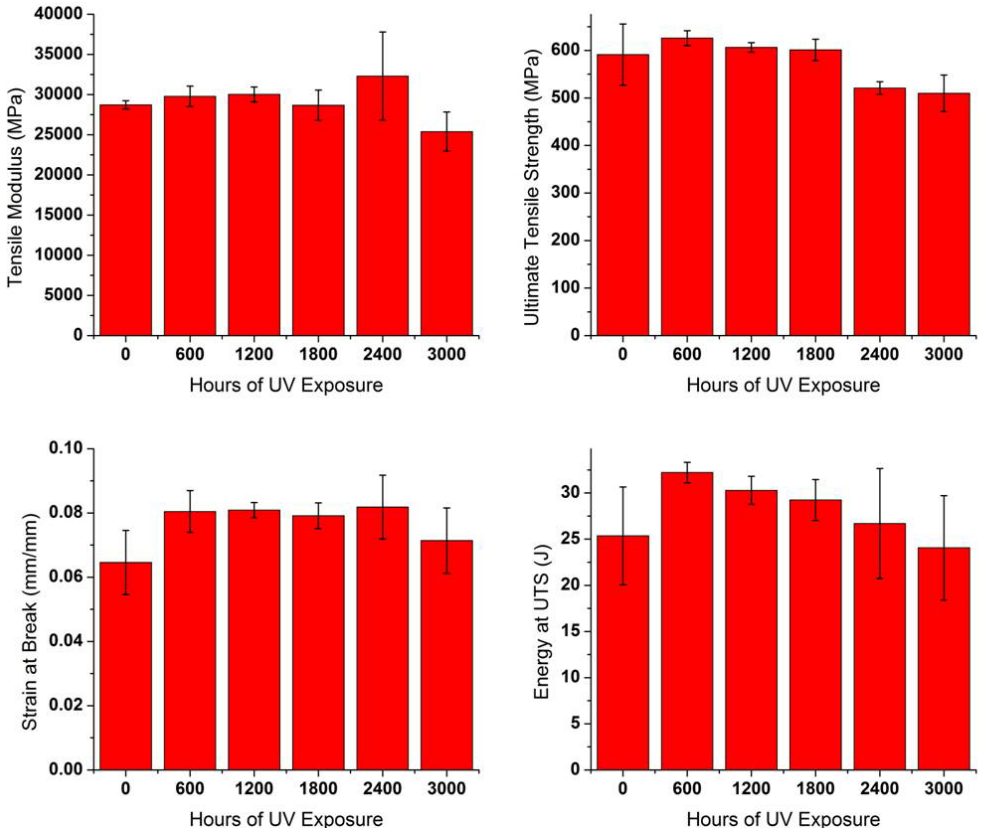


**Figure 5.2 – Tensile properties for S2 Glass® composites after six exposure periods including a) tensile modulus b) ultimate tensile strength c) strain at break and d) energy at the ultimate tensile strength**

The tensile modulus reveals small changes during accelerated exposure; however, the decrease at 3000 hours is larger than one standard deviation from the initial modulus.

Also, the modulus exhibited a slight increase at 600 hours and 1200 hours before decreasing again at 1800 hours. Tensile modulus is dependent on the bulk polymer and fiber responses to small strains which would have not been drastically influenced until long exposure times. The slight increase in the modulus can be attributed to less polymer mobility in the elastic regime. A loss of mobility can occur from a variety of reasons, but the most pertinent cases, to this research, stem from either an increase in crosslinking reactions from ultraviolet exposure of the matrix or plasticizer. It is assumed that the phenolic polymer is lightly copolymerized with polyvinyl butyral (PVB) which has demonstrated self crosslinking when exposed to ultraviolet conditions.[2] Low concentrations of PVB have demonstrated PVB rich zones in a phenolic matrix allowing for possible entrapment of unreacted PVB.[3] Another possible contribution may be attributed to the increased crosslinking of unreacted phenolic polymer which is possible within the cross sections of the composites. The 2400 hour sample set produced only three acceptable failures (i.e., failures initiated within the gage section) leading to large deviations in the results.

The ultimate tensile strength displayed significant changes after 2400 hours of exposure. This time frame also correlated well with the emergence of fibers present at the composite surface. On average, a slight increase in ultimate tensile strength was observed before decreasing in later exposure periods. Similar to the tensile modulus, the initial increase can be attributed to less mobility of the matrix material from either increased crosslinking of the matrix or plasticizer. The ultimate tensile strength of the S2 Glass® composites was observed to occur within 0.5% strain of bulk composite failure. This suggests a brittle failure which is to be expected with a brittle fiber constituent in S2

Glass®. A relatively unchanging modulus during accelerated exposure with a decreasing ultimate tensile strength has also been observed in literature.[4] Porosity increased with increased ultraviolet exposure which was also observed with water uptake and electrochemical impedance results. The effect of pore formation may only influence the ultimate tensile strength as the modulus is calculated in small strain regions where fiber and interfacial properties dictate the bulk response.

The strain at break also demonstrated an increase after initial exposure, but little confidence of a statistical change was observed as the standard deviations overlap in these instances. This trend was counter intuitive as the increased crosslinking would suggest a decrease in the strain at break due to less matrix mobility. Further observation determined that slipping of the clamped composite was occurring which influenced the results. The slipping caused higher elongations which would increase the strain at break value for the S2 Glass® fiber composites.

Energy at the ultimate tensile strength was observed to slightly increase before decreasing with increased exposure. The energy is calculated as the area under the stress-strain curve from initial loading until the ultimate tensile strength occurs. Therefore, the energy is dependent on both the stress and strain aspects. This suggests that the initial increase had both an increase in ultimate tensile strength and strain as factors causing a large initial increase in the energy. After the initial increase in energy, the later measurements were influenced by the ultimate tensile strength decreasing while the strain remained relatively constant resulting in an overall decrease in the energy. This result can be explained by the ultimate tensile strength decreasing from the creation and expansion of voids while the strain remained unchanged due to the slipping which was occurring.

As the peel ply was attached during exposure of the Kevlar® fiber composites, very little difference was observed in the tensile properties. The intensity of ultraviolet radiation allowed to pass through the peel ply increased from 0.06 watts/square meter ($W/m^2$) to 0.12 $W/m^2$, at 340 nanometer wavelength, over the span of 3000 hours of exposure when applied at 1.35 $W/m^2$. Overall, the amount of degradation reactions possible (i.e., the number of photons subjected to the composite) for the 3000 hour exposure samples would theoretically have less degradation reactions than that of the 600 hour samples weathered without the peel ply. This fact demonstrates that the results would show little difference from the initial results. Figure 5.3 displays the tensile properties of the phenolic matrix/Kevlar® fiber composites.

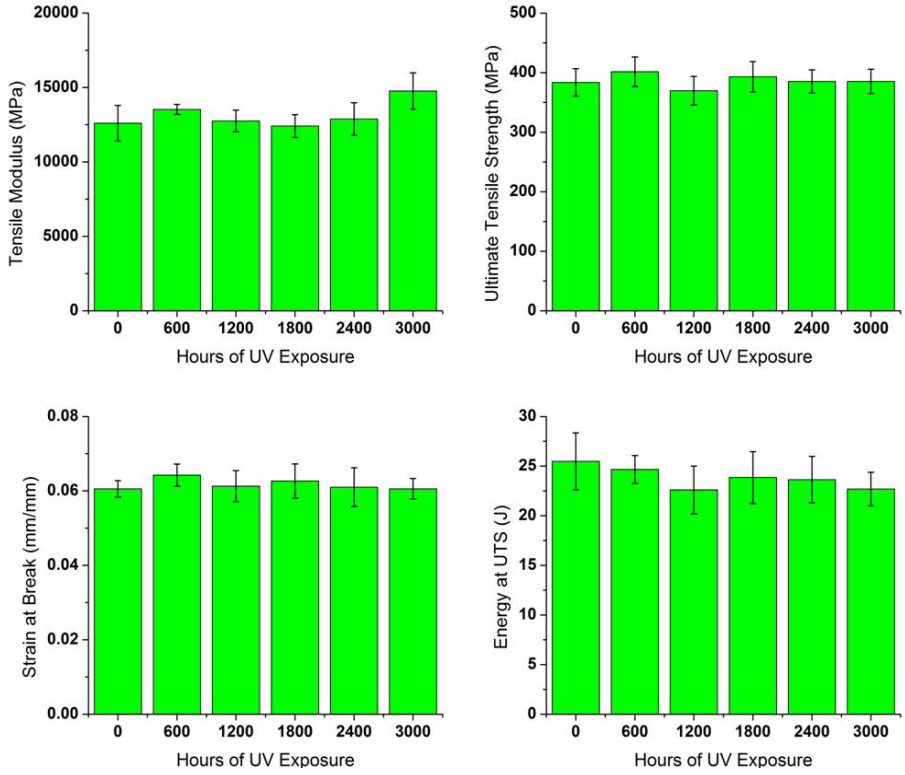


**Figure 5.3 - Tensile properties for Kevlar® fiber composites after six exposure periods including a) tensile modulus b) ultimate tensile strength c) strain at break and d) energy at the ultimate tensile strength**

As expected, the tensile modulus remained statistically unchanged from the initial values. This can be explained by the lack of penetration of the ultraviolet radiation during exposure. However, a small increase, of the average, was observed at 3000 hours, but little statistical confidence was assigned to this observation. Similarly, the ultimate tensile strength was not observed to change during increased exposure as pore creation and expansion could not occur which would change the crack initiation and propagation attributes. Strain at break values remained unchanged from the lack of ultraviolet exposure while the energy at ultimate tensile strength displayed a slight decrease in value but small confidence was assigned to this observation.

The small intensity of the ultraviolet radiation passing through the peel ply allowed for minor discoloration in the composites, but Figure 5.3 reveals that the tensile mechanical properties remained unchanged. Again, the unchanged properties are attributed to the lack of photodegradation reactions that occurred due to ultraviolet screening by the peel ply.

**5.3 Flexural Properties of PMCs Exposed to Ultraviolet Conditions**

Three point bending experiments were utilized to perform flexural measurement of the "thick" composite samples. By using a span distance (i.e., distance between two bottom supports) of four times the thickness of the composite, the short beam interlaminar shear strength (ILSS) could be determined. This ratio of span to thickness produces interlaminar shearing to occur which is not representative of an elastic flexural response; therefore, flexural modulus could not be calculated. From the ILSS measurement, it was determined that an overall trend of increasing ILSS was observed during the ultraviolet exposure. However, very little confidence is associated with this result which was observed for the S2 Glass® fiber composites in Figure 5.4.

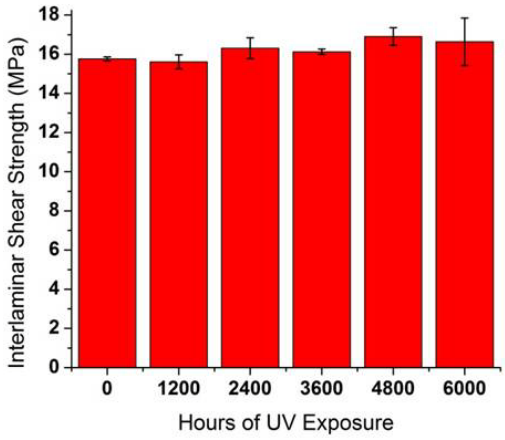


**Figure 5.4 - ILSS of S2 Glass® fiber composites**

Flexural responses (i.e., out of plane loading) are more dependent on the matrix material because fibers are not aligned for this loading, unless z-direction stitching is applied, as opposed to the tensile experimentation which is largely dependent on the fiber.[5] The ILSS demonstrated very little change during the exposure as the interlaminar shearing occurs typically within the middle most fiber plies. This was explained by the lack of penetration of the ultraviolet radiation into the inner most layers. Photodegradation of polymers tends to be a surface phenomenon as the depth of ultraviolet radiation penetration is low for a solar spectrum centered about the 340 nanometer wavelength (i.e., less than 20 micrometer).[6] This stems from the high absorption of visible and ultraviolet radiation in polymers along with the relatively low energy of this radiation wavelength. Even though the penetration depth is shallow, a noticeable increase in the ILSS of the S2 Glass® fiber composites was observed. However, a larger sample set would be necessary to determine the validity of this observation. The mode of failure for this experimentation demonstrated predominantly interlaminar shearing while compressive matrix cracking became more apparent after longer ultraviolet exposure.

The “thick” cross section phenolic matrix/Kevlar® fiber composites were also examined via flexural loading. Figure 5.5 displays the ILSS values for the Kevlar® fiber composite specimens with respect to the accelerated exposure times.

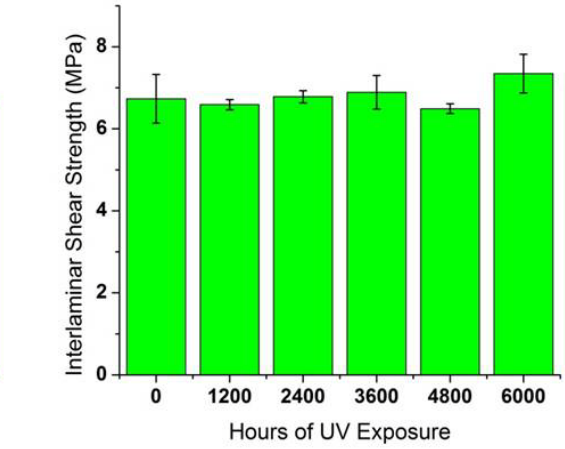


**Figure 5.5 - ILSS of Kevlar® fiber composites**

The interlaminar shear strength values were recorded although the predominant mode of failure was a combination of compressive and inelastic deformation, but some instances of interlaminar shearing were observed. Post-manufacturing of the Kevlar® fiber composites resulted in difficult determination of possible shear cracking locations. Also, with flexural loading, the maximum tensile and compressive stresses occur at the surfaces which correspond with the area most influenced by photodegradation. Since both the Kevlar® fiber and phenolic matrix are aromatic, the surfaces were photodegraded during ultraviolet exposure which could have led to greater porosity and, thus, more sites for compressive crack propagation. At six thousand hours of exposure the ILSS of the Kevlar® composites displayed an increase from the previous averaged values. However, the standard deviations were large lending little confidence to the increased ILSS value observed at this duration of weathering.

### 5.4 Ballistic Resistance of PMCs Exposed to Ultraviolet Conditions

Fragment simulating projectiles (FSPs) were utilized in the comparison of ballistic resistant capabilities of the two composite systems exposed to ultraviolet exposure. Table 5.1 reveals the ballistic results for the S2 Glass® fiber composites.

**Table 5.1 – Ballistic results for S2 Glass® fiber composites**

| Sample Identification | Projectile Mass (grams) | Measured Entrance Velocity (meters/second) | Projectile Surface Penetration (millimeter) | Cross-Sectional Penetration (millimeter) |
|---|---|---|---|---|
| **0 Hours Trial #1** | 17.30 | 88.70 | 4.47 | 3.72 |
| **0 Hours Trial #2** | 17.70 | 77.72 | 6.08 | 4.81 |
| **1200 Hours Trial #1** | 17.60 | N/A | 6.05 | 4.62 |
| **1200 Hours Trial #2** | 16.90 | 135.94 | 6.19 | 5.43 |
| **2400 Hours Trial #1** | 15.80 | N/A | 6.42 | 4.45 |
| **2400 Hours Trial #2** | 17.70 | 136.86 | 6.37 | 6.11 |
| **3600 Hours Trial #1** | 16.60 | N/A | 6.24 | 5.38 |
| **3600 Hours Trial #2** | 17.00 | 54.86 | 4.42 | 4.53 |
| **4800 Hours Trial #1** | 16.60 | 157.28 | 6.56 | 4.84 |
| **4800 Hours Trial #2** | 17.10 | N/A | 4.41 | 4.12 |
| **6000 Hours Trial #1** | 16.70 | 146.30 | 6.28 | 5.13 |
| **6000 Hours Trial #2** | 16.50 | 71.02 | 6.58 | 6.17 |

Two replicates per exposure period were subjected to ballistic characterization. The projectile mass was recorded as the kinetic energy is dependent on the mass and velocity of the projectile before impacting the composites. It was noted that the entrance velocity had large discrepancies which are attributed to the chronographs detecting the sabot particulates after reaching the sabot stripper. By using data from previous studies at this pressure, the average velocity for this composite set was determined to be 147 meters/second (m/s) by disregarding the unrealistically low velocities. The velocity measured constitutes a high velocity impact (i.e., > 100 m/s) for these samples. The penetration depth of the projectile was determined via two methods, including a surface measurement and a cross-sectional approach which was deemed more accurate as the depth was measured from an

uninfluenced ballistic exposed surface. The ballistic affected zone of the S2 Glass® fiber composites displayed fiber failure with an explosive nature as broken fiber and fiber ends were readily exposed. This failure mode was also observed in the tensile experimentation. Figure 5.6 displays the explosive failure observed for the S2 Glass® fiber composites.

**Figure 5.6 – Ballistic impact surface characteristics of S2 Glass® fiber composites**

Normalization of the penetration depth, with mass, accounts for the variation in the projectile mass and, thus, the variation in projectile energy. Figure 5.7 exhibits the normalized penetration depth as a function of the ultraviolet exposure time.

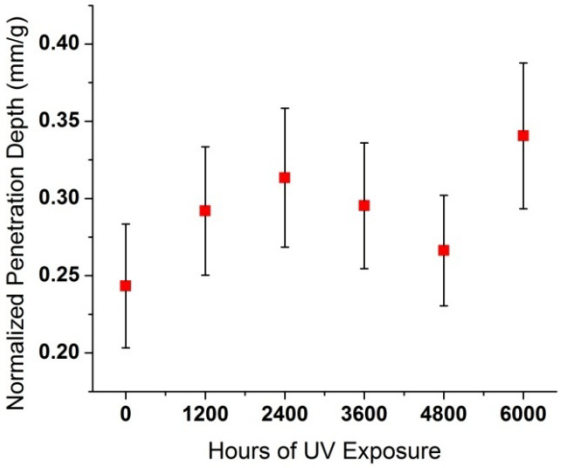


**Figure 5.7 - Normalized penetration depth of S2 Glass® fiber composites**

At 6000 hours of ultraviolet exposure, a one standard deviation of difference was observed in the normalized penetration depth. On average, all values of penetration depth were greater than the unexposed samples. Since the cross-sectional penetration depth was measured from an unaffected area, the slight decreases at 3600 and 4800 hours of exposure may be due to the removal of the topmost polymeric layer. The same amount of fiber plies would have been subjected to the projectile, but the distance between the impact area and top most surfaces would have decreased due to photodegradation. However, very low confidence was assigned to the increasing trend. Also, very little confidence is assigned to the difference between 0 and 6000 hours as only two replicates were subjected to ballistic measurement.

Examination of the Kevlar® fiber composites via ballistic penetration measurements demonstrated deeper penetration than the S2 Glass® fiber composites. However, the penetration depth was strongly dependent on the fiber material and the amount of plies of contact. The ballistic results for the Kevlar® fiber composites are displayed in Table 5.2.

**Table 5.2 - Ballistic results for Kevlar® fiber composites**

| Sample Identification | Projectile Mass (g) | Measured Entrance Velocity (m/s) | Projectile Surface Penetration (mm) | Cross-Sectional Penetration (mm) |
|---|---|---|---|---|
| **0 Hours Trial #1** | 17.30 | N/A | 4.38 | 3.80 |
| **0 Hours Trial #2** | 17.90 | 151.79 | 6.13 | 7.18 |
| **1200 Hours Trial #1** | 16.10 | N/A | 8.11 | 5.80 |
| **1200 Hours Trial #2** | 16.60 | 153.31 | 8.35 | 6.98 |
| **2400 Hours Trial #1** | 16.40 | N/A | 7.14 | 6.14 |
| **2400 Hours Trial #2** | 16.30 | N/A | 5.08 | 5.01 |
| **3600 Hours Trial #1** | 16.70 | N/A | 8.41 | 6.94 |
| **3600 Hours Trial #2** | 16.70 | N/A | 8.22 | 7.91 |
| **4800 Hours Trial #1** | 16.90 | 45.02 | 8.16 | 7.60 |
| **4800 Hours Trial #2** | 16.90 | N/A | 7.43 | 7.39 |
| **6000 Hours Trial #1** | 17.00 | 63.70 | N/A | 7.02 |
| **6000 Hours Trial #2** | 16.10 | 89.61 | 7.64 | 6.68 |

In the S2 Glass® fiber composites, 50 plies were utilized to create the 25.4 millimeter cross-sectional thickness while 45 plies were needed to produce the same thickness in the Kevlar® fiber composites. Therefore the results do not necessarily dictate that the Kevlar® composites did not perform as well as the S2 Glass® fiber composites on a per ply basis. Also, a larger difference was observed between the surface penetration and cross-sectional penetration depths. The difference in the two penetration depths can be accounted for by the fiber and matrix material being moved in the transverse direction with respect to the impact surface causing a bulging at the impact surface. The penetration surface also demonstrated a different mode of failure compared to the S2 Glass® fiber composites. A plugging effect was observed more frequently in the Kevlar® fiber composites along with a cleaner penetration surface. Plugging is a process where a surface layer creates a circular "plug" of material which must be forced through the bulk material and is known to occur more frequently with flat headed projectiles.[7] This plugging phenomenon is displayed in Figure 5.8 where the plug is observed within the impact area.

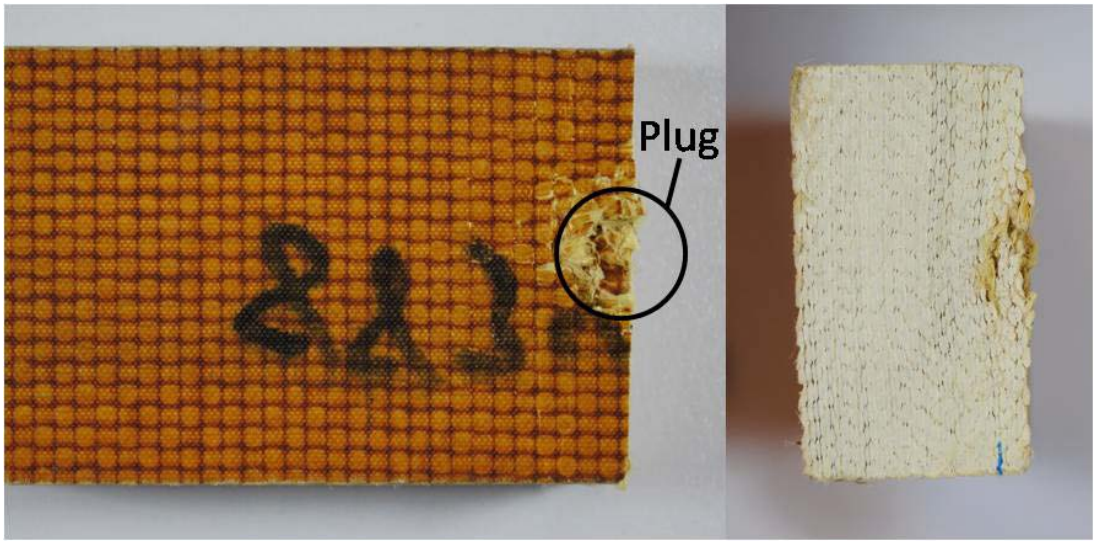


**Figure 5.8 – Ballistic impact surface characteristics of Kevlar® fiber composites**

Even with plug formation, the normalized penetration depth also exhibited an increasing trend for the Kevlar® fiber composites with respect to the ultraviolet exposure time. The normalized penetration depth for the Kevlar® fiber composites are displayed in Figure 5.9.

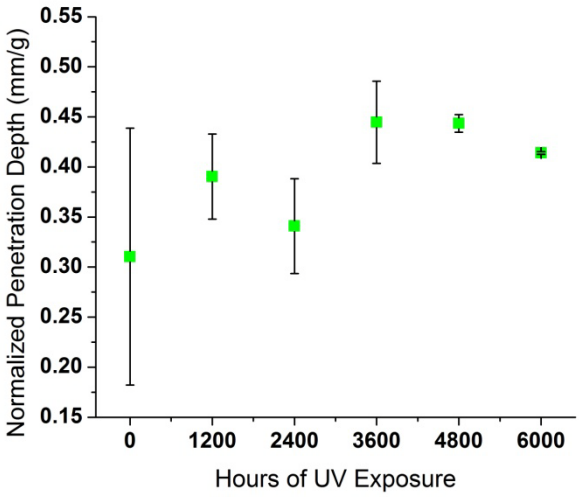


**Figure 5.9 - Normalized penetration depth of Kevlar® fiber composites**

On average, an increasing trend was observed from the initial penetration depth. A large deviation was observed at 0 hours of ultraviolet exposure which was dependent on the small number of trials associated with this data. The small number of replicates provides little confidence in the trend observed for the ballistic resistance of the Kevlar® fiber composites. For the phenolic matrix/Kevlar® fiber composites, both the matrix and fibrous materials were degraded during ultraviolet exposure which may be a factor in the deeper penetration upon ultraviolet exposure. As mentioned previously, the penetration depth is dependent on the number of plies the projectile contacts which is widely varied in these composites as fiber plies are not flat with respect to the penetration surface. This attribute made the determination of penetrated plies difficult.

## 5.5 Correlation of Mechanical Properties to EIS Circuit Model Constituents

The main objective of this research was to obtain a correlation of the electrochemical impedance and the mechanical properties. Of the three impedance modeled circuit elements, the pore resistance was selected as the most applicable characteristic to correlate to the mechanical properties, specifically the ultimate tensile strength. Both the average pore resistance and average ultimate tensile strength are displayed as a function of accelerated ultraviolet exposure for the "thin" S2 Glass® fiber composites in Figure 5.10.

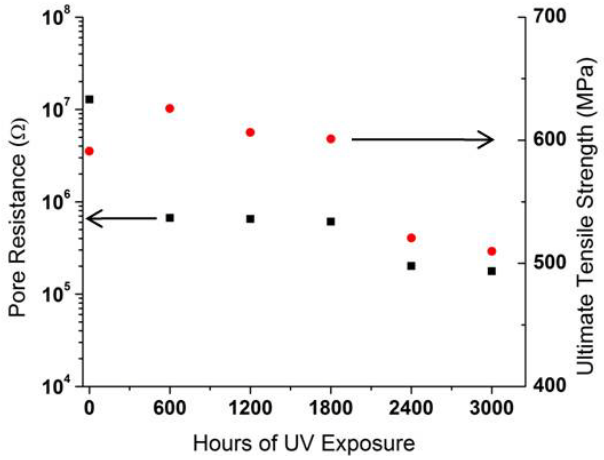


**Figure 5.10 – Composite pore resistance and ultimate tensile strength as a function of accelerated ultraviolet exposure for "thin" S2 Glass® fiber composites**

A large decrease after 2400 hours of accelerated exposure was present in both the pore resistance and ultimate tensile strength. The relative stabilities of both the pore resistance and ultimate tensile strength in the intermediate weathering periods also demonstrated a positive correlation between the two material properties. However, the initial increase in the ultimate tensile strength of the S2 Glass® fiber was met with a decrease in the pore resistance. The increase in porosity (i.e., lower pore resistance) with an increase in ultimate tensile strength has been observed during short ultraviolet exposure

durations in literature.[8] This was counter intuitive as increasing porosity was expected to lower the ultimate tensile strength as more defects are present, but the hardening of the matrix by various mechanisms outweigh the decrease from pore development.[9]

The correlation between the pore resistance and ultimate tensile strength of the S2 Glass® fiber composites was furthered studied to determine the relationship. Figure 5.11 exhibits the trend between the two properties for the data after 600 hours of accelerated ultraviolet weathering.

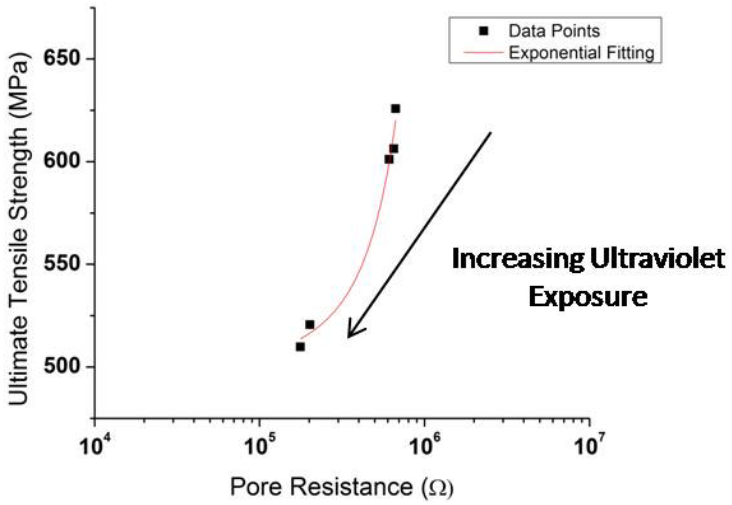


**Figure 5.11 – Exponential relation between the ultimate tensile strength and pore resistance for the S2 Glass® fiber composites**

The exponential relationship can be expressed in multiple variations which were studied for determination of the applicability of the fit. The two most popular forms, which also had high $R^2$ correlation, along with the constants are detailed in Table 5.3.

**Table 5.3 – Exponential fitting summary for the pore resistance and ultimate tensile strength relationship**

| Equation | $Y_0$ | A | B | $R^2$ |
|---|---|---|---|---|
| (5.1) $y = Y_0 + Ae^{bx}$ | 471.7 | 26.6 | $2.57E^{-6}$ | 0.978 |
| (5.2) $y = Ae^{bx}$ | ---- | 479.2 | $3.78E^{-7}$ | 0.983 |

From the equations, it was concluded that the fitting yielded a strong correlation as the correlation value was approaching one. However, the small sample set is conducive to a high correlation regardless of the type of fitting. The exponential function was applied to the data set as the boundary condition of a completely porous composite displayed reasonable approximation. As the pore resistance approaches zero, these two exponential functions approach 498 MPa (Equation 5.1) and 479 MPa (Equation 5.2) which are reasonable approximations given the extent of degradation which had occurred over the selected weathering periods. After 3000 hours of accelerated ultraviolet exposure, fiber was readily apparent on both exposed surfaces which signifies that most matrix removal from ultraviolet degradation had occurred in this duration. Therefore, it is assumed that the ultimate tensile strength would not decrease to a significant amount after this exposure period further justifying the use of the exponential models and good correlation to boundary conditions applied for the model.

**5.6 Conclusions**

It was concluded that the ultraviolet exposure had an influence on the mechanical properties as changes were observed in both the S2 Glass® fiber composites and Kevlar® fiber composites. The peel ply covering the "thin" Kevlar® fiber composites hindered the ultraviolet absorption, but a fraction of the intensity was observed to penetrate through the protective layer to induce degradation. Although the "thick" composite samples were administered to lengthy accelerated exposure periods, little change was found in the interlaminar shear strength. The ballistic resistance of these composites also displayed greater penetrations with increased exposure, but a small sample sizes promotes low confidence in these results.

Tensile properties of the S2 Glass® fiber composites demonstrated the most change from exposure to ultraviolet specifically in the area of ultimate tensile strength. The tensile modulus of these composites demonstrated an initial increase until a decrease was observed at the 3000 hour exposure point. Ultimate tensile strength followed a similar trend with an initial increase which then decreased dramatically at 2400 hours of exposure. These trends can be explained by an increase in crosslinking in either the phenolic matrix or changes involved with the plasticizer. The increased crosslinking of PVB has been reported in literature and can increase the modulus of these composite materials. Increased crosslinking of aromatic matrix materials also have been reported to initially increase the modulus and strength of composites. The strain at break, which occurred approximately at the ultimate tensile strength, increased initially and remained relatively unchanged, but some slipping was observed in these samples which may have altered the true strain observed at failure. Lastly, the energy at the ultimate tensile strength was observed to increase initially and decrease with increasing exposure. This was attributed to the change in the ultimate tensile strength as it decreased while the strain remained unchanged after the initial increase.

Phenolic matrix/Kevlar® fiber composites were inadvertently exposed to the accelerated ultraviolet source with an intact peel ply still attached. This layer acted as a screen to the ultraviolet exposure, but the investigation of the weathered peel ply demonstrated that an intensity of 0.12 watts/square meter (at 340 nanometer wavelength) was being subjected to the sample after long exposure periods. The most profound result was the appearance of a tensile modulus increase at 3000 hours. This was thought to occur from matrix hardening as was observed in the S2 Glass® composites initially. Other tensile

properties exhibited little statistical change from the initial properties as the peel ply screened ultraviolet radiation from causing significant photodegradation.

The ILSS displayed very little change in either composite as this characteristically involved fracture from shearing which occurs within the inner most composite plies. Ultraviolet penetration into these "thick" composites is not deep enough to drastically influence this property. Also, the depth of ultraviolet penetration was dependent on the absorption coefficient of these materials. As the S2 Glass® was transparent in this radiation regime, the small changes in ILSS may be attributed to the deeper penetration of ultraviolet radiation. The presence of compressive cracking at the surface, observed in both composite systems, can be attributed to the surface hardening which occurs upon photodegradation. The surface also corresponds to the largest compressive and tensile stresses in flexural loading which is another reason for cracks initiating at the surface. In the ILSS results, a sample set of three composites was used leading to large deviations from the mean and less statistical confidence in the results.

Ballistic characterization of these composites demonstrated a deeper penetration with increased exposure. By normalizing the penetration depth to the mass of the projectile (i.e., the only known constituent of the kinetic energy), a more conclusive investigation could be performed on the penetration depth. The mechanism of failure was also observed to be different between the two fiber types as the S2 Glass® fiber composites demonstrated an explosive failure while a cleaner penetration surface was observed with the Kevlar® fiber composites. The deeper penetration was not statistically significant as a small sample set provided large deviations in the data. Kevlar® fiber composites demonstrated a deeper penetration of the FSP than the S2 Glass® fiber which was expected as the S2 Glass® fiber

does not undergo photodegradation from ultraviolet exposure. The penetration depth is largely dependent on the number of fiber plies that comes in contact with the projectile. As the fiber weave made the discerning of the plies penetrations difficult. Therefore, the S2 Glass® fiber is not necessarily a better ballistic deterrent fiber as fiber size and fiber loading in the composite is a very important aspect.

The relationship between the ultimate tensile strength and pore resistance obtained from circuit modeling demonstrated a strong correlation. After numerous variations of curve fitting, it was determined that an exponential fitting more appropriately correlated to the boundary conditions. As the pore resistance approached a low value (i.e., effectively the resistance of the electrolyte) the ultimate tensile strength of the S2 Glass® composites approached a value between 479 MPa and 498 MPa. These values were deemed acceptable as the top layer polymeric region was almost completely removed at 3000 hours leading to an ultimate tensile strength which would not be drastically influenced until the ultraviolet radiation reached the middle most ply.

**5.7 References**


1. Singh, B., M. Gupta, and A. Verma, *The durability of jute fibre-reinforced phenolic composites.* Composite Science and Technology, 2000. **60**(4): p. 581-589.
2. Saad, G.R., E. El-Shafee, and M. Sabaa, *Dielectric and mechanical properties in the photodegradation of poly (vinyl butyral) films.* Polymer Degradation and Stability, 1995. **47**(2): p. 209-215.
3. Ismail, I., Z. Ishak, M. Jaafar, S. Omar, M.F.Z. Abidin, and H.F.A. Marzuki, *Thermomechanical Properties of Toughened Phenolic Resole Resin.* Solid State Science and Technology, 2009. **17**(1): p. 155-165.
4. Correia, J.R., S. Cabral-Fonseca, F.A. Branco, J.G. Ferreira, M.I. Eusebio, and M.P. Rodrigues, *Durability of pultruded glass-fiber-reinforced polyester profiles for structural applications.* Mechanics of Composite Materials, 2006. **42**(4): p. 325-338.
5. Rugg, K.L., B.N. Cox, and R. Massabò, *Mixed mode delamination of polymer composite laminates reinforced through the thickness by z-fibers.* Composites Part A: Applied Science and Manufacturing, 2002. **33**(2): p. 177-190.

6. Hinderliter, B. and S. Croll, *Monte Carlo approach to estimating the photodegradation of polymer coatings.* Journal of Coatings Technology and Research, 2005. **2**(6): p. 483-491.
7. Ulven, C., U.K. Vaidya, and M.V. Hosur, *Effect of projectile shape during ballistic perforation of VARTM carbon/epoxy composite panels.* Composite Structures, 2003. **61**(1-2): p. 143-150.
8. Huang, G., *Degradation of glass fibre/polyester composites after ultraviolet radiation.* Materials & Design, 2008. **29**(7): p. 1476-1479.
9. Hammami, A. and N. Al Ghuilani, *Durability and environmental degradation of glass vinylester composites.* Polymer Composites, 2004. **25**(6): p. 609-616.

# CHAPTER 6. GENERAL CONCLUSIONS AND FUTURE WORK

## 6.1 General Conclusions

After exposure to accelerated ultraviolet exposure, it was determined that a multitude of material characteristics were altered. Surface characteristics including gloss, color, water contact angle, and surface roughness were monitored to determine the influence of the ultraviolet exposure on the phenolic matrix composites containing either S2 Glass® or Kevlar® fibers. As expected, gloss and color were visually observed to change with exposure time while the contact angle and surface profilometry results demonstrated increasing surface roughness, possibly from pore creation. All these surface effects have been widely reported in literature. Electrochemical impedance spectroscopy (EIS) was utilized to monitor the bulk impedance of the composites after accelerated exposure was administered. From the EIS data, circuit modeling demonstrated that both capacitive and resistive elements were observed in the impedance response. Modeling each element individually allowed further characterization of the bulk degradation mechanisms. Mechanical analysis performed in tension demonstrated the most conclusive changes in the ultimate tensile strength for the S2 Glass® fiber composites. Also, ballistic resistance experimentation exhibited an increased penetration with exposure time, but large deviations in the data caused a low confidence in this observation.

First, the applicability of using EIS for a non-destructive evaluation (NDE) technique was investigated. It was determined that composites immersed in water for a brief duration could be measured via EIS. The EIS spectra demonstrated both a resistive (i.e., pore resistance) and capacitive (i.e., composite capacitance) response in the mid to high frequencies. Circuit modeling of the spectra was performed to obtain the magnitude

of each circuit modeled element. For the "thin" S2 Glass® composites, a large decrease in the pore resistance was observed from the initial to final exposure periods. Porosity increases with increased ultraviolet exposure which allows easier motion of electrons and ions and ,thus, lower impedance. An initial increase in the capacitive value was also observed for these composites before decreasing toward the original value. Increased water uptake should cause the capacitive value to continually increase, but the decrease in capacitance was associated with a smaller contact area as fiber became exposed. The "thin" phenolic matrix/Kevlar® fiber composite were subjected to EIS experimentation with the peel ply intact. After experimentation with the peel ply removed, it was determined that the peel ply was porous enough that the pore resistance was not influenced. However, the water uptake of this layer did change the magnitude of the capacitance, so the initial results observed are not truly representative of the actual composite capacitance. Both "thick" composite systems did not display significant differences in the capacitive elements with increasing exposure time. Water uptake was not large enough to influence the bulk dielectric constant and, correspondingly, the capacitance was not influenced. The pore resistance was observed to decrease in both systems with increasing exposure from the porosity increasing with increased ultraviolet exposure.

Another interesting phenomenon that occurred as measured by EIS experimentation was the appearance of a low frequency impedance increase. The phase angle remained resistive while an increase in the impedance suggested an almost capacitive incline at the low frequencies. This phenomenon has not been observed in literature, so further analysis was conducted to determine the cause for this phenomenon. Performing single frequency measurements at a low frequency (i.e., 0.1 Hertz) displayed that an evaporation process

was occurring in the ambient experimental chamber. The evaporation influence at the low frequencies was not modeled in the circuit modeled results. By selecting the correct frequency range during circuit modeling, the possibility of error in the results from this undocumented phenomenon was avoided.

The EIS results suggested that porosity was occurring from ultraviolet exposure. Therefore, traditionally reported surface characteristics were monitored during exposure to examine the extent of degradation. A color change was visually observed after the first weathering duration in both the "thick" and "thin" composites. Color measurements displayed that, after the final exposure period, large changes in color were present. Color characteristics are an indication the ultraviolet exposure caused photodegradation reactions within the material. The degradation reactions created new functional groups or alter the existing functional groups to change the absorption of visible light and, thus, change the color of the sample. Most specifically in the literature, a yellowing occurs in clear and white polymers. In the case with the phenolic matrix composites, the yellowness decreased during exposure. However, the emergence of fiber verified that significant degradation was occurring, causing the removal of the top polymeric layer. This claim was further reinforced as the gloss values for the 60° and 85° angles increased during exposure which is attributed to fiber bridging. Fiber bridging was not easily observed by surface profilometry, but the increases in surface roughness before fiber emergence (i.e., before 1200 hours of exposure) signified that a roughening was occurring. The roughening effect was also observed within the water contact angle as the water contact angle was observed to decrease with exposure time. However, the water contact angle is not only dependent of surface roughness as it also depends on the chemical composition at the surface. An intact

peel ply attached to the "thin" Kevlar® fiber composites hindered absorption of the ultraviolet radiation. Therefore, color and gloss results of the Kevlar fiber composites were not reported for the "thin" samples as the peel ply color and gloss were not of concern in this study.

The increase in porosity, suggested by EIS and surface characterization, was further studied with destructive mechanical measurements in tensile and flexural configuration. It was determined that the "thin" S2 Glass® fiber composites demonstrated a significant decrease in the ultimate tensile strength while the modulus demonstrated an increase with exposure time before decreasing at long exposure times. The hardening of the matrix via increased crosslinking of the matrix or plasticizer is commonly observed in literature. At long exposure times, the porosity greater influences both the modulus and ultimate tensile strength as the pores act as locations for easier crack propagation. A slipping of the tabs attached for experimentation was noted which may have resulted in misleading strain at break information, but the energy at the ultimate tensile strength was observed to increase initially before decreasing. The "thin" Kevlar® fiber composites displayed little mechanical change as the peel ply prevented any significant ultraviolet degradation. All properties observed remained unmodified from the original value, but a small increase in the modulus was observed at 3000 hours of exposure which was thought to be caused by matrix hardening.

Flexural properties were different for the two composite systems which was attributed to both the possible difference in matrix composition as well as fiber absorption properties. The S2 Glass® fiber composites displayed a slight increase in the interlaminar shear strength (ILSS) but little statistical confidence was associated with this observation.

Kevlar® fiber composites demonstrated that the ILSS remained unchanged except for a slight increase at 6000 hours which, again, was not statistically different. The relatively unchanged vales for both ILSS vales were due to the location of the interlaminar shearing. As ultraviolet radiation only penetrates a small distance into the composites, the interlaminar properties would not be greatly influenced as the location of failure was within the middle of the structure. The "thick", or one inch, cross-sections were too thick for monitoring a substantial ILSS change. However, the modes of failure in the ILSS measurements were different for the two composite systems. The S2 Glass® fiber composites demonstrated interlaminar shearing failure. Kevlar® fiber composites displayed surface compression cracking and inelastic deformation, but the edge view of the post-manufactured composites displayed some instances of interlaminar shearing. The compressive cracking occurred at the surface which was also becoming harder with increased ultraviolet exposure. A combination of surface hardening and the location of the largest compressive stresses at the surface lead to surface compression cracking.

Ballistic experimentation determined that the normalized penetration depth exhibited an increasing trend with increased exposure. By normalizing the penetration depth with the mass of the projectile, which was the only known constituent involved in the impact energy, a better understanding of the material's ballistic resistance could be determined. The Kevlar® fiber composites displayed deeper penetration of the fragment simulating projectile (FSP) than the S2 Glass® fiber composites. These depths of penetration were more dependent on the composition and number of fiber plies which could not be accurately counted due to complex orientation of the fiber plies. Also, the increased penetration depth has a low confidence as the sample set of two replicates was

not conducive in this type of experimentation. The mode of failure was also different for the two composites. The S2 Glass® fiber composites displayed explosive failure in the impact zone as S2 Glass® fiber was broken in a buckling manner to expose fiber ends. The Kevlar® fiber composites demonstrated a much cleaner penetration surface, but the occurrence of plugging was observed frequently. A plug of composite is developed at the surface and is pushed into the impact zone via the FSP.

### 6.2 Future Work

One of the major drawbacks of the completed research occurred due to the peel ply attachment on the "thin" Kevlar® fiber composites utilized for tensile experimentation. The Kevlar® fiber composition, being aromatic, was ideal to determine the influence of accelerated exposure where the two composite constituents would degrade. A repeated ultraviolet exposure should be conducted with the peel ply removed to determine the correlation between the pore resistance and ultimate tensile strength for this composite system.

Longer exposure periods would be preferred as well to determine if the tensile modulus and ultimate tensile strength would continue to decrease. Also, different exposure durations could be utilized to determine the applicability of the exponential model for prediction of the ultimate tensile strength as a function of the pore resistance. A larger sample set would also be more conducive for minimizing the standard deviation and thus increasing the confidence in trends observed.

Although the "thick" composite samples were a better reflection of the geometries utilized in ballistic resistant applications, the cross section was not conducive to flexural properties of composites weathered with ultraviolet exposure. Noticeable EIS and surface

characteristics were observed during exposure, but upon investigation of the flexural properties, little change was observed in the Kevlar® fiber composites. The ILSS results may exhibit more change if smaller cross-sections were utilized. Thinner composite thicknesses would be more conducive to exhibiting mechanical property differences as ultraviolet penetration is of the order of 20 microns.

Ballistic experimentation performed in this work was not the ideal for determining the ballistic limit as the sample geometry was not correct. Future work in this area would benefit from larger panel dimensions with thinner cross sections. This would require more EIS experimentation as the influence of ultraviolet radiation is dependent on the penetration depth. The ballistic limit would then be another quantitative result which could be correlated with the pore resistance and perhaps even the capacitive values which may display information regarding the interfacial properties.

In terms of EIS experimentation, a study of the electrode size would be interesting as a large area is preferred. Electrons travel via the least impeded path which would coincide with pores formed during weathering. At this point, it is assumed that the impedance measured over a large area would be at the deepest pore where mechanical failure would be likely to occur. If the EIS technique would be utilized for NDE of non-conducting composites, a large surface area electrode would be ideal for fewer measurements which would further reduce the cost of an already inexpensive method. A study determining the largest usable electrode size while maintaining correct sensitivity would be very beneficial. Adversely, the use of local EIS (LEIS) could also be useful in determining the precise area where the high porosity, or low impedance, is occurring within the composite specimen.

A simultaneous single frequency EIS and ultrasonic NDE technique would be a novel study correlating data from EIS and a widely accepted ultrasonic technique. Both these techniques could be carried out in a water medium with some type of external stimuli to induce pores and delaminations. Ultrasonic techniques do not use an electronic signal for conducting measurements which would not provide errors in the EIS measurements. The difficultly in the measurement would be the interference of metallic electrodes with the ultrasonic waves. To avoid the possible interference, different configurations of ultrasonic transducers and receivers could be utilized for measurements as opposed to the most traditional transmission methods to avoid the interference.